Shear Thinning Fluid Mixing in Unbaffled Stirred Vessels

by
Nihat Yavuz

A dissertation submitted to the Graduate Faculty of
North Carolina State University
in partial fulfillment of the
requirements for the degree of
Doctor of Philosophy

Food Science

Raleigh, North Carolina

2016

APPROVED BY:

_____	_____
Dr. K.P. Sandeep Committee Chair	Dr. Josip Simunovic
_____	_____
Dr. Christopher R. Daubert	Dr. Kenan Gundogdu

ABSTRACT

YAVUZ, NIHAT. Shear Thinning Fluid Mixing in Unbaffled Stirred Vessels. (Under the direction of Dr. K.P. Sandeep).

Mixing is a common operation used in many process industries. Highly viscous fluids are often mixed in stirred vessels equipped with various impellers. However, certain performance issues arise due to the nature of these fluids. Isolated mixing regions (IMRs) are formed in laminar flow. For impellers located at the center of the vessels, IMRs appear right above and below the impeller and only after impractically long times, they dissipate by diffusion. Increasing rotational speed or using large diameter impellers such as an anchor or helical ribbon minimize IMRs at the expense of increased power consumption. Several strategies have been developed to eliminate IMRs. Insertion of baffles, variable rotational speed/direction protocols, and multiple impellers are proven to be effective in improving mixing under laminar flow conditions. The presence of extra surface area resulting in possible cleaning problems and the need for advanced control systems necessitate simpler solutions. Therefore, mixing of 1% carboxymethyl cellulose (CMC) solution in an unbaffled stirred vessel was studied in two parts. In the first part, the objective was to investigate the effects of eccentricity (locating impeller away from the center of the vessel) and modification of a standard pitched blade turbine (PBT) on laminar mixing and power consumption. Numerical analysis was also conducted to replicate the same experimental conditions. Laminar mixing was evaluated by the evolution of a tracer dye within the vessel. The measurements were made using the planar laser induced fluorescence (PLIF) method. Increasing eccentricity reduced the size of IMRs and increased concentration homogeneity without increasing power consumption. A Dual-flow PBT, which is a modified PBT

generates simultaneous upward and downward flow, did not perform better than PBT for all the cases studied. The Metzner-Otto constant (K_s) was also calculated for both impellers to determine Power curves for further use in the second part of the study. The objective of the second part was to scale-up the results obtained in the first part based on equal values of Reynolds (Re) number, tip speed, and power per volume. For PBT, similar % area coverage and concentration distribution values were achieved with all three scale-up criteria. Time to reach the same end point and power consumption were the main differences between each criteria. Scale-up with equal power per volume resulted in achieving the end point faster than that with the other two methods while power consumption was the lowest for scale-up based on equal Re. For Dual-flow PBT, only equal Re number was successful in achieving good mixing, thereby suggesting that the dynamic behavior of the impeller may be affected significantly by scale-up.

BIOGRAPHY

Nihat Yavuz was born in Mersin, Turkey on February 25th, 1985. He received his B.S. degree in Food Engineering from University of Mersin in 2007. While enrolled as a M.S. student in the same department and working for a spice company as a process engineer, he received a fellowship from the Turkish Ministry of National Education to study abroad. He started his graduate studies again in the department of Biological Systems Engineering at Virginia Tech and earned his M.S. degree in 2010. He then moved to Raleigh, NC, to pursue a Ph.D. degree in the department of Food, Bioprocessing, and Nutrition Sciences under the supervision of Dr. K.P. Sandeep in 2011.

ACKNOWLEDGMENTS

I would like to thank my advisor, Dr. K.P. Sandeep for all his guidance, encouragement, and patience during my studies. This work wouldn't be complete without him and I appreciate all the opportunities he provided.

I would also like to thank all my committee members, Dr. Josip Simunovic, Dr. Christopher Daubert, and Dr. Kenan Gundogdu for their advice, suggestions, and time.

Much appreciation and gratitude are extended to Karl Hedrick III, Michael Bumgardner, Jack Canady, Chris Pernell, Randy Kotzian, and Gary Cartwright for their help in experimental set up and runs.

Special thanks to Ediz Batmaz and Nestle Nutrition for lending us their experimental equipment.

TABLE OF CONTENTS

LIST OF TABLES vii

LIST OF FIGURES ix

CHAPTER 1 1

Literature Review 1

1. Basics of Mixing 1

2. Stirred Vessels 2

3. Mixing Measures 5

4. Measurement Methods 8

4.1. Mixing Level Methods 8

4.2. Power Measurement Methods 14

4.3. Computational Fluid Dynamics 15

4.4. Dimensional Analysis 16

5. Laminar Flow in Stirred Vessels 20

6. Scale-up of Stirred Vessels 23

References 24

CHAPTER 2 40

Shear thinning fluid mixing in unbaffled stirred vessels. Part 1: Hydrodynamic characterization 40

Abstract 40

1. Introduction 41

2. Materials and Methods 44

2.1. Materials 44

2.2. Set-up for mixing system 45

2.3. Planar Laser Induced Fluorescence Experiments 46

2.4. Power Measurement 48

2.5. Numerical Studies 49

3. Results and Discussions 51

3.1. PLIF Measurements 51

3.2. Effect of Eccentricity on Laminar Mixing 52

3.3. Effect of Impeller Type on Laminar Mixing 53

3.4. Power Consumption 55

4. Conclusion 56

References 57

CHAPTER 3 89

Shear thinning fluid mixing in unbaffled stirred vessels. Part 2: Scale-Up 89

Abstract 89

1. Introduction 90

2. Material and Methods 92

2.1. Materials 92

2.2. Mixing system 92

2.3. Scale-up Methods 93

2.4. Planar Laser Induced Fluorescence Experiments 94

2.5. Power Measurement 95

2.5. Numerical Studies 95

3. Results and Discussions 96

3.1. Determination of rpm at large scale 96

3.2. Effects of scale-up on mixing performances 97

4. Conclusion 100

References 101

CONCLUDING REMARKS 123

RECOMMENDATIONS FOR FUTURE STUDIES 126

LIST OF TABLES

CHAPTER 1

Table 1. The impeller diameter (D) to vessel diameter (T) ratios for a standard vessel configuration 4

Table 2. Various laser power/energy levels and camera resolutions used for different vessel diameters 13

CHAPTER 2

Table 1. Rheological parameters of 1% (w/v) CMC within shear rate range of 10-800 1/s .. 62

Table 2. Viscosity of light corn syrup 62

Table 3. Effect of number of elements on power and computation time in a mesh convergence study 68

Table 4. Specific power consumption (W/m^3) for 1.0% CMC 81

Table 5. Experimental and numerical values of Po*Re 84

Table 6. Experimental and numerical values of K_S 87

CHAPTER 3

Table 1. Geometrical dimensions of the small and large scale vessels 104

Table 2. Large scale rpm values for each scale-up rule 108

Table 3. Specific power consumption (W/m^3) comparison for experimental and numerical measurements 111

Table 4. Change in Re and tip speed with scale-up 112

Table 5. CoV values when uncovered area% is less than 5 and at the end of the experiments (3 hrs.) 119

LIST OF FIGURES

CHAPTER 1

Figure 1. Stirred vessel configuration and the flow generated by an impeller 3

Figure 2. Change in the intensity of segregation (I) while the scale of segregation (S) is relatively constant 6

Figure 3. Change in the scale of segregation (S) while the intensity of segregation (I) is constant at 1.7321 7

Figure 4. Evolution of a dimensionless concentration over time..... 9

Figure 5. A generic set-up of PLIF method 11

Figure 6. Visual interpretations of CFD results. 17

Figure 7. Power curve of a Newtonian fluid for Anchor and Rushton impellers 19

Figure 8. Mixing at Re = 25 with an axial impeller..... 21

CHAPTER 2

Figure 1. Geometry of the mixing system 63

Figure 2. Pitched blade turbine (a) and Dual-flow pitched blade turbine (b) 64

Figure 3. Calibration curve of Rhodamine 6G..... 65

Figure 4. Linear portion of the calibration curve of Rhodamine 6G 66

Figure 5. Geometry of the mixing system with a stationary outer domain and a rotating inner domain..... 67

Figure 6. PLIF images of DF-PBT and PBT for E = 0 69

Figure 7. PLIF images of DFPBT and PBT for E = 0.25 70

Figure 8. PLIF images of DF-PBT and PBT for E = 0.50 71

Figure 9. Isolated mixing regions seen at different locations 72

Figure 10. % Uncovered area for DF-PBT 73

Figure 11. % Uncovered area for PBT 74

Figure 12. CoV for DF-PBT 75

Figure 13. CoV for PBT 76

Figure 14. Velocity vectors at fluid surface at 100 rpm for PBT 77

Figure 15. Velocity vectors at the vessel center at 100 rpm for PBT 78

Figure 16. Axial velocity at the tip of the impeller at 300 rpm for DF-PBT 79

Figure 17. Velocity vectors at center of the vessel center at 300 rpm for DF-PBT 80

Figure 18. Power number vs Reynolds number for light corn syrup (PBT) 82

Figure 19. Power number vs Reynolds number for light corn syrup (DF-PBT) 83

Figure 20. Effect of rps on Ks for PBT 85

Figure 21. Effect of rps on Ks for DF-PBT 86

Figure 22. Non-Newtonian power curve for E = 0.50 88

CHAPTER 3

Figure 1. Grayscale vs concentration of Rhodamine 6G for large scale vessel..... 105

Figure 2. Linear calibration curve of Rhodamine 6G for large scale vessel..... 106

Figure 3. Uniformity of the lase sheet for calibration image at 20 µg/L 107

Figure 4. Isosurface representations of velocity magnitudes at the small scale 109

Figure 5. Isosurface representations of velocity magnitudes on the large scale..... 110

Figure 6. PLIF images for PBT at the end of 3 hrs..... 113

Figure 7. PLIF images for DF-PBT at the end of 3 hrs. 114

Figure 8. The change in % uncovered area% over time for PBT at small scale..... 115

Figure 9. The change in uncovered area% over time for DF-PBT at small scale..... 116

Figure 10. Change in % uncovered area over time for PBT at large scale 117

Figure 11. Change in % uncovered area over time for DF-PBT at large scale..... 118

Figure 12. Velocity vectors at the vessel center for PBT 120

Figure 13. Velocity vectors at the laser measurement plane for PBT 121

Figure 14. Velocity vectors at the fluid surface for PBT..... 122

CHAPTER 1

Literature Review

1. Basics of Mixing

Mixing, which results in the reduction of inhomogeneity in a system, is a common unit operation in processing industries such as chemical, food, and pharmaceutical. Depending on the application, the size of the system can change from small containers to industrial size bioreactors for batch operations or from microscopic channels to large diameter pipelines for continuous operations. The differences between concentration, color, temperature, or droplet/bubble sizes are few examples of the source of inhomogeneity among many others. Complete mixing occurs when the degree of inhomogeneity has the same value at every point in the system. Under practical conditions, complete mixing is really hard to achieve. Therefore, reducing the inhomogeneity to predetermined levels is the main goal to meet quality criteria for customer satisfaction and legal claims (Cullen and O'Donnell 2009).

The applications of mixing can be classified based on the phases to be mixed (Chhabra 2003). A quick summary of the applications is given below:

- Miscible liquid-liquid (homogenization, heat/mass transfer, chemical reactions)
- Immiscible liquid-liquid (emulsification, extraction)
- Liquid-solid mixing (suspensions, dissolution of powders)

- Gas-liquid mixing (fermentation, oxidation, chlorination)
- Liquid-solid - gas (slurries)
- Solid-solid (powders)

Chavan and Mashelkar (1980) described effective mechanisms of mixing as the breakage of the inhomogeneity sources into smaller parts, deformation by shear and tensile stresses, transport by natural or forced convection, and diffusion. The mixing equipment, processing parameters, and physical properties of the phases determine which mechanisms are dominant during mixing. These mechanisms usually take place at different length scales (Cullen and O'Donnell 2009). Three scales are defined for investigation of various mixing applications as follows:

- Macromixing (mixing at the equipment volume by convective flow)
- Micromixing (deformation and diffusion based mixing close to molecular level)
- Mesomixing (in between macro and micromixing)

2. Stirred Vessels

Stirred vessels are widely used as mixing equipment. The standard configuration of a stirred vessel includes a vertical cylindrical vessel and an impeller attached to a shaft which is rotated by a motor. An example of stirred vessel configuration and the flow types

generated by an impeller is given in Figure 1. Axial flow which is parallel to the shaft is represented by the arrows ‘A’ and the radial flow which is directed perpendicular to the shaft is shown by arrows ‘C’. The rotational movement around the shaft axis is the tangential flow (arrow ‘B’). When tangential flow is dominant, the fluid rotates like a solid body in the vessel and the relative positions of the phases to be mixed do not change. The radial and axial components of the flow should be increased as opposed to tangential component for effective mixing (Fellows 2009).

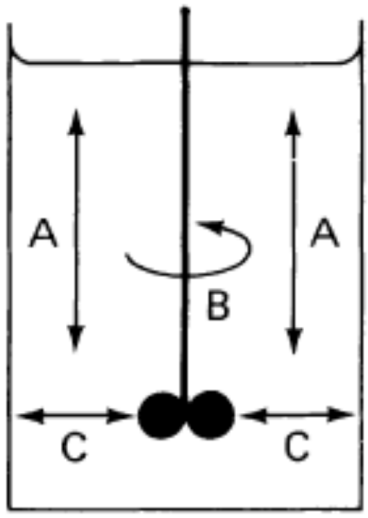

Figure 1. Stirred vessel configuration and the flow generated by an impeller (Fellows 2009)

The volume of vessels may vary from the order of mL for pharmaceutical applications to the order of cubic meters for fermentation applications. While cylindrical vessels are quite common, different shapes such as flat, conical, rounded, and, profiled can

be used for the bottom of the vessels for easy cleaning, suspension of solids, or improved efficiency (Houcine and others 2000). Marine, Rushton, pitched blades, hydrofoils, anchor, gates, planetary, and rotor stators are some of the impeller types used in stirred vessels. There is more than one way to classify all these impellers. The flow type (axial, radial, mixed), phases to be mixed (dispersion and dissolution into liquids, particulate blending, solid-liquid mixing for doughs/pastes), relative positions in the vessel (close clearance to vessel walls, low clearance to the bottom of the vessel) can be selected base on the convenience they provide (Niranjan and others 1994; Tekchandaney 2012). For a standard vessel, fluid height is set equal to the vessel diameter. In this case, the recommended range of impeller diameter to vessel diameter ratios are given in Table 1.

Table 1. The impeller diameter (D) to vessel diameter (T) ratios for a standard vessel configuration (Tekchandaney 2012)

Impeller	**D/T**
Propeller	0.25 – 0.33
Pitched-blade turbine	0.5 – 0.7
Hydrofoil	0.4 – 0.5
Rushton / Bar turbine	0.66 – 0.75
Paddle	0.50 - 0.70
Anchor / Helical	0.90 – 0.95

With so many options available for equipment selection and the diverse nature of phases that can be mixed, various problems arise in evaluating mixing. Developing standards for mixer comparison, models describing changes during mixing, determining the degree of mixing, and, design/control methods of the equipment are highlighted by Lindley (1991).

3. Mixing Measures

Before deciding which measurement methods are going to be used for a mixing application, the concept of scale of scrutiny must be considered. (Danckwerts 1952) defined the scale of scrutiny as the minimum size of segregated regions causing the mixture to be perceived as unmixed. For any given mixture, the closer the mixture is viewed, the more unmixed it will seem to be. The end usage of the mixture should be kept in mind when the scale of scrutiny is determined and the choice of measurement equipment for mixing must be able to collect data based on this scale.

Danckwerts (1952) also defined the scale and intensity of segregation and gave detailed calculations for these two characteristic measures of mixing. Practically, droplet/bubble sizes or the areas uncovered by tracers can be used to determine the scale of segregation while coefficient of variation, which is the ratio of standard deviation to the mean value, can be used to determine the intensity of segregation. The size of unmixed regions and concentration variations are expressed using the scale and intensity of segregations, respectively (Rielly and others 1994). Both values must be considered at the same time in order to understand mixing better. In Figure 2, four different mixing scenarios

are given. Without the intensity of segregation values, the relatively same scale of segregation values are inadequate to represent the true nature of mixing. For three different scale of segregation values, same intensity of segregation value is incapable of capturing the state of mixing, either (Figure 3).

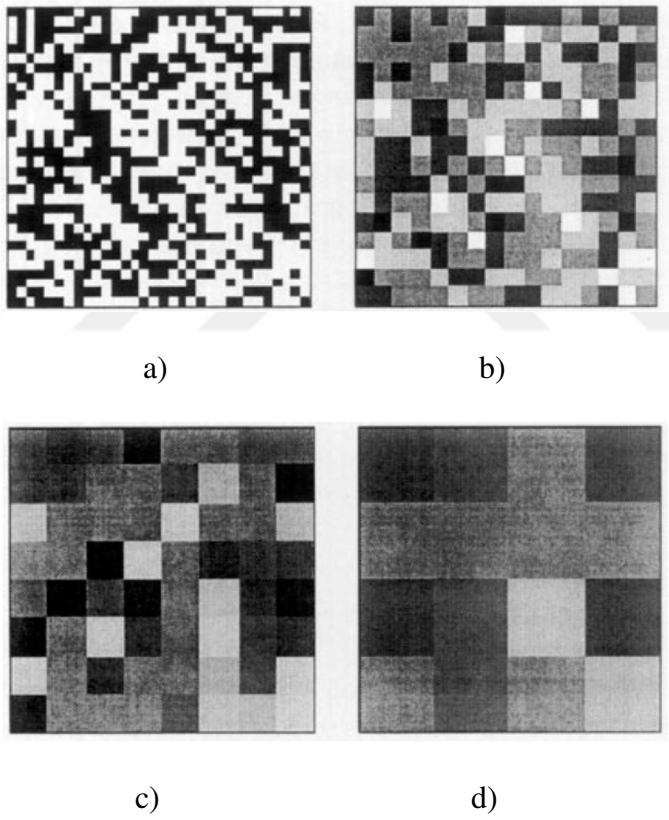

Figure 2. Change in the intensity of segregation (I) while the scale of segregation (S) is relatively constant a) S = 0.492 – I = 1.000, b) S = 0.572 – I = 0.239, c) S = 0.525 – I = 0.084, d) S = 0.457 – I = 0.028 (Rielly and others 1994)

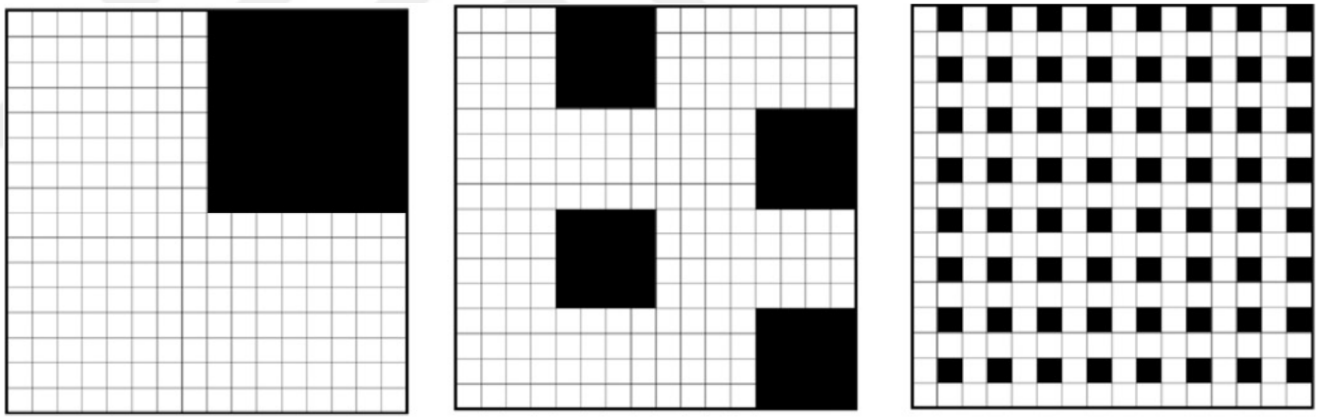

a) b) c)

Figure 3. Change in the scale of segregation (S) while the intensity of segregation (I) is constant at 1.7321

a) S = 8, b) S = 4, c) S = 1 (Kukukova and others 2009)

4. Measurement Methods

Experimental and computational methods are available to evaluate mixing in stirred vessels. The level of mixing and power consumption are key measurements for evaluation of mixing and common measurement methods are described in the following section.

4.1. Mixing Level Methods

Methods to determine the level of mixing can be classified in many ways. One of the ways to classify the methods is whether they are invasive or non-invasive. Invasive methods make use of probes for pH, temperature or conductivity measurements (Ascanio 2015). Since limited amount of data can be collected with probes, mixing can be analyzed with the evolution of an average concentration value over time (Figure 4.) When the concentration reaches a predetermined value with a ±5% interval, mixing is considered to be complete (Rielly and others 1994). However, the effect of the probe location on mixing time should be kept in mind if comparison between different equipment/studies is necessary (Szoplik and Karcz 2008).

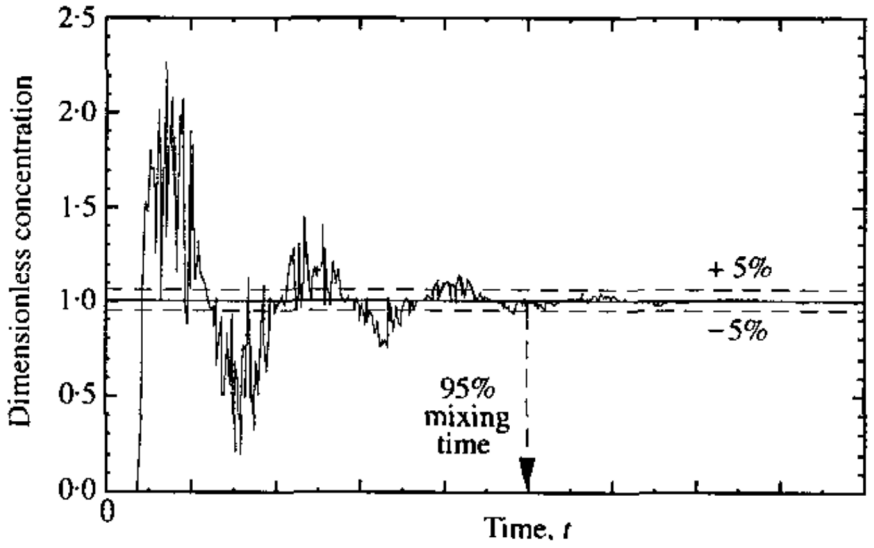

Figure 4. Evolution of a dimensionless concentration over time (Rielly and others 1994).

For multiphase mixing applications, invasive methods which use light sources such as strobe lights or capillary suction tubes for external analysis are available for droplet/bubble size measurements (Guevara-López and others 2008, Laakkonen and others 2005).

Color changes due to acid-base reactions or oxidation have been used to develop non-invasive methods for evaluation of mixing. The study of Cabaret and others (2007a) is an example of this method. Tracer dyes such as bromocresol purple, methyl red, or phenolphtalein are added to the fluid. The pH level is then adjusted by the injection of acidic or basic solutions in order to start the desired color changes. The change is recorded with a camera over time. From the recorded images, R, G, and, B values of individual pixels are

used for further calculations. The level of mixing is usually depicted using mixing curves. The pixels with color components or a brightness level above a threshold value are counted and the ratio of these pixels to the total number of pixels is plotted against time. Curve fitting methods are also used with the equation given below to identify dynamics of mixing:

$$A = A_{max}*(1 - e^{-mt})$$

where A is an area estimation based on the number of pixels, A_{max} is the maximum value that can be achieved, m is the rate of change for A and t is time, respectively. A discussion on the effects of acid to base ratio, selection of threshold value, and illumination around the vessel was also given by Cabaret and others (2007a). Flow patterns can also be visualized with colorimetric methods. Slow or completely unmixed locations within the vessels equipped with different impellers were studied and the effects of processing parameters were investigated (Norwood and Metzner 1960; Yao and others 1998; Alvarez and others 2002b; Alvarez and others 2005; Bonnot and others 2007; Cabaret and others 2007a). A major drawback of colorimetric methods is the requirement of transparent fluids and vessels. Reflections from the surroundings and capabilities of the camera may affect the quality of measurements. The fact that the fluid has uniform initial tracer distribution must also be verified for accuracy and objectivity of the experiments.

Planar laser induced fluorescence (PLIF) is another non-invasive method. The main difference of this method from the colorimetric method is that a laser source is required for

illumination of fluorescent dyes injected into the vessels. Upon interaction with the laser light, a fluorescent light at a different wavelength is emitted by the dye. The intensity of fluorescence is related to dye concentration, thus allowing mixing evaluation. A typical PLIF set-up is presented in Figure 5.

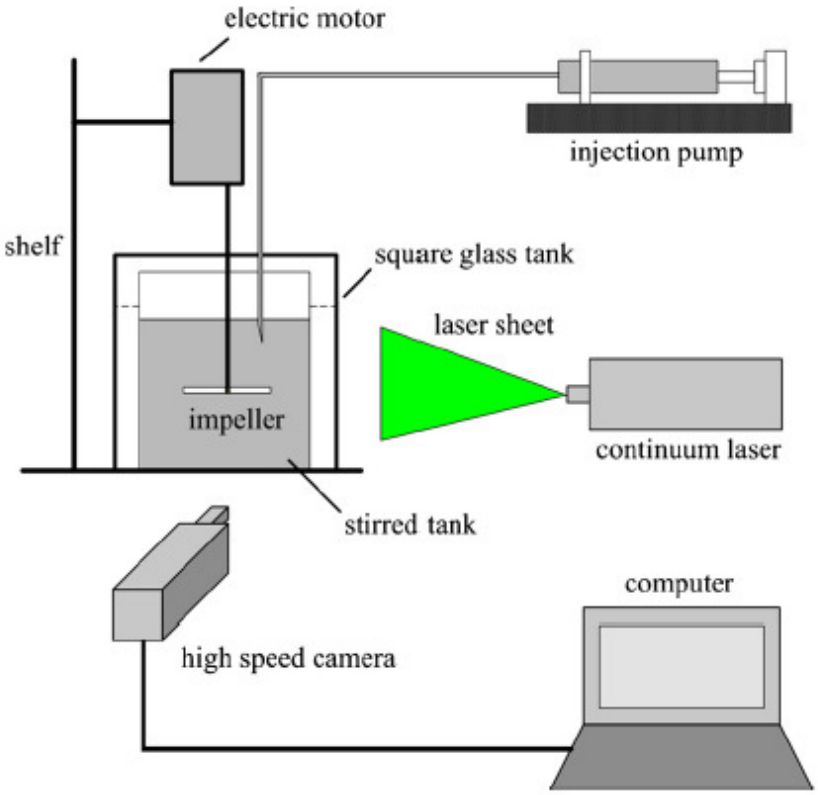

Figure 5. A generic set-up of PLIF method (Hu and others 2012)

Crimaldi (2008) reviewed the equipment and experimental configurations of the PLIF method thoroughly. Continuous or pulsed laser sources (argon-ion or Nd:YAG) operating at

488, 514.5, and 532 nm are commonly used. The laser beam is converted into a sheet using cylindrical lenses or scanning mirrors so that measurements from the entire vertical or horizontal cross section of the vessel can be taken at the same time. A variety of cameras have been used in the PLIF method. Camera resolution, bit depth, and frame rate can be considered as selection criteria for the cameras. A narrow-band filter must be used with the cameras to block the laser light and let only the fluorescent light to be recorded. Fluorescein, Rhodamine 6G, and Rhodamine B are the major fluorescent dyes used for PLIF. However, these dyes are toxic which requires extra time and care in preparation, handling, and waste disposal. Zähringer (2014) found that Vitamin B_2 and B_6 have similar fluorescence properties and can be used as alternative solutions. At increased power levels and longer exposure time to laser, the dyes may lose their fluorescence. This effect is called photobleaching and should be taken into account for the quality of measurements (Larsen and Crimaldi 2006). Fluid temperature, pH, and the lenses used for generating the laser sheet also affect the measurements. The concentration level of the dyes need to be adjusted based on a calibration procedure. The relationship between the fluorescence intensity and concentration is linear up to a certain maximum concentration value. However, the exact maximum value shows a great variation in literature. The most probable reason for it is the different laser power/energy levels used for different sizes of vessels. Examples of the aforementioned variation are given in Table 2. Even though the camera resolution is almost the same in these examples, additional attention may be required due to the effect of CCDs as highlighted by Crimaldi (2008).

Table 2. Various laser power/energy levels and camera resolutions used for different vessel diameters

Vessel Diameter (m)	Laser Source		Camera Resolution (Pixels)	Reference
	Power (W)	Energy (mJ)		
0.288	1.4	-	512 x 512	(Houcine and others 1996)
0.29	2	-	1280 x 1024	(Fall and others 2001)
0.24	-	30	1076 x 1024	(Arratia and Muzzio 2004)
0.035 - 0.060	-	50	1024 x 1024	(Hall and others 2005)
0.10	1.5	-	1280 x 1024	(Hu and others 2012)
0.19		50	1280 x 1024	(Busciglio and others 2014)

As in the case of colorimetric methods, PLIF has been used to study flow profiles, as well (Arratia and Muzzio 2004; Alvarez and others 2005; Hu and others 2012; Bulnes-Abundis and Alvarez 2013; Zhang and others 2013; Busciglio and others 2014). If concentration values at specific points and cross-sectional areas of complex flow profiles are needed for evaluating mixing, PLIF may be chosen over colorimetric methods.

Although it is not as common as colorimetric and PLIF methods, electrical resistance tomography is also available for characterization of mixing in stirred vessels. The electrical resistance distribution is calculated using a series of electrodes installed around the vessel measure voltage or currents. Mixing is evaluated with the addition of tracers that cause a significant change in the electrical resistance of the fluid. The images of flow profiles are constructed using the software designed for this purpose. When multiple measurements are taken at various heights of the vessel, individual images can be combined for three dimensional representation (Sharifi and Young 2011). The method has been used to study both single and multiple phase mixing applications (Pakzad and others 2008; Hosseini and others 2010; Patel and others 2013). A distinctive advantage of electrical resistance tomography is that it can be used with non-transparent fluids and vessels.

4.2. Power Measurement Methods

Electrical and calorimetric measurements, dynamometers, torquemeters, and strain gauges were reviewed by (Ascanio and others 2004) as the major power measurement methods for stirred vessels. Advantages and disadvantages of each method were given based on the ease of installation, cost, sensitivity, and accuracy. Overall, it was concluded that for inexpensive methods such as making electrical measurements with wattmeters have lower sensitivity than methods that use torquemeters and strain gauges. However, as the equipment gets more advanced, installation gets more complicated. Chapple and others (2002) discussed the application of a torque transducer for power measurement during mixing of Newtonian

solutions with a pitched blade impeller. The importance of alignment (between the shaft, torque transducer, and the motor), minimizing vibration (with bearings attached to the shaft), the time required to obtain a stable signal, and data acquisition have been shown as the critical factors for reliable measurements. Similar set ups can also be seen for close clearance impellers such as Maxblend® and helical ribbon (Fradette and others 2007; Maingonnat and others 2008). Experimental considerations for electrical measurements and dynamometers were given by Hjorth and others (2000) and Brucato and others (2010), respectively.

4.3. Computational Fluid Dynamics

Data necessary for mixing analysis can be obtained with computational methods, too. Computational fluid dynamics (CFD) provides numerical solutions of Navier-Stokes equations for conservation of mass, momentum, and energy. Finite element and finite volume techniques are widely used numerical techniques for the solution using appropriate boundary conditions (Norton and Sun 2006). For modelling of stirred vessels, the Navier-Stokes equations must be modified to describe the nature of flow due to the rotational movement of the shaft and impeller. Since this can be done in multiple ways, the details can be found in reference manuals of commercial software or the codes generated by individual users. Numerical analysis methods also return only approximate solutions rather than an exact solution and the accuracy is dependent on the assumptions made. These two factors require validation of the models with experimental data. Usually, velocity profiles and power consumption data have been used for validation purposes (Ein-Mozaffari and Upreti 2010).

The visual interpretation of results is one of the powerful feauture of CFD studies. In Figure 6, counter, vector, and isosurface of velocity plots are shown from different studies. In addition to flow profiles and power consumption measurements for different stirred vessel configurations (Li and others 2005; Buwa and others 2006; Anne-Archard and others 2006; Taghavi and others 2011), the locations of slow mixing, unmixed regions, and mixing times have also been studied numerically (Lamberto and others 1999; Harvey III and others 2000; Szalai and others 2004; Iranshahi and others 2006; Arratia and others 2006; Bulnes-Abundis). Multiple measurements can be taken at every point of the vessel geometry with one CFD model. Thus, the number of experiments required for mixing analysis can be greatly reduced when CFD is used as a prediction tool beforehand.

4.4. Dimensional Analysis

Several process parameters affect mixing in stirred vessels. Fluid viscosity, density, rotational speed of the impeller, and the geometrical ratios between the impeller and vessel are major factors which have been studied extensively (Knoch 1999; Houcine and others 2000; Ochieng and Onyango 2008; Youcefi and Youcefi 2015). When the effects of these major factors on mixing need to be determined, an experimental procedure can be designed by using different values for one factor while keeping all the others constant. However, this will result in a huge number of experiments when it is repeated for all factors.

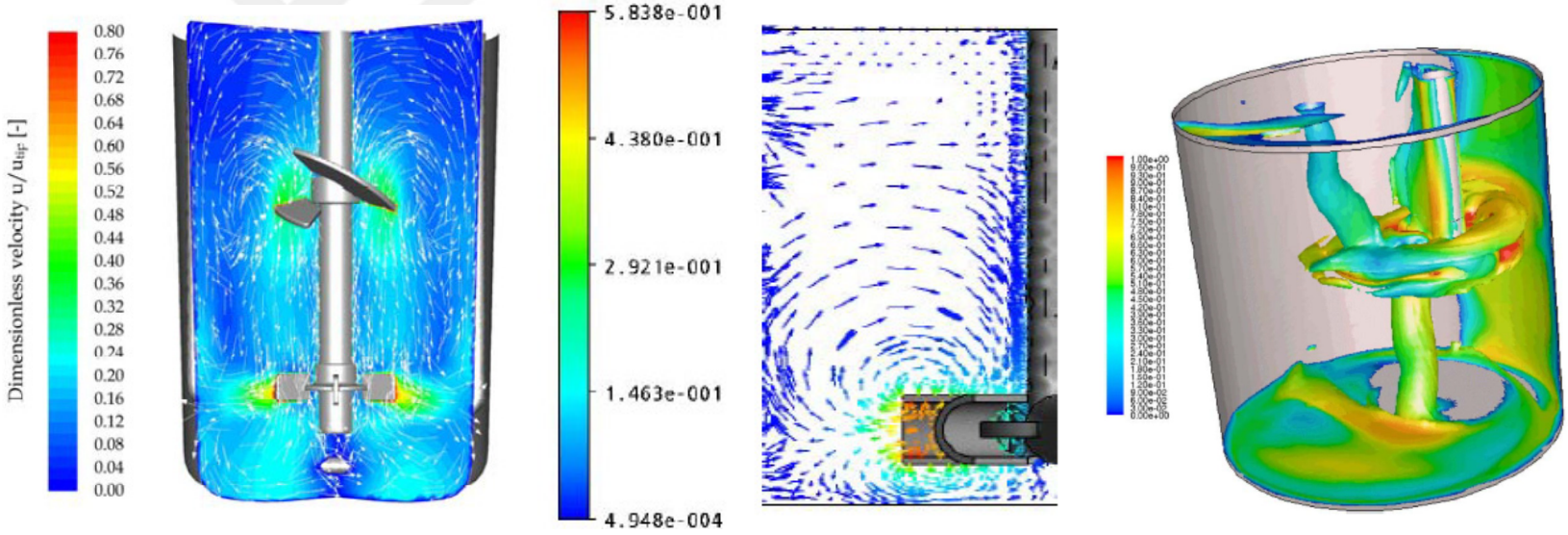

a) b) c)

Figure 6. Visual interpretations of CFD results a) Velocity counter (Kaiser and others 2011), b) velocity vectors (Ameur and others 2012), and c) isosurface of velocity magnitudes (Montante and others 2006). The change in color bars from blue to red indicates increased values of velocity.

The concept of dimensional analysis based on the Buckingham pi theorem may then be used to describe mixing in stirred vessels with fewer number of dimensionless factors which will minimize experimental efforts. The details of the method can be found in the literature (Zlokarnik 1998; Geankoplis 2003; Singh and Heldman 2009). Reynolds, Power, Froude, Weber, Prandtl, and pumping numbers are few examples of such dimensionless numbers. Modifications of these numbers may be needed for planetary and rotor-stator mixers since characteristic dimension and velocity of these impellers require new definitions as opposed to the traditional impeller diameter and rotational speed (Delaplace and others 2005; Doucet and others 2005; Delaplace and others 2007; Delaplace and others 2012). Descriptive curves for power consumption, mixing time or other mixing measures are usually obtained by plotting the representative dimensionless number on the y axis and plotting Reynolds number (Re) on the x axis. Power curves for anchor and Rushton impellers are given in Figure 7.

A linear decrease in Power numbers is seen at low Reynolds numbers (Re) and relatively constant values are seen at higher Re. Re values up to 10 indicate laminar flow in stirred vessels while turbulent flow occurs for Re greater than 10^4. In between these values, transitional flow is observed (Smith 2003). However, the limits for each flow type is not strict and different values such as 100 for the end of laminar region was proposed by Lamberto and others (1999). Re is calculated using the following equation:

$$Re = (\rho * N * D)/\mu$$

where ρ is the density (kg/m^3), N is the rotational speed of the impeller (1/s), D is the impeller diameter (m), and μ is the fluid viscosity (Pa.s).

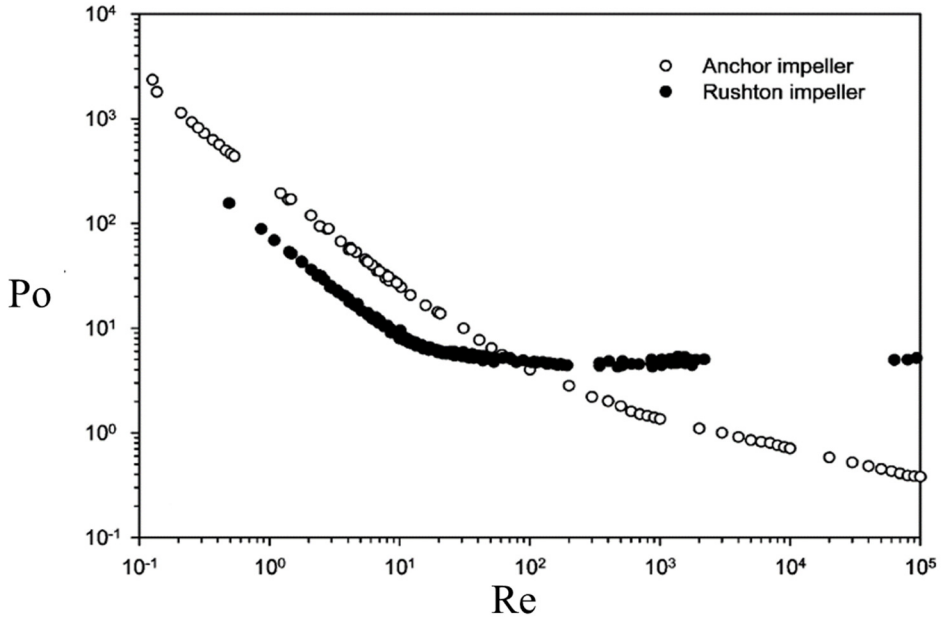

Figure 7. Power curve of a Newtonian fluid for Anchor and Rushton impellers (Foucault and others 2005)

This calculation for Newtonian is straightforward. Due to the shear rate dependent viscosity values of non-Newtonian fluids, alternative solutions are needed. An average shear rate approximation has been proposed by Metzner and Otto (1957). The average shear rate is assumed to be proportional to the rotational speed of the impeller and is given by:

$$\dot{\gamma} = K_s * N$$

where $\dot{\gamma}$ is the average shear rate (1/s) and K_s is the Metzner-Otto constant. For most impellers, the value of K_s is between 10 and 13 except for close clearance impellers wherein it is between 25 and 30 (Chhabra 2003). Castell-Perez and Steffe (1990) explained three methods, namely Power Curve, Torque Curve, and Slope Method to determine K_s and discussed the advantages and disadvantages of each method. While the Power Curve method requires more effort, the Slope method is more susceptible to experimental errors than the other two methods. Glenn and Daubert (2003) proposed the Matching Stress Method to estimate K_s. Rieger and Novak (1973) and Sánchez Pérez and others (2006) developed similar concepts for average shear rate estimation. The common point of these estimations is that they are valid only for laminar flow in stirred vessels. The error induced by these assumptions for transitional and turbulent flows must be assessed carefully. Wassmer and Hungenberg (2005) introduced a model that could be used for all flow types during mixing of non-Newtonian fluids.

5. Laminar Flow in Stirred Vessels

Laminar flow in stirred vessels is encountered commonly since several fluids used in process industries have high viscosity values. Mixing of highly viscous fluids is challenging due to the characteristic features of laminar flow. Isolated mixing regions (IMR), separation of the vessel at the impeller height, and slow mixing at the fluid surface have been observed by Alvarez and others (2002a) and visualization with a colorimetric method is shown in

Figure 8. Mixing will be completed only after impractically long times due the presence of these features.

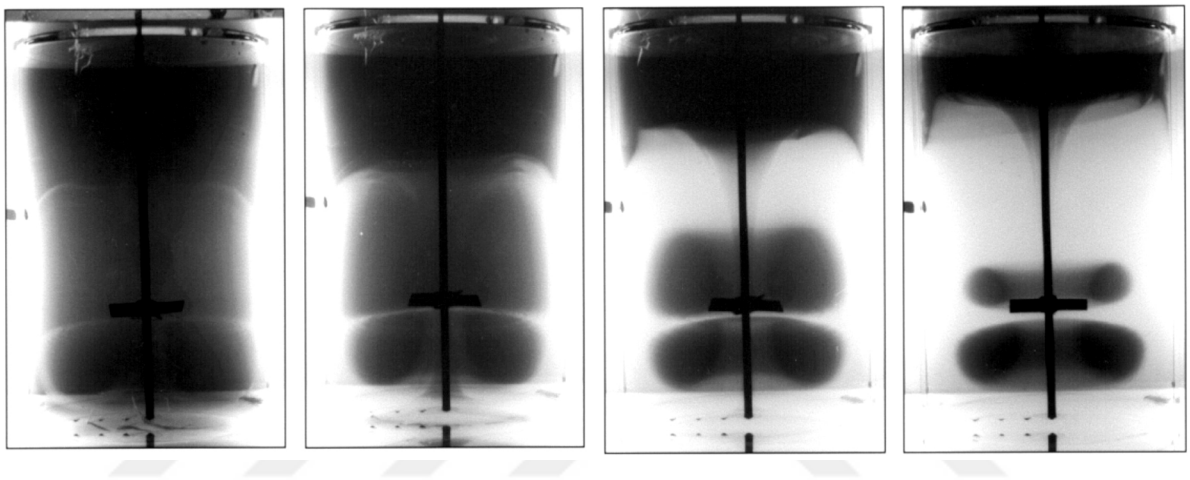

Figure 8. Mixing at Re = 25 with an axial impeller (Alvarez and others 2002b)

Increased rotational speed and impeller diameter may not be an option because of the high power consumption and limitations on the hardware capabilities. Installation of baffles to promote axial flow for improved mixing has been shown as an effective way for laminar and turbulent flow (Hashimoto and others 2011; Wang and others 2013). The size of IMRs and total mixing time can be reduced significantly during mixing by using multiple impellers on the same shaft or using a dual shaft configuration (Alvarez-Hernández and others 2002; Bonnot and others 2007; Cabaret and others 2007b). The relative position of the impellers to one other is the key parameter for successful mixing using these methods. Both baffles and

multiple impellers introduce additional elements into the vessel. Increased efforts may be required during installation and cleaning of the vessels. Instead of operating at a constant rotational speed and direction, mixing can be completed in very short times (in the order of few minutes) by applying variable speed and direction protocols (Lamberto and others 1996; Yao and others 1998; Lamberto and others 1999; Ascanio and others 2002). However, motors capable of running in both directions and advanced speed control equipment are necessary in these methods. Modifications of the standard impellers have been investigated under laminar flow conditions, as well. Wang and others (2013) and Kato and others (2007) changed the design of pitched blade impellers to generate simultaneous upward and downward flow. At similar power consumption levels, smaller IMRs were created with the modified impellers as opposed to the standard ones. Locating impellers away from the center of the vessel has been shown as the most practical solution since no changes in manufacturing and equipment is needed in addition to the already existing ones. No significant increase in power consumption also adds value to this approach. The increase in the chaotic flow with reduced symmetry in the geometry is the main reason behind the success of eccentrically located impellers. The performance of both axial and radial impellers have been tested in the literature (Alvarez and others 2002b; Cabaret and others 2008; Ng and Ng 2013; Bulnes-Abundis and Alvarez 2013; Zhang and others 2013).

6. Scale-up of Stirred Vessels

Stirred vessel design and optimization is completed at laboratory scales (1-20 L) first to keep the cost and time requirements at minimum. The results obtained at the laboratory scale must be replicated for the pilot-plant and actual production with a scale-up protocol. The exact similarity between two scales is achieved if there is geometric, kinematic, and dynamic similarities. Geometrical similarity is maintained by designing stirred vessels having the same ratios between important parameters such as impeller and vessel diameters, fluid height, impeller clearance etc. Kinematic similarity is observed if the same velocity ratios exist at corresponding points in the vessel. Dynamic similarity ensures that gravitational, inertial, and surface tension forces acting on the vessel have the same ratios (Tekchandaney 2012). In practice, all three similarities cannot be maintained at the same time due to manufacturing limitations and the complex nature of fluid flow. Therefore, the parameter with the most significant effect on mixing is kept constant between different scales. Wilkens and others (2003) listed a number of scale-up rules including equal values of power per volume, Reynolds number, Froude number, tip speed, torque per volume, blend time, and bulk fluid velocity. The change in flow profiles, power consumption, and mixing time have been used to compare different scale-up rules (Rieger and Novák 1972; Rieger and Novák 1974; Böhme and Stenger 1988; Ståhl Wernersson and Trägårdh 1999; Vrábel and others 2000; Li and others 2005b).

References

Alvarez MM, Guzmán A, Elías M. 2005. Experimental visualization of mixing pathologies in laminar stirred tank bioreactors. Chemical Engineering Science 60:2449-2457.

Alvarez MM, Zalc JM, Shinbrot T, Arratia PE, Muzzio FJ. 2002a. Mechanisms of mixing and creation of structure in laminar stirred tanks. AIChE Journal 48(10):2135-2148.

Alvarez MM, Arratia PE, Muzzio FJ. 2002b. Laminar Mixing in Eccentric stirred tank systems. The Canadian Journal of Chemical Engineering 80(4):546-557.

Alvarez-Hernández MM, Shinbrot T, Zalc J, Muzzio FJ. 2002. Practical chaotic mixing. Chemical Engineering Science 57(17):3749-3753.

Ameur H, Bouzit M, Helmaoui M. 2012. Numerical study of fluid flow and power consumption in a stirred vessel with a Scaba 6SRGT impeller. Chemical and Process Engineering 32(4):351-366.

Anne-Archard D, Marouche M, Boisson HC. 2006. Hydrodynamics and Metzner–Otto correlation in stirred vessels for yield stress fluids. Chemical Engineering Journal 125(1):15-24.

Arratia PE, Kukura J, Lacombe J, Muzzio FJ. 2006. Mixing of shear-thinning fluids with yield stress in stirred tanks. AIChE Journal 52(7):2310-2322.

Arratia PE, Muzzio FJ. 2004. Planar laser-induced fluorescence Method for analysis of mixing in laminar flows. Industrial Engineering Chemistry & Research 43(20):6557-6568.

Ascanio G, Castro B, Galindo E. 2004. Measurement of power consumption in stirred vessels-A Review. Chemical Engineering Research & Design 82(9):1282-1290.

Ascanio G. 2015. Mixing time in stirred vessels: A review of experimental techniques. Chinese Journal of Chemical Engineering 23(7):1065-1076.

Ascanio G, Brito-Bazán M, Brito-De La Fuente E, Carreau PJ, Tanguy PA. 2002. Unconventional configuration studies to improve mixing times in stirred tanks. The Canadian Journal of Chemical Engineering 80(4):558-565.

Böhme G, Stenger M. 1988. Consistent scale-up procedure for the power consumption in agitated non-newtonian fluids. Chemical Engineering Technology 11(1):199-205.

Bonnot S, Cabaret F, Fradette L, Tanguy PA. 2007. Characterization of mixing patterns in a coaxial mixer. Chemical Engineering Research & Design 85(8):1129-1135.

Brucato A, Cipollina A, Micale G, Scargiali F, Tamburini A. 2010. Particle suspension in top-covered unbaffled tanks. Chemical Engineering Science 65(10):3001-3008.

Bulnes-Abundis D, Alvarez MM. 2013. The simplest stirred tank for laminar mixing: Mixing in a vessel agitated by an off-centered angled disc. AIChE Journal 59(8):3092-3108.

Busciglio A, Grisafi F, Scargiali F, Brucato A. 2014. Mixing dynamics in uncovered unbaffled stirred tanks. Chemical Engineering Journal 254:210-229.

Buwa V, Dewan A, Nassar AF, Durst F. 2006. Fluid dynamics and mixing of single-phase flow in a stirred vessel with a grid disc impeller: Experimental and numerical investigations. Chemical Engineering Science 61(9):2815-2822.

Cabaret F, Fradette L, Tanguy PA. 2008. Effect of shaft eccentricity on the laminar mixing performance of a radial impeller. The Canadian Journal of Chemical Engineering 86(6):971-977.

Cabaret F, Bonnot S, Fradette L, Tanguy PA. 2007a. Mixing time analysis using colorimetric methods and image processing. Industrial & Engineering Chemistry Research 46(14):5032-5042.

Cabaret F, Rivera C, Fradette L, Heniche M, Tanguy PA. 2007b. Hydrodynamics Performance of a Dual Shaft Mixer with Viscous Newtonian Liquids. Chemical Engineering Research & Design 85(5):583-590.

Castell-Perez ME, Steffe JF. 1990. Evaluating shear rates for power law fluids in mixer viscometry. Journal of Texture Study 21(4):439-452.

Chapple D, Kresta SM, Wall A, Afacan A. 2002. The Effect of impeller and tank geometry on power number for a pitched blade turbine. Chemical Engineering Research & Design 80(4):364-372.

Chavan VV, Mashelkar RA. 1980. Mixing of viscous Newtonian and Non-Newtonian fluids. In: A. S. Mujumdar, editor. Advances in transport processes. Wiley Eastern/Wiley Halsted. p 210-252.

Chhabra RP. 2003. Fluid mechanics and heat transfer with non-Newtonian liquids in mechanically agitated vessels. In: J. P. Hartnett, editor. Advances in heat transfer. San Diego: Academic Press. p 77-178.

Crimaldi JP. 2008. Planar laser induced fluorescence in aqueous flows. Experiments in Fluids 44(6):851-863.

Cullen PJ, O'Donnell CP. 2009. Mixing in the food industry: Trends and Challenges. In: P. J. Cullen, editor. Food mixing. Blackwell Publishing Ltd. p 1-5.

Danckwerts PV. 1952. The definition and measurement of some characteristics of mixtures. Applied Scientific Research, Section A 3(4):279-296.

Delaplace G, Guérin R, Leuliet JC. 2005. Dimensional analysis for planetary mixer: Modified power and Reynolds numbers. AIChE Journal 51(12):3094-3100.

Delaplace G, Thakur RK, Bouvier L, André C, Torrez C. 2007. Dimensional analysis for planetary mixer: Mixing time and Reynolds numbers. Chemical Engineering Science 62(5):1442-1447.

Delaplace G, Coppenolle P, Cheio J, Ducept F. 2012. Influence of whip speed ratios on the inclusion of air into a bakery foam produced with a planetary mixer device. Journal of Food Engineering 108(4):532-540.

Doraiswamy D, Grenville RK, Etchells AW. 1994. Two-Score years of the Metzner-Otto correlation. Industrial & Engineering Chemistry Research 33(10):2253-2258.

Doucet L, Ascanio G, Tanguy PA. 2005. Hydrodynamics characterization of rotor-stator mixer with viscous fluids. Chemical Engineering Research & Design 83(10):1186-1195.

Ein-Mozaffari F, Upreti SR. 2010. Investigation of mixing in shear thinning fluids using computational fluid dynamics. In: H. Woo, editor. Computational fluid dynamics. InTech. p 77-102.

Elson TP. 1990. X-Ray flow visualization of flow patterns during the mixing of yield stress, Newtonian and dilatant fluids. Chemical Engineering Communications 94(1):143-158.

Fall A, Lecoq O, David R. 2001. Characterization of mixing in a stirred tank by planar laser induced fluorescence (P.L.I.F.). Chemical Engineering Research & Design 79(8):876-882.

Fellows PJ. 2009. 4 - Mixing and forming. In: P. J. Fellows, editor. Food processing technology (Third edition). Woodhead Publishing. p 157-187.

Foucault S, Ascanio G, Tanguy PA. 2005. Power characteristics in coaxial mixing: Newtonian and non-Newtonian fluids. Industrial & Engineering Chemistry Research 44(14):5036-5043.

Fradette L, Thomé G, Tanguy PA, Takenaka K. 2007. Power and mixing time study involving a Maxblend® impeller with viscous Newtonian and Non-Newtonian fluids. Chemical Engineering Research & Design 85(11):1514-1523.

Geankoplis CJ. 2003. Transport processes and separation process principles (Includes Unit Operations). 4th ed. New Jersey: Prentice Hall. 1026 p.

Glenn TA, Daubert CR. 2003. A mixer viscometry approach for blending devices. Journal of Food Process Engineering 26(1):1-16.

Guevara-López E, Sanjuan-Galindo R, Córdova-Aguilar MS, Corkidi G, Ascanio G, Galindo E. 2008. High-speed visualization of multiphase dispersions in a mixing tank. Chemical Engineering Research & Design 86(12):1382-1387.

Hall JF, Barigou M, Simmons MJH, Stitt EH. 2005. Comparative study of different mixing strategies in small high throughput experimentation reactors. Chemical Engineering Science 60(8–9):2355-2368.

Harvey III AD, West DH, Tufillaro NB. 2000. Evaluation of laminar mixing in stirred tanks using a discrete-time particle-mapping procedure. Chemical Engineering Science 55(3):667-684.

Hashimoto S, Natami K, Inoue Y. 2011. Mechanism of mixing enhancement with baffles in impeller-agitated vessel, part I: A case study based on cross-sections of streak sheet. Chemical Engineering Science 66(20):4690-4701.

Hashimoto S, Ito H, Inoue Y. 2009. Experimental study on geometric structure of isolated mixing region in impeller agitated vessel. Chemical Engineering Science 64(24):5173-5181.

Hjorth S, Karlsson L, Friberg P, Boon L. 2000. An analysis of the use of electrical power measurements for process control in large-scale stirred vessels. The Canadian Journal of Chemical Engineering 78(6):1127-1132.

Hosseini S, Patel D, Ein-Mozaffari F, Mehrvar M. 2010. Study of solid–liquid mixing in agitated tanks through electrical resistance tomography. Chemical Engineering Science 65(4):1374-1384.

Houcine I, Plasari E, David R. 2000. Effects of the stirred tank's design on power consumption and mixing time in liquid phase. Chemical Engineering Technology 23(7):605-613.

Houcine I, Vivier H, Plasari E, David R, Villermaux J. 1996. Planar laser induced fluorescence technique for measurements of concentration fields in continuous stirred tank reactors. Experiments in Fluids 22(2):95-102.

Hu Y, Wang W, Shao T, Yang J, Cheng Y. 2012. Visualization of reactive and non-reactive mixing processes in a stirred tank using planar laser induced fluorescence (PLIF) technique. Chemical Engineering Research & Design 90(4):524-533.

Iranshahi A, Heniche M, Bertrand F, Tanguy PA. 2006. Numerical investigation of the mixing efficiency of the Ekato Paravisc impeller. Chemical Engineering Science 61(8):2609-2617.

Kaiser SC, Löffelholz C, Werner S, Eibl D. 2011. CFD for characterizing standard and single-use stirred cell culture bioreactors. In: I. Minin, editor. Computational fluid dynamics technologies and applications. InTech. p 97-122.

Kato Y, Tada Y, Ban M, Nagatsu Y, Yanagimoto K. 2007. Application of asymmetric impellers to mixing at unsteady speed within a single revolution. Kagaku Kogaku Ronbunshu 33(1):16-19.

Knoch A. 1999. Influence of non-Newtonian flow behavior on mixing process characteristics. Chemical Engineering Technology 22(2):112-118.

Kukukova A, Aubin J, Kresta SM. 2009. A new definition of mixing and segregation: Three dimensions of a key process variable. Chemical Engineering Research & Design 87(4):633-647.

Kumaresan T, Joshi JB. 2006. Effect of impeller design on the flow pattern and mixing in stirred tanks. Chemical Engineering Journal 115(3):173-193.

Laakkonen M, Moilanen P, Aittamaa J. 2005. Local bubble size distributions in agitated vessels. Chemical Engineering Journal 106(2):133-143.

Lamberto DJ, Alvarez MM, Muzzio FJ. 1999. Experimental and computational investigation of the laminar flow structure in a stirred tank. Chemical Engineering Science 54(7):919-942.

Lamberto DJ, Muzzio FJ, Swanson PD, Tonkovich AL. 1996. Using time-dependent RPM to enhance mixing in stirred vessels. Chemical Engineering Science 51(5):733-741.

Larsen LG, Crimaldi JP. 2006. The effect of photobleaching on PLIF. Experiments in Fluids 41(5):803-812.

Li M, White G, Wilkinson D, Roberts KJ. 2005. Scale up study of retreat curve impeller stirred tanks using LDA measurements and CFD simulation. Chemical Engineering Journal 108:81-90.

Lindley JA. 1991. Mixing processes for agricultural and food materials: 1. Fundamentals of mixing. Journal of Agricultural Engineering Research 48:153-170.

Machado MB, Nunhez JR, Nobes D, Kresta SM. 2012. Impeller characterization and selection: Balancing efficient hydrodynamics with process mixing requirements. AIChE Journal 58(8):2573-2588.

Maingonnat JF, Doublier JL, Lefebvre J, Delaplace G. 2008. Power consumption of a double ribbon impeller with newtonian and shear thinning fluids and during the gelation of a iota-carrageenan solution. Journal of Food Engineering 87(1):82-90.

Metzner AB, Taylor JS. 1960. Flow patterns in agitated vessels. AIChE Journal 6(1):109-114.

Metzner AB, Otto RE. 1957. Agitation of non-Newtonian fluids. AIChE Journal 3(1):3-10.

Montante G, Bakker A, Paglianti A, Magelli F. 2006. Effect of the shaft eccentricity on the hydrodynamics of unbaffled stirred tanks. Chemical Engineering Science 61(9):2807-2814.

Ng KC, Ng EYK. 2013. Laminar mixing performances of baffling, shaft eccentricity and unsteady mixing in a cylindrical vessel. Chemical Engineering Science 104:960-974.

Niranjan K, Smith DLO, Rielly CD, Lindley JA, Phillips VR. 1994. Mixing processes for agricultural and food materials: Part 5, Review of mixer types. Journal of Agricultural Engineering Research 59(3):145-161.

Norton T, Sun D. 2006. Computational fluid dynamics (CFD) – an effective and efficient design and analysis tool for the food industry: A review. Trends in Food Science & Technology 17(11):600-620.

Norwood KW, Metzner AB. 1960. Flow patterns and mixing rates in agitated vessels. AIChE Journal 6(3):432-437.

Ochieng A, Onyango MS. 2008. Homogenization energy in a stirred tank. Chemical Engineering and Processing: Process Intensification 47:1853-1860.

Pakzad L, Ein-Mozaffari F, Chan P. 2008. Measuring mixing time in the agitation of non-Newtonian fluids through electrical resistance tomography. Chemical Engineering Technology 31(12):1838-1845.

Patel D, Ein-Mozaffari F, Mehrvar M. 2013. Using tomography to characterize the mixing of non-Newtonian fluids with a Maxblend impeller. Chemical Engineering Technology 36(4):687-695.

Rieger F, Novak V. 1973. Power consumption of agitators in highly viscous non-Newtonian liquids. Transactions of the Institution of Chemical Engineers 51:105-111.

Rieger F, Novák V. 1974. Power consumption scale-up in agitating non-newtonian fluids. Chemical Engineering Science 29(11):2229-2234.

Rieger F, Novák V. 1972. Scale-up method for power consumption of agitators in the creeping flow regime. Chemical Engineering Science 27(1):39-44.

Rielly CD, Smith DLO, Lindley JA, Niranjan K, Phillips VR. 1994. Mixing processes for agricultural and food materials: Part 4, Assessment and monitoring of mixing systems. Journal of Agricultural Engineering Research 59(1):1-18.

Sánchez Pérez JA, Rodríguez Porcel EM, Casas López JL, Fernández Sevilla JM, Chisti Y. 2006. Shear rate in stirred tank and bubble column bioreactors. Chemical Engineering Journal 124:1-5.

Sharifi M, Young B. 2011. 3-Dimensional spatial monitoring of tanks for the milk processing industry using electrical resistance tomography. Journal of Food Engineering 105(2):312-319.

Singh RP, Heldman DR. 2009. Introduction to food engineering. 4th ed. San Diego, CA: Academic Press. 864 p.

Smith PG. 2003. Mixing and seperation. In: P. G. Smith, editor. Introduction to food process engineering. Springer Science & Business Media. p 397-436.

Solomon J, Elson TP, Nienow AW, Pace GW. 1981. Cavern sizes in agitated fluids with a yield stress. Chemical Engineering Communications 11:143-64.

Ståhl Wernersson E, Trägårdh C. 1999. Scale-up of Rushton turbine-agitated tanks. Chemical Engineering Science 54(19):4245-4256.

Szalai ES, Arratia P, Johnson K, Muzzio FJ. 2004. Mixing analysis in a tank stirred with Ekato Intermig® impellers. Chemical Engineering Science 59(18):3793-3805.

Szoplik J, Karcz J. 2008. Mixing time of a non-Newtonian liquid in an unbaffled agitated vessel with an eccentric propeller. Chemical Papers 62(1):70-77.

Taghavi M, Zadghaffari R, Moghaddas J, Moghaddas Y. 2011. Experimental and CFD investigation of power consumption in a dual Rushton turbine stirred tank. Chemical Engineering Research & Design 89(3):280-290.

Takahashi K, Takeno Y, Takahata Y. 2015. Comparison of mixing performances among several spatial chaotic mixing methods. Journal of Chemical Engineering Japan 48(7):518-522.

Tekchandaney JR. 2012. Mixers. In: Process plant equipment: Operation, control, and reliability. M.D. Holloway, C. Nwaoha, O.O. Onyewuenyi, editors. John Wiley & Sons, Inc. p 245-296.

Thakur RK, Vial C, Djelveh G, Labbafi M. 2004. Mixing of complex fluids with flat-bladed impellers: effect of impeller geometry and highly shear-thinning behavior. Chemical Engineering and Processing: Process Intensification 43(10):1211-1222.

Triveni B, Vishwanadham B, Madhavi T, Venkateshwar S. 2010. Mixing studies of non-Newtonian fluids in an anchor agitated vessel. Chemical Engineering Research & Design 88(7):809-818.

Vrábel P, van der Lans RGJM, Luyben KCAM, Boon L, Nienow AW. 2000. Mixing in large-scale vessels stirred with multiple radial or radial and axial up-pumping impellers: modelling and measurements. Chemical Engineering Science 55(23):5881-5896.

Wang S, Wu J, Bong E. 2013. Reduced IMRs in a mixing tank via agitation improvement. Chemical Engineering Research & Design 91(6):1009-1017.

Wassmer K, Hungenberg K. 2005. A Unified model for the mixing of non-Newtonian fluids in the laminar, transition, and turbulent region. Macromolecular Materials and Engineering 290(4):294-301.

Wilkens RJ, Henry C, Gates LE. 2003. How to scale-up mixing processes in non-Newtonian fluids. Chemical Engineering Progress 9944-9952.

Wilkens RJ, Miller JD, Plummer JR, Dietz DC, Myers KJ. 2005. New techniques for measuring and modeling cavern dimensions in a Bingham plastic fluid. Chemical Engineering Science 60(19):5269-5275.

Woziwodzki S. 2014. Mixing of viscous Newtonian fluids in a vessel equipped with steady and unsteady rotating dual-turbine impellers. Chemical Engineering Research & Design 92(3):435-446.

Wu J, Zhu Y, Pullum L. 2001.Impeller Geometry Effect on Velocity and Solids Suspension. Chemical Engineering Research & Design 79(8):989-997.

Yao WG, Sato H, Takahashi K, Koyama K. 1998. Mixing performance experiments in impeller stirred tanks subjected to unsteady rotational speeds. Chemical Engineering Science 53(17):3031-3040.

Youcefi S, Youcefi A. 2015. Power consumption and mixing time in rheologically complex fluids by a two-bladed impeller. Journal of Mechanical Science and Technology 29(2):543-548.

Zähringer K. 2014. The use of vitamins as tracer dyes for laser-induced fluorescence in liquid flow applications. Experiments in Fluids 55(4):1-11.

Zhang M, Hu Y, Wang W, Shao T, Cheng Y. 2013. Intensification of viscous fluid mixing in eccentric stirred tank systems. Chemical Engineering and Processing: Process Intensification 6636-6643.

Zlokarnik M. 1991. Dimensional analysis and scale-up in chemical engineering. Berlin: Springer-Verlag. 176 p.

Zlokarnik M. 1998. Problems in the application of dimensional analysis and scale-up of mixing operations. Chemical Engineering Science 53(17):3023-3030.

CHAPTER 2

Shear thinning fluid mixing in unbaffled stirred vessels. Part 1: Hydrodynamic characterization

Nihat Yavuz, K.P. Sandeep

Department of Food, Bioprocessing, and Nutrition Sciences, North Carolina State University, Box 7624, Raleigh, NC 27695-7624

Abstract

A shear thinning fluid (1% CMC) was used to study mixing under laminar flow conditions in an unbaffled vessel. The effects of eccentricity (E = 0, 0.25, and, 0.50) and impeller type (Pitched blade turbine and Dual-Flow Pitched blade turbine) were studied in terms of distribution of a tracer solution, power consumption, and velocity profiles (obtained from numerical analysis). While Isolated mixing regions (IMR) existed for E = 0, increased eccentricity was found to be effective in removing IMRs and resulted in better area coverage of the tracer solution. The Dual-Flow Pitched blade turbine (DF-PBT) was designed to provide both upward and downward flow at the same time to induce more chaotic flow. Though numerical analysis showed this type of flow generated, its performance based on area coverage and power consumption was not better than the standard Pitched blade turbine (PBT). Power consumption was not affected by increased eccentricity. Thus, an eccentric location of an impeller is best for improved laminar mixing in stirred vessels.

1. Introduction

Stirred vessels are widely used in many process industries for various mixing applications. The main function of mixing in these applications is to reduce concentration, droplet/bubble size or temperature differences so that the desirable reactions or structure development takes place. Achieving a certain level of mixing is crucial to meeting the predetermined product quality (Cullen and O'Donnell 2009). Several factors including impeller type, fluid properties, and geometric ratios between the impeller and the vessel affect mixing performance. Mixing time, power consumption, and flow patterns have been used as performance criteria along with many others (Metzner and Taylor 1960; Cabaret and others 2007a; Machado and others 2012). Highly viscous fluids (corn syrup, fruit/vegetable puree, ketchup, etc.) and non-Newtonian flow behavior pose extra challenges in stirred vessel design and evaluation of mixing.

During mixing of high viscosity fluids, the flow type is considered to be laminar. While the flow velocity is high mostly in the impeller region, the velocity of the fluid near the surface and walls are very low. The axial flow is limited and tangential flow is more dominant (Metzner and Taylor 1960). For the symmetric vessel configurations in which the impeller is located at the center, isolated mixing regions (IMR) are formed under laminar flow conditions and it is usually divided into two parts at the impeller mid-plane. Acid-base reactions, fluorescent dyes, X-ray methods, and computational fluid dynamics (CFD) have been used to study the relationship between the process parameters and formation of IMRs (Norwood and Metzner 1960; Elson 1990; Alvarez and others 2005; Cabaret and others

2007a; Hashimoto and others 2009). These torus shaped regions are usually formed right above and below impellers such as the Ruston turbines and pitched blade impellers. Unless the impeller speed and location are manually changed, diffusion is the only mechanism that can eliminate IMRs. Since this will take an impractically long time, alternative methods have been developed. Installation of baffles (Hashimoto and others 2011; Wang and others 2013) mixing with multiple impellers (Bonnot and others 2007; Cabaret and others 2007a; Woziwodzki 2014) have been shown to completely eliminate or reduce the size of IMRs. When relatively easy and fast cleaning is also an important design factor, impeller location, speed, and design can be manipulated without usage of any extra equipment inside the vessel. Both Lamberto and others (1996) and Yao and others (1998) showed that IMRs could be removed with time-periodic rpm protocols. A typical time-periodic rpm protocol was applied by operating at one fixed rpm value (50, 100, 150, 200, and, 250 rpm) for a certain amount of time (20 s) followed by operating at increased rpm values by 50, 100, and 150 rpm for the same amount of time. While complete mixing was achieved in 2 min. with a time-periodic protocol, IMRs were still visible after 40 min. for the steady rpm protocol. Significant improvements were also possible by changing the direction of rotation periodically (Yao and others 1998). Modifications to existing impellers have also been proven to be effective. Alvarez-Hernández and others (2002) redesigned a 6-bladed Rushton turbine by moving a blade upwards and an adjacent one downward by half the blade height. The new turbine reduced mixing time and isolated regions in comparison to the regular Rushton turbine and a disk impeller. Modified pitched blade impellers which provide upward and downward flow

at the same time was used by both Kato and others (2007) and Wang and others (2013). The smallest IMRs were observed for a six-bladed 45 degree alternating pitch blade impeller and a 45 degree up and down two bladed impeller. Commercially available impellers such as Ekato MIG, INTERMIG (Schopfheim, Germany), and, the CounterFlow from Philadelphia Mixing Solutions (Palmyra, Pa) are also developed based on the same idea of simultaneous upward and downward flow. The methods mentioned so far require additional equipment or alteration of the existing ones. Increased chaotic flow has been identified as the source of elimination of IMRs. Another way of imparting chaos in laminar flow by using already available equipment is eccentricity. Locating impellers away from the center of a stirred vessel have been studied for axial, radial, and disc impellers. Even though contradictory results have been reported for the effect of eccentricity as the Re number increases, eccentric location of impeller has been proven to be very effective for mixing enhancement under laminar flow (Ascanio and others 2002; Alvarez and others 2002; Cabaret and others 2008; Ng and Ng 2013; Zhang and others 2013; Bulnes-Abundis and Alvarez 2013; Takahashi and others 2015).

Dimensionless numbers are usually derived to compare the effects of each method on different equipment and scales. However, this task could be problematic for non-Newtonian fluids due to the shear rate dependent apparent viscosity. Since shear rates at different order of magnitudes are present in stirred vessels, an average shear rate must be defined. An approximation to determine an average apparent viscosity has been developed by Metzner and Otto (1957) and widely used since then. The details for determination of the relationship

between the impeller speed and average shear rate can be found in the literature (Castell-Perez and Steffe 1990, Doraiswamy and others 1994). Alternative approaches of average shear rate approximations have also been developed by Rieger and Novák (1972), Wassmer and Hungenberg (2005b), and Sánchez Pérez and others (2006).

As the effectiveness of the methods for improving mixing under laminar flow have been studied mostly for Newtonian fluids, this paper is the first part of a study which aims to investigate the effects of eccentricity and impeller modification for simultaneous upward and downward flow on non-Newtonian shear thinning fluid mixing in an unbaffled vessel. In this first part, concentration measurements of a tracer dye with planar laser induced fluorescence technique, power measurements, and numerical analysis with Comsol 5.2 (Comsol Inc, 1 New England Executive Park, Burlington, MA) have been conducted for hydrodynamic characterization.

2. Materials and Methods

2.1. Materials

Carboxymethyl cellulose powder (Pre-Hydrated® Ticalose® CMC 2500, TIC Gums, Belcamp, MD) and light corn syrup (Golden Barrel, Good Food Inc., Honey Brook, PA) were used to prepare the working fluids. 1% (w/v) carboxymethyl cellulose (CMC) solution was prepared by dissolving the CMC powder in distilled water and kept at ~20 ^{o}C overnight to remove air bubbles. Light corn syrup was used in its original form (77-79 Brix). The rheological properties of the fluids at various temperatures were measured by using a Haake

VT550 viscometer (Gebruder Haake GmbH, Karlsruhe, Germany) and are given in Table 1 and Table 2. The density (ρ, kg/m^3) of the fluids were determined to be 1001 ± 0.87 and 1395 ± 3.36 kg/m^3 for 1% (w/v) CMC and light corn syrup solutions, respectively. The physical properties of the fluids at 20 ^oC were used for further calculations.

2.2. Set-up for mixing system

Mixing experiments were conducted in a cylindrical flat-bottomed unbaffled transparent vessel (Figure 1.). The vessel had a diameter of D = 0.254 m. When the fluid height (H) was equal to the diameter of the tank, the working volume of fluid was 12.87 L. A custom made standard 45^o four-blade pitch blade impeller (PBT) and a modified version of the same impeller (DF-PBT) were used (Figure 2.) in the study. The modification was based on the idea of reversing the direction of the two opposing blades on the standard impeller so that both upward and downward flow would be generated at the same time. The impellers were attached to a Servodyne 50000-20 electrical motor operating at 3 A, 115 V (Cole-Parmer Instrument Co., Niles, IL). The impellers were placed at three different locations inside the vessel. The locations were expressed in terms of their the eccentricity value (E):

$$E = e/r$$

where e is the distance between the center of the shaft and the center of the vessel and r is the radius of the vessel. Eccentricity values of 0.00, 0.25, and, 0.50 were selected for the experiments.

2.3. Planar Laser Induced Fluorescence Experiments

Planar laser induced fluorescence (PLIF) method was used to quantify single-phase mixing of the CMC solutions. A laser sheet was formed by using a 532 nm wavelength 0.450 W output powered diode pumped solid state laser system (RayPower 450, Dantec Dynamics Inc, Holtsville, NY) with cylindrical lenses. The laser sheet was adjusted to go through the vessel in a vertical direction at a location that was 0.0508 m away from the centerline of the vessel. Rhodamine 6G (Sigma-Aldrich, St. Louis, MO) was used as the fluorescent dye. Rhodamine 6G powder was dissolved in distilled water first, and then mixed with 1% CMC (w/v) at a ratio of 1:100 to prepare neutrally buoyant tracer solutions at desired concentrations. A digital camera (Sony Handycam HDR-CX150, Sony Corporation, Tokyo, Japan) with a narrow-band filter (9080C0541, Dantec Dynamics Inc., Holtsville, NY) was used to record images before and after injection of the tracer solution. The images recorded before injection were used as the background image. A Matlab (2013b, The Mathworks, Inc., Natick, MA) code was written to complete the following steps:

a) Cropping the original images to define an area of interest because of the reflections caused by the free liquid surface and the surroundings

b) Converting colored images to grayscale images

c) Removing of background images from the images after injection to determine the fluorescent intensity in terms of grayscale values

The concentration value of each pixel was then determined based on a calibration procedure. High concentration tracer solutions were mixed with the CMC solution inside the vessel to result in final concentrations between 0 and 300 µg/L for calibration purposes. For each concentration level, an average grayscale value was calculated. A calibration curve (Figure 3) between the concentration and average gray scale values were plotted. Only the linear portion of the calibration curve (up to 30 µg/L) was used for calculations (Figure 4).

During experiments, 30 mL of 8750 µg/L tracer solution was injected through the surface of the CMC solution in approximately 41 seconds to result in 20 µg/L average concentration if 100% mixing would be achieved.

Two measurements were used to quantify mixing. The regions which were relatively darker than the rest of the image were identified. An average value of 5 µg/L was determined to be a threshold value of the concentration to define these regions. The ratio of number of pixel having an intensity less than 5 µg/L to the total number of pixels was defined as the fraction of Uncovered Area. In addition to this measurement, the coefficient of variation (CoV), which was the ratio of standard distribution and mean values of concentration values were also determined. A correction method which was similar to the one used by Zhang and others (2013) was applied to all concentration values used in these calculations. Based on the calibration curve in Figure 3, the degree of linearity between concentration and grayscale values decreased at concentration level of after 30 µg/L and completely went away at

concentration level of 150 µg/L. Therefore, 30 µg/L was chosen as a pseudo maximum concentration. Any value greater than this maximum value was set to 30 µg/L.

The mixing experiments were conducted at 50, 100, and 300 rpm for 1.5 hrs of recording time at all values of eccentricity.

2.4. Power Measurement

Power consumption was determined using the following equation:

$$P = 2\pi N M_c$$

where N is the impeller speed in revolution per second (1/s), M_c is the corrected torque (Nm) which was the difference between the measured torque with and without the working fluid. A torque transducer (T5-1-A1A, Interface Inc. Scottsdale, AZ) which had a measurement range between 0.1 Nm and 1 Nm was installed between the motor and the shaft. A pillow bearing was used to limit vibration. Even with the support of the bearing, excessive vibration was present for rpm values above 475. The torque transducer was warmed up for 5 min. and the measurements were taken at various rpm (25, 50, 75, 100, 175, 300, and 450 rpm) for the following 3 min. at a sampling rate of 1.0 Hz.

The relationship between power consumption and other process parameters (fluid density, viscosity, impeller diameter and speed) were also expressed with a Power number (Po) vs Reynolds number (Re) curve. With Po and Re being determined using the following equations:

$$Po = P/\rho*N^3*D^5$$

$$Re = \rho*N*D^2/\eta$$

where D is impeller diameter (m), ρ is density (kg/m^3), and η is apparent viscosity (Pa.s). In order to calculate the apparent viscosity of CMC solution, an average shear rate was estimated using the matching viscosity method based on the Metzner-Otto correlation given below:

$$\dot{\gamma} = K_s*N$$

where $\dot{\gamma}$ is the average shear rate (1/s) and K_s is the Metzner-Otto constant (Castell-Perez and Steffe 1990).

2.5. Numerical Studies

A commercial software, COMSOL 5.2 (Comsol Inc, 1 New England Executive Park, Burlington, MA), was used for numerical studies of mixing. Experimentally measured material properties, the operating parameters used in the experiments, and the same equipment geometry were used to set up the models under Rotating Machinery-Laminar Flow interface in the CFD module. The model was solved with the frozen rotor and time-dependent approaches which reformulated the Navier-Stokes equations in rotating coordinate systems. The mixing system geometry was built using COMSOL 5.2 interface. An outer stationary domain and an inner rotating domain with the shaft and impeller parts (Figure 5.)

were assembled. The geometry was meshed with tetrahedral, pyramid, prism, triangular, quadrilateral, edge, and, vertex elements. A mesh convergence study was completed by increasing the number of the elements to the point at which the results of power drawn by the impeller and the shaft was not affected. The power consumption was determined by:

$$P = \int_A 2\pi N(xFx - yFy)dA$$

where N is the impeller speed (1/s), Fx and Fy are the forces acting on every point of the impeller and the shaft surface. Based on the convergence studies completed at different rpm values, no significant change in power values was detected after the number of elements was increased to 2884161. An example at 25 rpm is shown in Table 3. Since no vortex formation was observed during the experiments, symmetry boundary condition was applied to the fluid surface. While no slip boundary condition was used on the vessel walls, the shaft and impeller surfaces were selected as rotating walls. A single point in the geometry was selected for a pressure point constraint and the pressure value was set to zero. Therefore, a pressure gradient in the model can be calculated and infinite number of solutions is avoided for a successful convergence. The initial velocity of the fluid was set to zero for all the studies. Power consumption and velocity profiles were used to characterize the hydrodynamics of the mixing system.

3. Results and Discussions

3.1. PLIF Measurements

The images taken 1.5 hours after the start of PLIF experiments are shown in Figures 6, 7, and 8 for impeller locations at E = 0, 0.25, and, 0.50, respectively. While the dark areas represent the isolated mixing regions (IMR), the bright areas represent regions of highly concentrated tracer solution. Even though no tracer solution is expected to enter IMRs, a grayscale value corresponding to 5 µg/L was found to be the average value within these regions. Therefore, a threshold value of 5 µg/L was used to determine the size of IMRs. A similar approach was also used by Zhang and others (2013). However, the ratio of threshold value to the expected final concentration (20%) is higher than the one used by Zhang and others (2013), namely 5% of the final concentration. The relatively low power of the laser source and large diameter of the stirred vessel in addition to the different camera quality could be the main reasons for this difference.

A larger upper and a smaller IMR are observed, especially for E = 0. Considering the effects of impeller clearance on IMR seen by Wang and others (2013), a small gap between the impeller and the bottom of the vessel in this study (C = T/4) is likely the main reason for this observation. Since the measurements were taken away from the center of the vessel, the cross-sectional areas of IMRs were not revealed. However, a preliminary experiment was conducted to capture images at different locations within the vessel. In Figure 9, a series of images show the change in cross-sectional areas of IMRs with measurement location. With more detailed experiments, the location with the minimum reflection for better quality

measurements or the location where the cross-sectional area is the largest for a worst-case scenario can be chosen.

3.2. Effect of Eccentricity on Laminar Mixing

IMRs, the separation of the vessel at the impeller height, and, slow mixing at the fluid surface which were identified by Alvarez and others (2002) as the characteristic features of the laminar mixing, are seen in Figure 6. As eccentricity increases, these features start to disappear. The size of both the upper and lower IMRs decrease with increase in eccentricity. However, the effect of eccentricity is more pronounced for the lower IMR than it is for the upper IMR. Only for PBT located at E = 0.50 and operating at 300 rpm, both the upper and lower IMRs are non-existent (Figure 8). Quantitative measurements of IMRs, % of uncovered area, and CoV, are shown in Figures 10 - 13. Based on the results of % uncovered area, the lowest rpm (50 rpm) at E = 0.25 results in a lower % uncovered area value than the highest rpm (300 rpm) does at E = 0. The same trend is also valid for values of E = 50. Thus, increasing eccentricity is more effective than increasing rpm alone to improve mixing under laminar flow conditions. Based on the criterion that $\leq 5\%$ uncovered area is an acceptable level of mixing, only five combinations (E = 0.50 for DF-PBT at 100 and 300 rpm; E = 0.50 for PBT at 50, 100, and, 300 rpm) meet this criteria. On the other hand, CoV results showed that significant concentration variation ($\geq 10\%$) still exists. Bright areas, which are the source of the concentration variation, can be seen in Figures 6, 7, and 8. The location of these areas moved from fluid surface to the sides and bottom of the vessel with increased eccentricity. In

Figure 14, the disruption of complete circular movement of the fluid is seen on the surface. As eccentricity increases, the flow is directed to the opposite direction of the impeller and the separation of the flow next to the impeller is observed. The velocity vectors at the vessel centerline for E = 0 show that the flow is directed upwards from the sides of the shaft and returns to the impeller from the vessel walls to complete two symmetrical circular loops. This top to bottom flow is effective up to the upper one-third region of the vessel. Above this point, the flow is more circular which can explain the slow mixing near the surface. The symmetrical flow structure is again disrupted with increased eccentricity and the top to bottom flow is extended to the fluid surface.

Even though uniform concentration values may not be achieved during viscous fluid mixing, CoV should still be considered as a useful measurement in addition to the area based measurements. The effect of eccentricity at low rpm values, which corresponds to low Re numbers, is contradictory to the effect seen by Zhang and others (2013) and was more similar to the results of Cabaret and others (2008). The reduction in the % of uncovered area and CoV with increased eccentricity is more effective when rpm increased from 50 to 300.

3.3. Effect of Impeller Type on Laminar Mixing

For all combinations of eccentricity and rpm, PBT performs better than DF-PBT in terms of % of uncovered area and CoV values. The results are contradictory to the findings of Kato and others (2007) and Wang and others (2013). In these studies, a 2-bladed and a 6-bladed 45^{o} pitched blade impeller were modified to generate simultaneous upward and

downward flow for laminar mixing at Re of 20 and 61, respectively. The size of IMRs were significantly reduced in both studies for Newtonian fluids. A time-dependent numerical analysis was conducted to see if DF-PBT provides simultaneous upward and downward flow. The Axial velocity component of the flow on a vertical line located at the tip of the impeller blade is presented in Figure 16. At 300 rpm, one impeller blade visits the vertical line every 0.05 s. The positive axial velocity values in Figure 16 indicate the upward flow while the downward flow is represented with negative values. Almost equal magnitudes of velocity were seen for both flow types and the velocity profiles were almost mirror images of one another. The velocity vectors at the vessel centerline are shown in Figure 17 for one complete revolution of the impeller. The symmetrical flow structure and distinct radial flow which separates the vessel into two parts at the impeller height remain constant in one revolution while the flow is directed towards the corners of the vessel and then back to the impeller. The main geometrical difference between DF-PBT and the others is that the blades are separated by larger gaps for the impellers used in the previous studies. This is likely causing the upward and downward flow to cancel each other's action before a total chaotic motion is developed and the performance is similar to that of a disc with no blades. Wang and others (2013) also pointed out the same effect with increased number of blades. Overall, the effect of eccentricity and rpm is similar for both PBT and DF-PBT. One particular exception for for DF-PBT is that mixing at 100 rpm results in a slightly smaller lower IMR than mixing at 300 rpm does.

3.4. Power Consumption

The results of eccentricity and impeller type on specific power consumption are given in Table 4. No significant difference is detected between E = 0 and E = 0.50 for a given rpm value. As the flow is effective only around the impeller and the shaft, any possible interaction between the vessel wall and impeller does not cause an increase in power consumption. Cabaret and others (2008) also made the same conclusion for a Rushton turbine operated under laminar flow conditions. DF-PBT has lower power values than PBT does at increased rpm values for all the eccentricity values. Extra vibration on the shaft was detected especially for DF-PBT during torque measurements without the fluid. Since the power consumption is calculated based on the difference between the torque values with and without the fluid, the extra vibration may have reduced the power values with DF-PBT.

The Newtonian power curves are plotted as the first step using the Metzner-Otto concept (Figures 18 and 19). The inverse relationship between the Po and Re are observed as expected. Unlike mixing under turbulent flow, Po*Re is constant during laminar mixing. The experimental and numerical values are reported in Table 5. The fluctuations in the experimental data is most likely due to the highly temperature dependent nature of corn syrup viscosity and the lack of temperature control in the mixing system. The range of Po*Re is in agreement with the values of 46-47 reported by Kato and others (2007) and lower than the values of 75 and 230 for Rushton and anchor impellers seen by Foucault and others (2005). Average values of Po*Re are used for determination of K_s values for PBT and DF-PBT. K_s is a constant up to 5 1/s and a sudden decrease is seen at 7.5 1/s (Figures 20 and 21). Since the

Metzner-Otto concept is valid only for laminar flow, the drop in K_s suggests the end of the laminar region for the mixing system used in this study. This change was also reported by Thakur and others (2004). The average K_s values given in Table 6 are used to plot non-Newtonian power curves (Figure 22). Within the laminar region the power curves of Newtonian and non-Newtonian fluids are similar. However, the deviation of the exponent from -1 is seen and this is due to experimental errors.

4. Conclusion

Mixing of a shear thinning non-Newtonian fluid under laminar flow conditions in an unbaffled vessel was investigated in terms of planar laser induced fluorescence measurements (PLIF) and power consumption. Numerical analysis was also conducted to reveal flow patterns. Eccentric locations of the impellers (E = 0, 0.25, and, 0.50) and modification of a regular pitched blade turbine to generate simultaneous upward and downward flow methods were used. The size of the unmixed regions were reduced by increased eccentricity. Significant concentration variations were still present even though the tracer solution covered more than 95% of the visualized area, suggesting coefficient of variation (CoV) values were still valuable measurements for quantification of laminar mixing. Velocity vectors were helpful for understanding the distribution of the tracer solution within the vessel. In future studies, this could be considered as a prediction tool to choose injection points of the tracer for faster mixing and locate measurement planes for better representation. Dual-flow pitched blade (DF-PBT) turbine did not perform better than

pitched blade turbine (PBT) for any of the cases studied. Since power consumption did not increase with increased eccentricity, additional methods combined with eccentricity may be used for improved laminar mixing.

References

Alvarez MM, Guzmán A, Elías M. 2005. Experimental visualization of mixing pathologies in laminar stirred tank bioreactors. Chemical Engineering Science 60(8-9):2449-2257.

Alvarez MM, Arratia PE, Muzzio FJ. 2002. Laminar mixing in eccentric stirred tank systems. The Canadian Journal of Chemical Engineering 80(4):546-557.

Alvarez-Hernández MM, Shinbrot T, Zalc J, Muzzio FJ. 2002. Practical chaotic mixing. Chemical Engineering Science 57(17):3749-3753.

Ascanio G, Brito-Bazán M, Brito-De La Fuente E, Carreau PJ, Tanguy PA. 2002. Unconventional configuration studies to improve mixing times in stirred tanks. The Canadian Journal of Chemical Engineering 80(4):558-565.

Bonnot S, Cabaret F, Fradette L, Tanguy PA. 2007. Characterization of mixing patterns in a coaxial mixer. Chemical Engineering Research & Design 85(8):1129-1135.

Bulnes-Abundis D, Alvarez MM. 2013. The simplest stirred tank for laminar mixing: Mixing in a vessel agitated by an off-centered angled disc. AIChE Journal 59(8):3092-3108.

Cabaret F, Fradette L, Tanguy PA. 2008. Effect of shaft eccentricity on the laminar mixing performance of a radial impeller. The Canadian Journal of Chemical Engineering 86(6):971-977.

Cabaret F, Bonnot S, Fradette L, Tanguy PA. 2007a. Mixing time analysis using colorimetric methods and image processing. Industrial & Engineering Chemistry Research 46(14):5032-5042.

Cabaret F, Rivera C, Fradette L, Heniche M, Tanguy PA. 2007b. Hydrodynamics performance of a dual shaft mixer with viscous newtonian liquids. Chemical Enginering Research and Design 85(5):583-590.

Castell-Perez ME, Steffe JF. 1990. Evaluating shear rates for power law fluids in mixer viscometry. Journal of Texture Study 21(4):439-452.

Cullen PJ, O'Donnell CP. 2009. Mixing in the food industry: Trends and challenges. In: P.J. Cullen, editor. Food Mixing. Blackwell Publishing Ltd. p 1-5.

Doraiswamy D, Grenville RK, Etchells AW. 1994. Two-Score years of the Metzner-Otto correlation. Industrial & Engineering Chemistry Research 33(10):2253-2258.

Elson TP. 1990. X-Ray flow visualisation of flow patterns during the mixing of yield stress, Newtonian and dilatant fluids. Chemical Engineering Communications 94(1):143-158.

Foucault S, Ascanio G, Tanguy PA. 2005. Power characteristics in coaxial mixing: Newtonian and non-Newtonian fluids. Industrial & Engineering Chemistry Research 44(14):5036-5043.

Hashimoto S, Natami K, Inoue Y. 2011. Mechanism of mixing enhancement with baffles in impeller-agitated vessel, part I: A case study based on cross-sections of streak sheet. Chemical Engineering Science 66(20):4690-4701.

Hashimoto S, Ito H, Inoue Y. 2009. Experimental study on geometric structure of isolated mixing region in impeller agitated vessel. Chemical Engineering Science 64(24):5173-5181.

Kato Y, Tada Y, Ban M, Nagatsu Y, Yanagimoto K. 2007. Application of asymmetric impellers to mixing at unsteady speed within a single revolution. Kagaku Kogaku Ronbunshu 33(1):16-19.

Lamberto DJ, Muzzio FJ, Swanson PD, Tonkovich AL. 1996. Using time-dependent RPM to enhance mixing in stirred vessels. Chemical Engineering Science 51(5):733-741.

Machado MB, Nunhez JR, Nobes D, Kresta SM. 2012. Impeller characterization and selection: Balancing efficient hydrodynamics with process mixing requirements. AIChE Journal 58(8):2573-2588.

Metzner AB, Taylor JS. 1960. Flow patterns in agitated vessels. AIChE Journal 6(1):109-114.

Metzner AB, Otto RE. 1957. Agitation of non-Newtonian fluids. AIChE Journal 3(1):3-10.

Ng KC, Ng EYK. 2013. Laminar mixing performances of baffling, shaft eccentricity and unsteady mixing in a cylindrical vessel. Chemical Engineering Science 104:960-974.

Norwood KW, Metzner AB. 1960. Flow patterns and mixing rates in agitated vessels. AIChE Journal 6(3):432-437.

Rieger F, Novák V. 1972. Scale-up method for power consumption of agitators in the creeping flow regime. Chemical Engineering Science 27(1):39-44.

Sánchez Pérez JA, Rodríguez Porcel EM, Casas López JL, Fernández Sevilla JM, Chisti Y. 2006. Shear rate in stirred tank and bubble column bioreactors. Chemical Engineering Journal 124:1-5.

Takahashi K, Takeno Y, Takahata Y. 2015. Comparison of mixing performances among several spatial chaotic mixing methods. Journal of Chemical Engineering of Japan 48(7):518-522.

Thakur RK, Vial C, Djelveh G, Labbafi M. 2004. Mixing of complex fluids with flat-bladed impellers: effect of impeller geometry and highly shear-thinning behavior. Chemical Engineering and Processing: Process Intensification 43(10):1211-1222.

Wang S, Wu J, Bong E. 2013. Reduced IMRs in a mixing tank via agitation improvement. Chemical Engineering Research & Design 91(6):1009-1017.

Wassmer K, Hungenberg K. 2005. A Unified model for the mixing of non-Newtonian fluids in the laminar, transition, and turbulent region. Macromolecular Materials and Engineering 290(4):294-301.

Wilkens RJ, Miller JD, Plummer JR, Dietz DC, Myers KJ. 2005. New techniques for measuring and modeling cavern dimensions in a Bingham plastic fluid. Chemical Engineering Science 60(19):5269-5275.

Woziwodzki S. 2014. Mixing of viscous Newtonian fluids in a vessel equipped with steady and unsteady rotating dual-turbine impellers. Chemical Engineering Research & Design 92(3):435-446.

Yao WG, Sato H, Takahashi K, Koyama K. 1998. Mixing performance experiments in impeller stirred tanks subjected to unsteady rotational speeds. Chemical Engineering Science 53(17):3031-3040.

Zhang M, Hu Y, Wang W, Shao T, Cheng Y. 2013. Intensification of viscous fluid mixing in eccentric stirred tank systems. Chemical Engineering and Processing: Process Intensification 66:36-43.

Table 1. Rheological parameters of 1% (w/v) CMC within shear rate range of 10-800 1/s

T (ºC)	n	K (Pa.s^n)
16	0.40 ± 0.00	6.27 ± 0.06
17	0.40 ± 0.01	6.19 ± 0.07
18	0.40 ± 0.00	6.15 ± 0.43
19	0.41 ± 0.01	5.82 ± 0.01
20	0.41 ± 0.01	5.59 ± 0.56

Table 2. Viscosity of light corn syrup

T (ºC)	μ (Pa.s)
22	15.85 ± 0.11
20	19.36 ± 0.05
18	27.31 ± 0.22

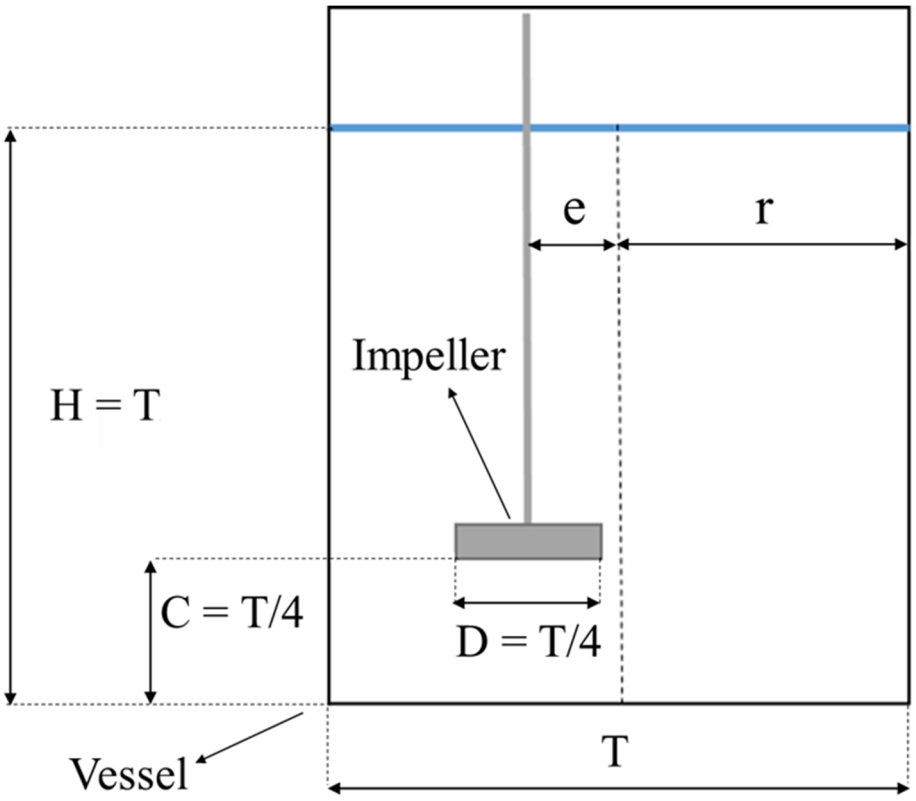

Figure 1. Geometry of the mixing system

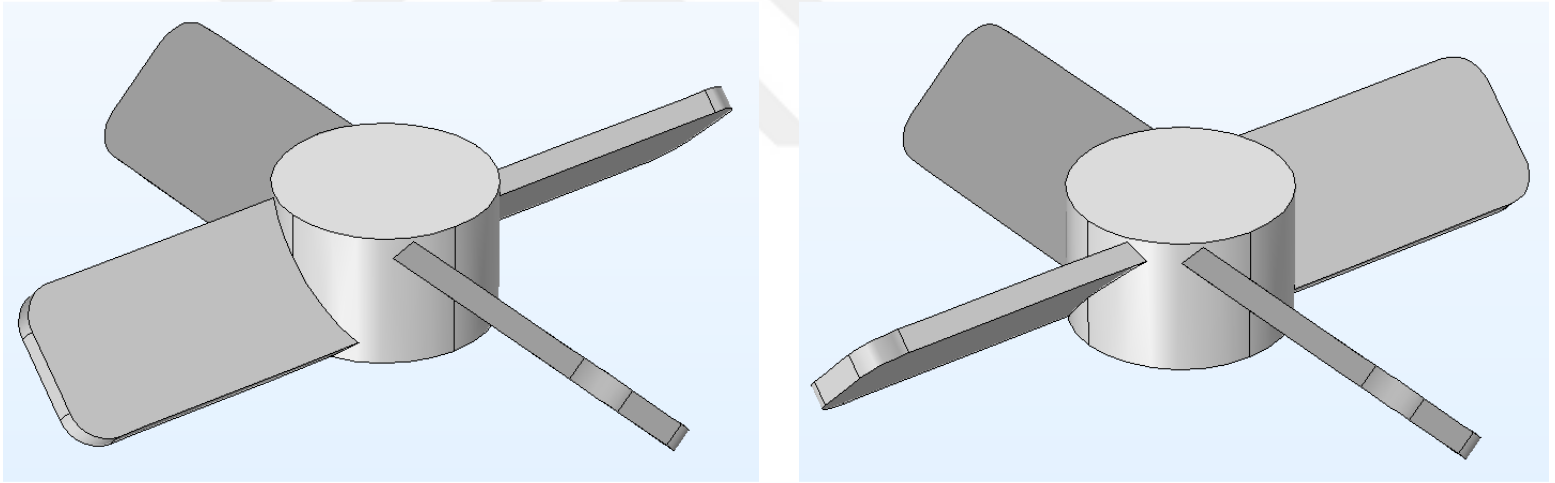

a) b)

Figure 2. Pitched blade turbine (a) and Dual-flow pitched blade turbine (b)

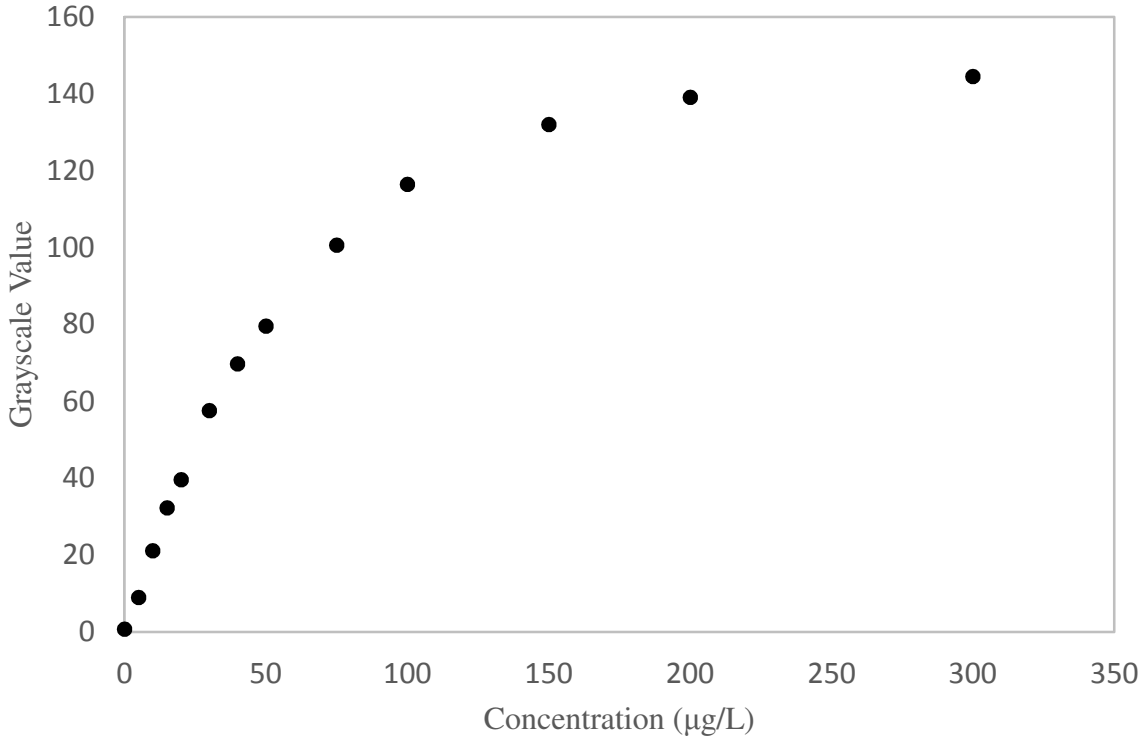

Figure 3. Calibration curve of Rhodamine 6G

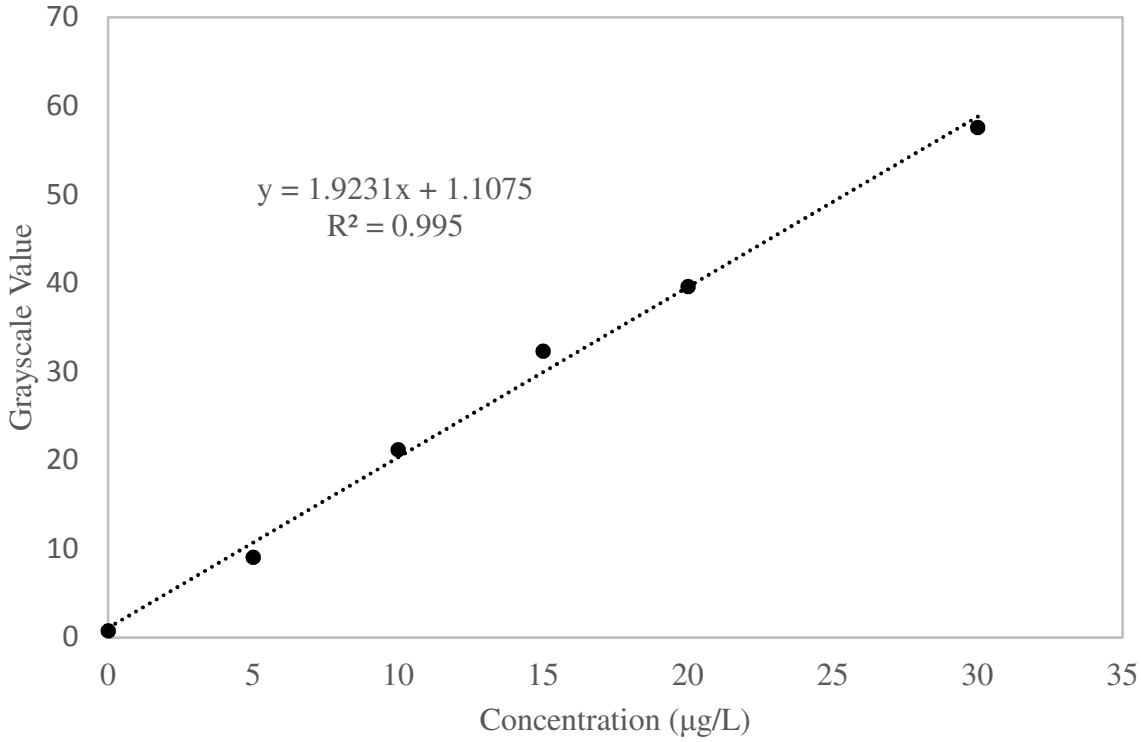

Figure 4. Linear portion of the calibration curve of Rhodamine 6G

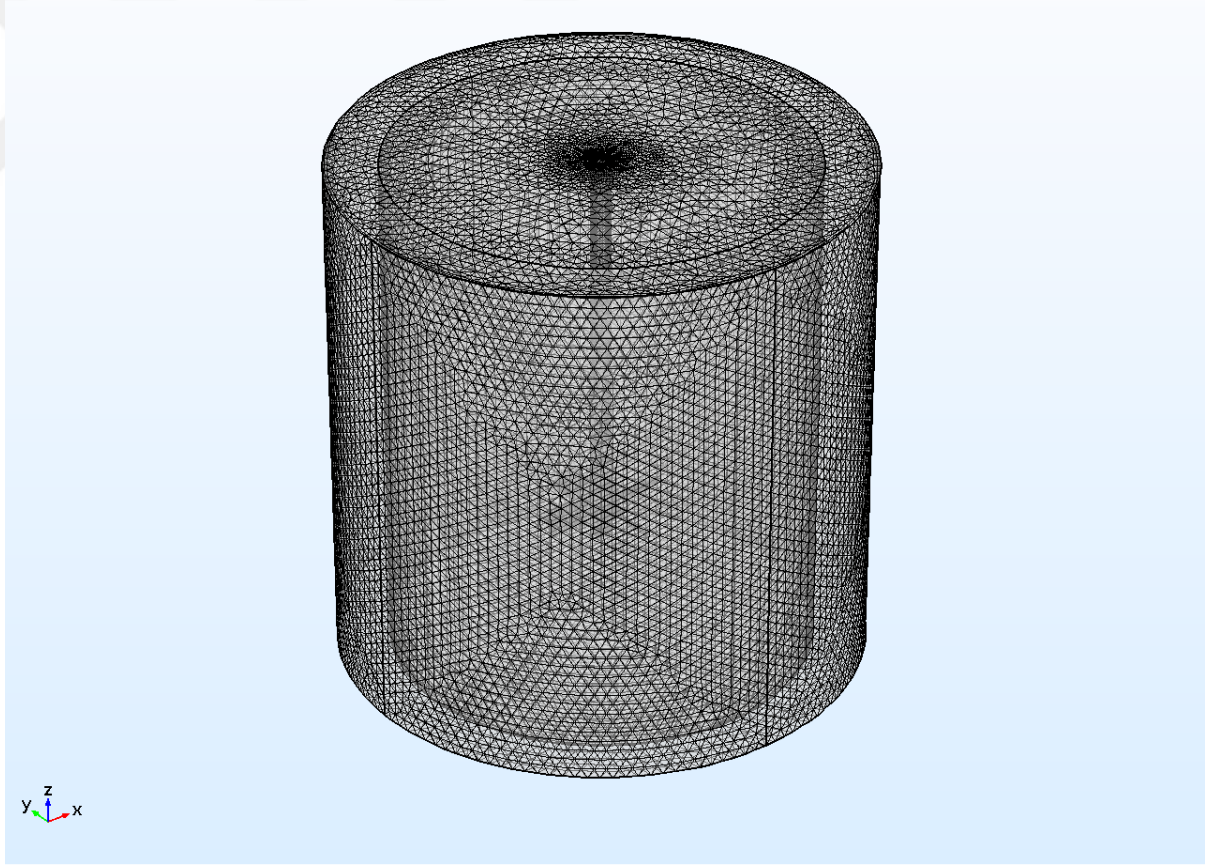

Figure 5. Geometry of the mixing system with a stationary outer domain and a rotating inner domain

Table 3. Effect of number of elements on power and computation time in a mesh convergence study

Number of elements	**Power* 10^{-3} (W)**	**Computation time (s)**
95860	5.15	252
218573	5.31	366
805452	5.83	1073
2884161	6.12	3871
4171448	6.10	7012
5599116	6.10	7836

DF-PBT			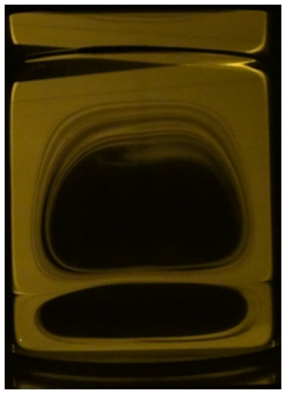
PBT	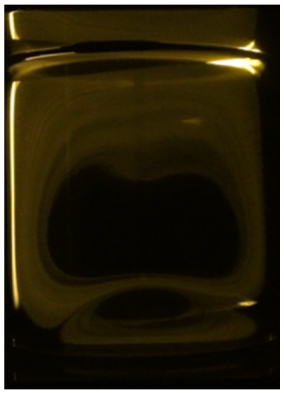	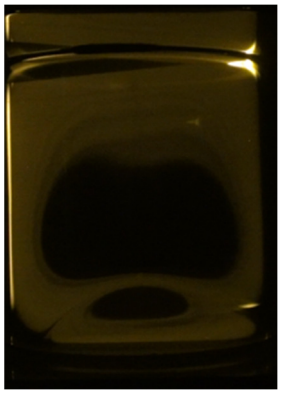	
	50 rpm	100 rpm	300 rpm

Figure 6. PLIF images of DF-PBT and PBT for E = 0

DF-PBT	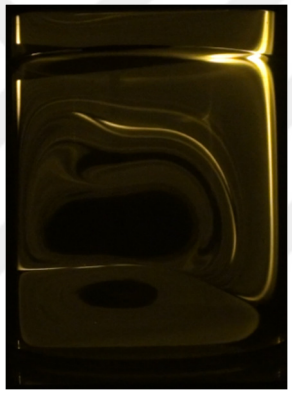		
PBT	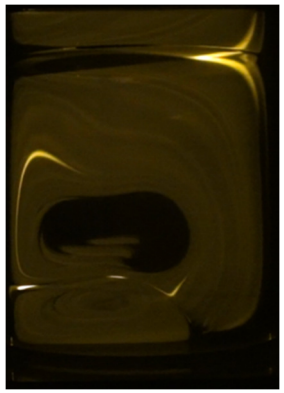		
	50 rpm	100 rpm	300 rpm

Figure 7. PLIF images of DFPBT and PBT for E = 0.25

DF-PBT	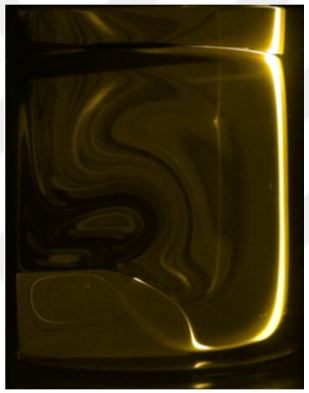	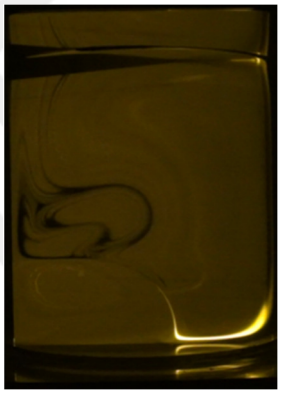	
PBT		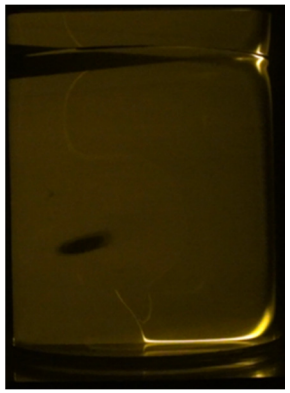	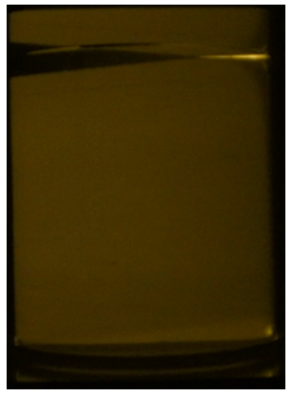
	50 rpm	100 rpm	300 rpm

Figure 8. PLIF images of DF-PBT and PBT for E = 0.50

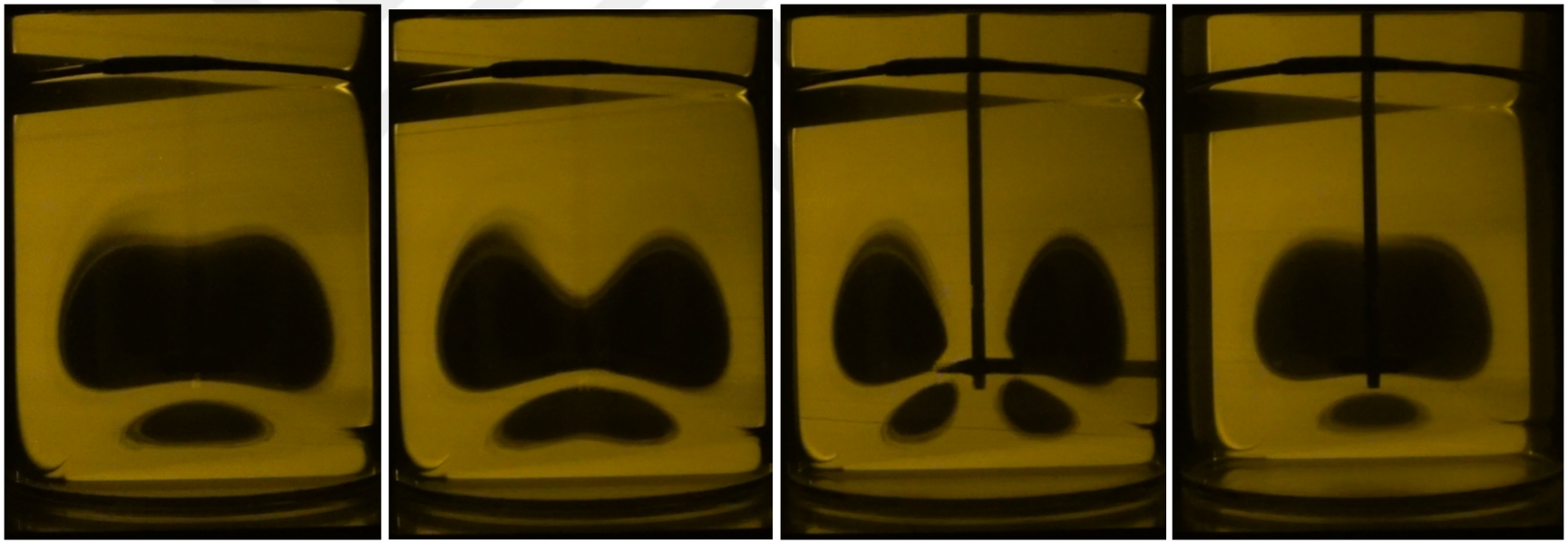

a) b) c) d)

Figure 9. Isolated mixing regions seen at different locations a) 0.0508 m in front of the center line, b) 0.03175 m in front of the center line, c) 0.01 m behind the center line, d) 0.0508 m behind the centerline

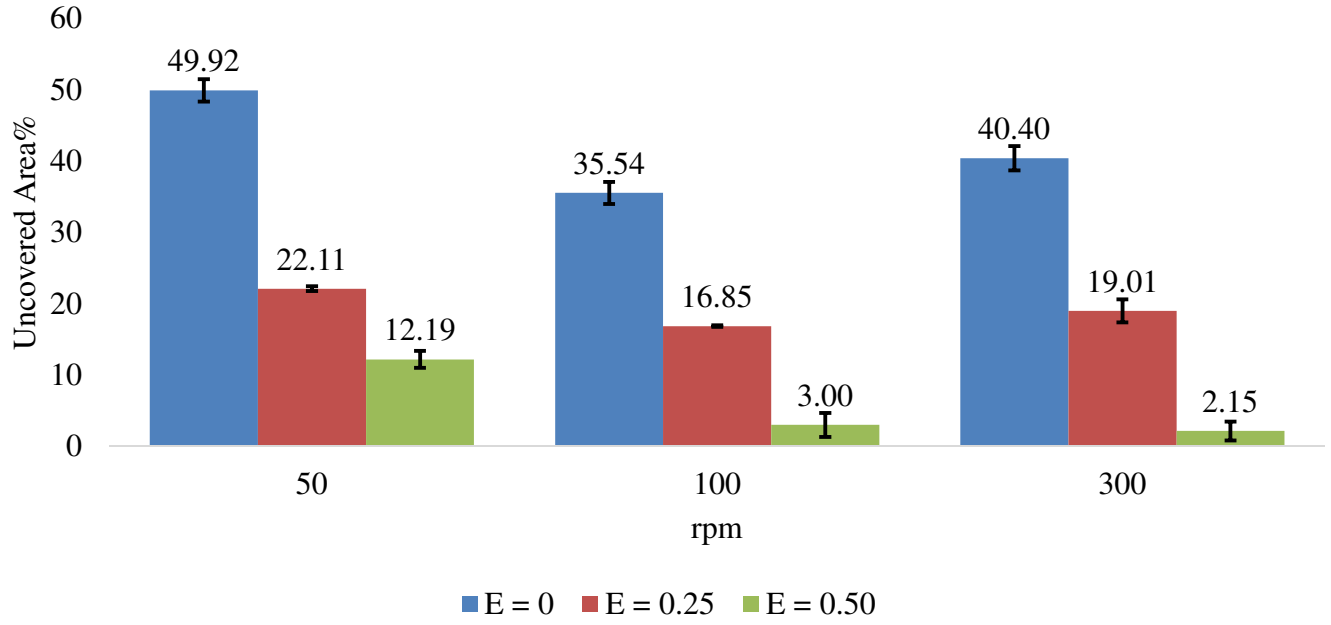

Figure 10. % Uncovered area for DF-PBT

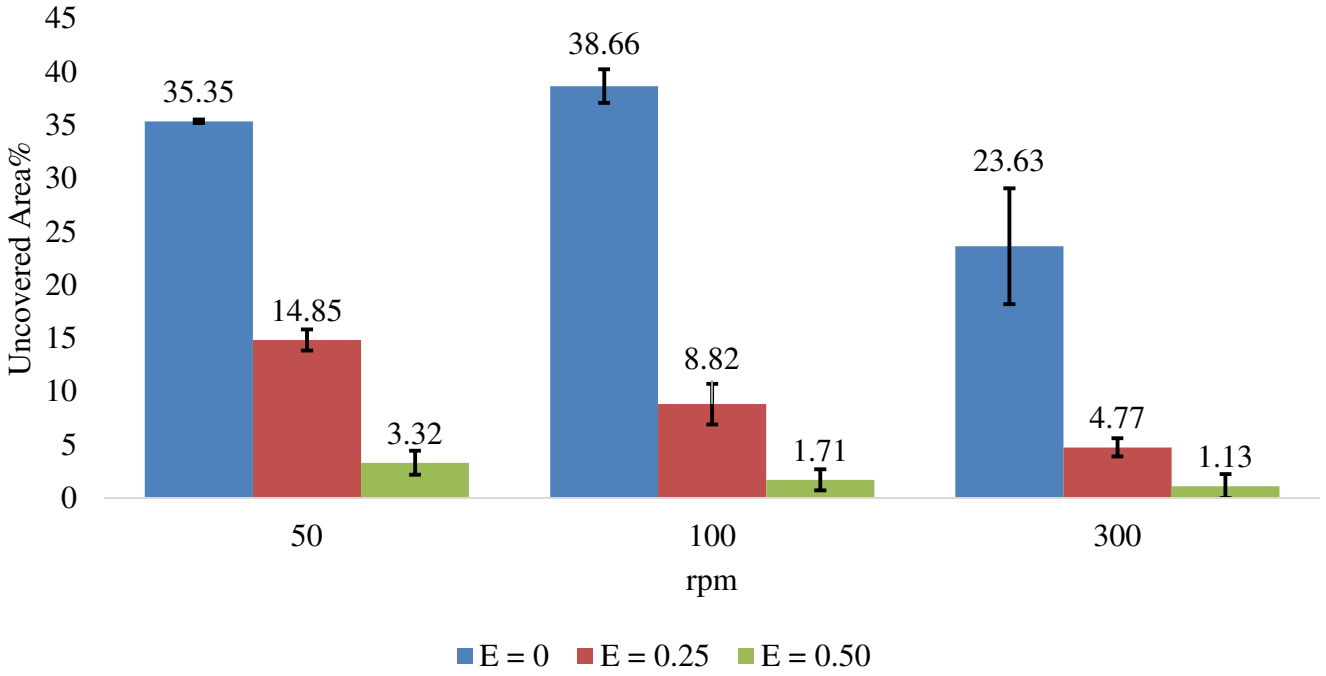

Figure 11. % Uncovered area for PBT

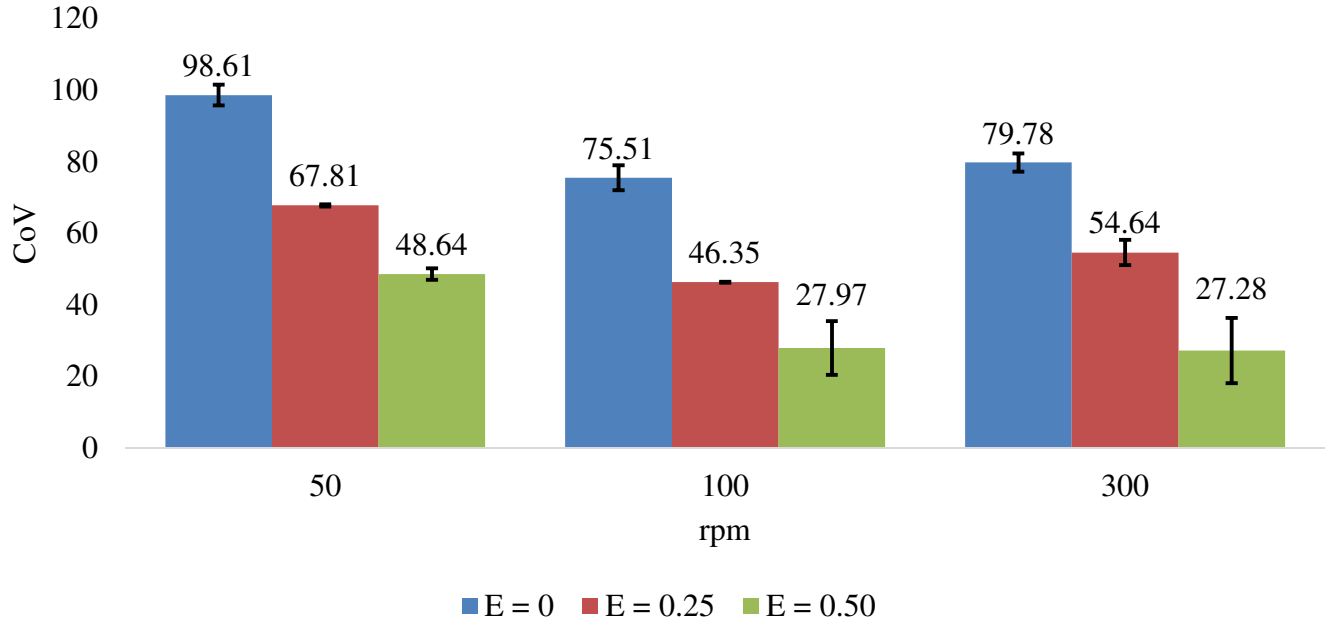

Figure 12. CoV for DF-PBT

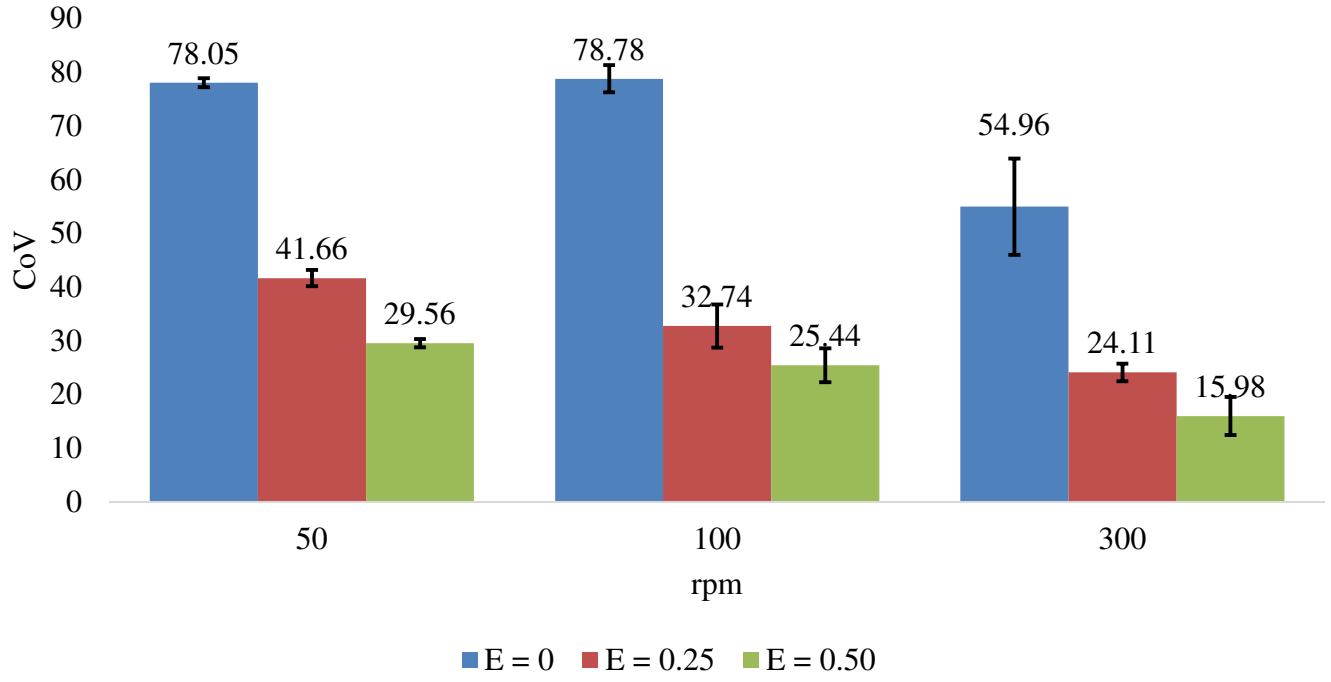

Figure 13. CoV for PBT

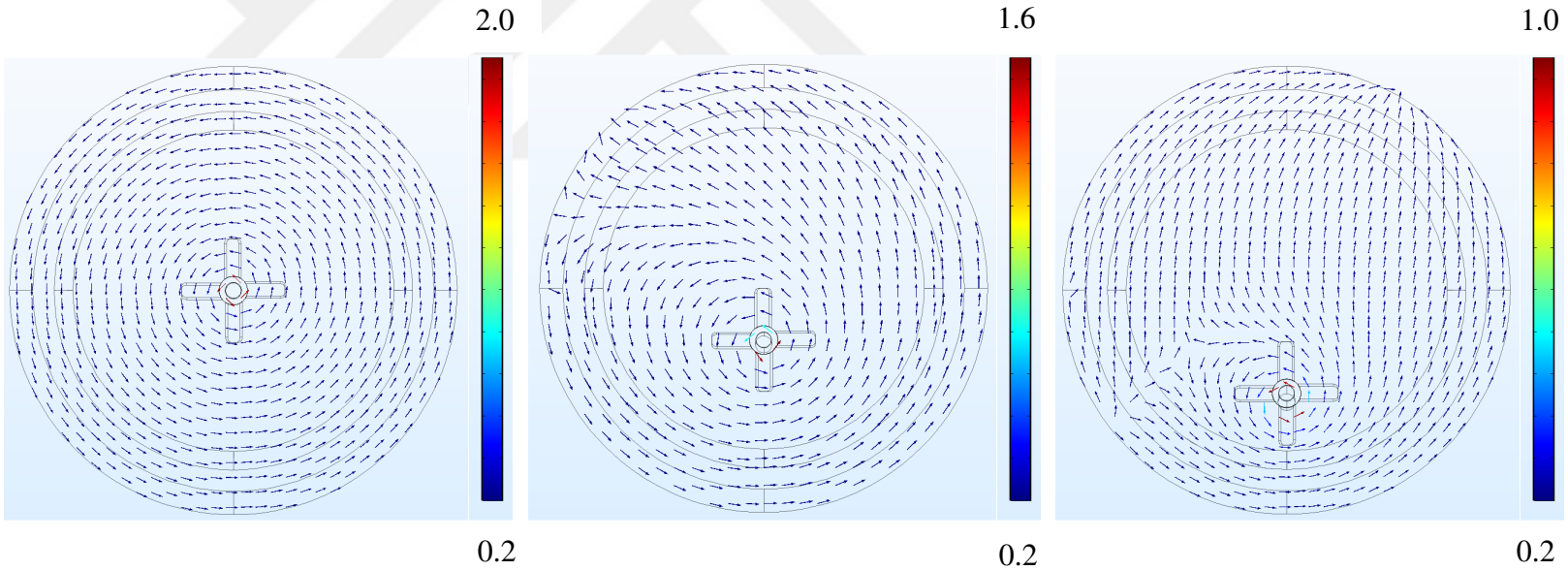

Figure 14. Velocity vectors at fluid surface at 100 rpm for PBT a) E = 0, b) E = 0.25, c) E = 0.50 (color bars shows normalized velocity magnitudes with the tip speed x 10^{-2})

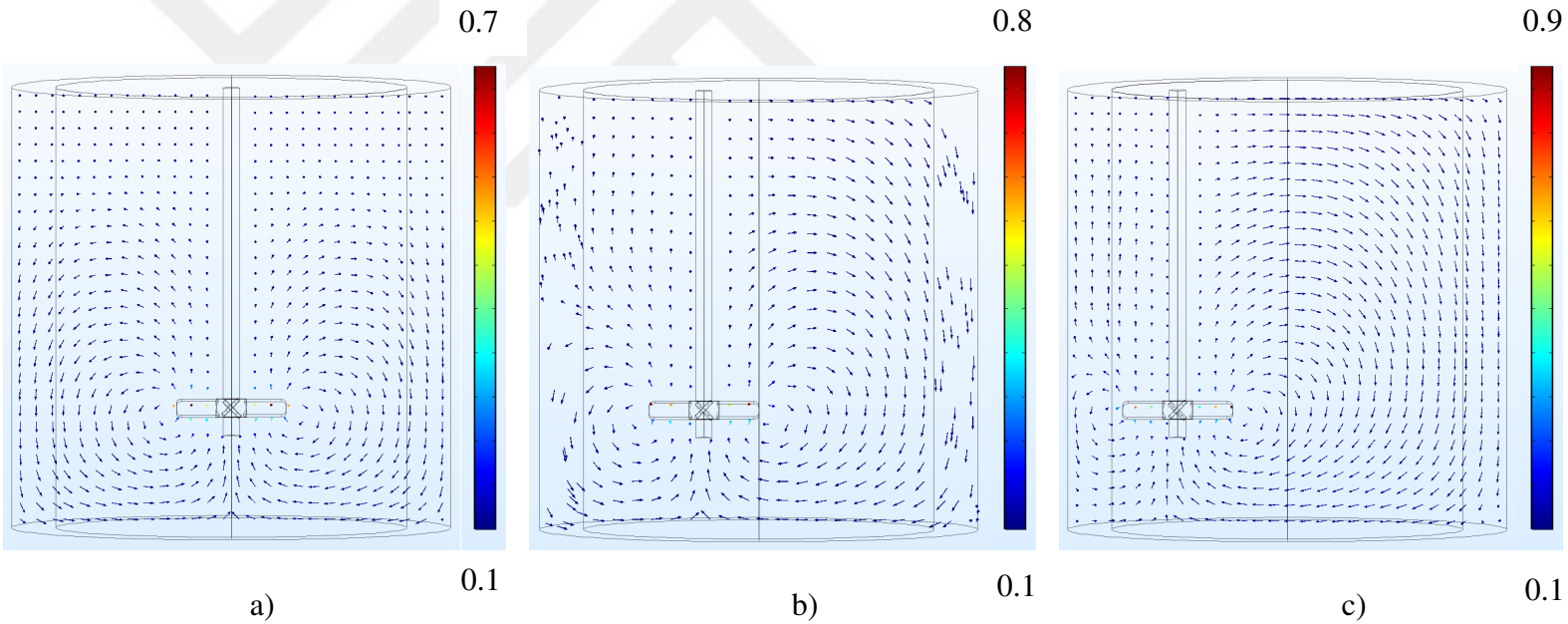

Figure 15. Velocity vectors at the vessel center at 100 rpm for PBT a) E = 0, b) E = 0.25, c) E = 0.50 (color bars shows normalized velocity magnitudes with the tip speed)

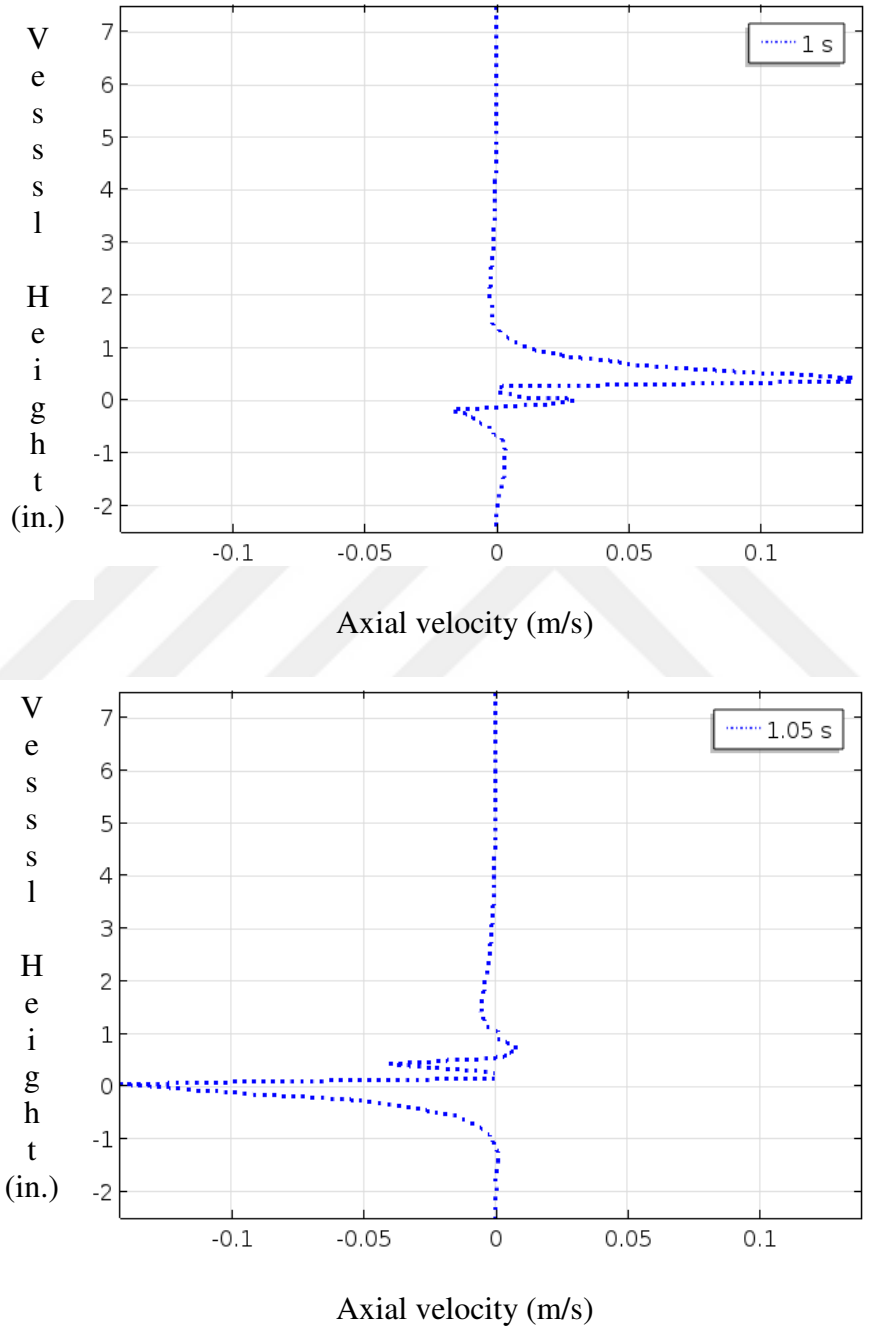

Figure 16. Axial velocity at the tip of the impeller at 300 rpm for DF-PBT (fluid surface at 7.5" – the bottom of the vessel at -2.5")

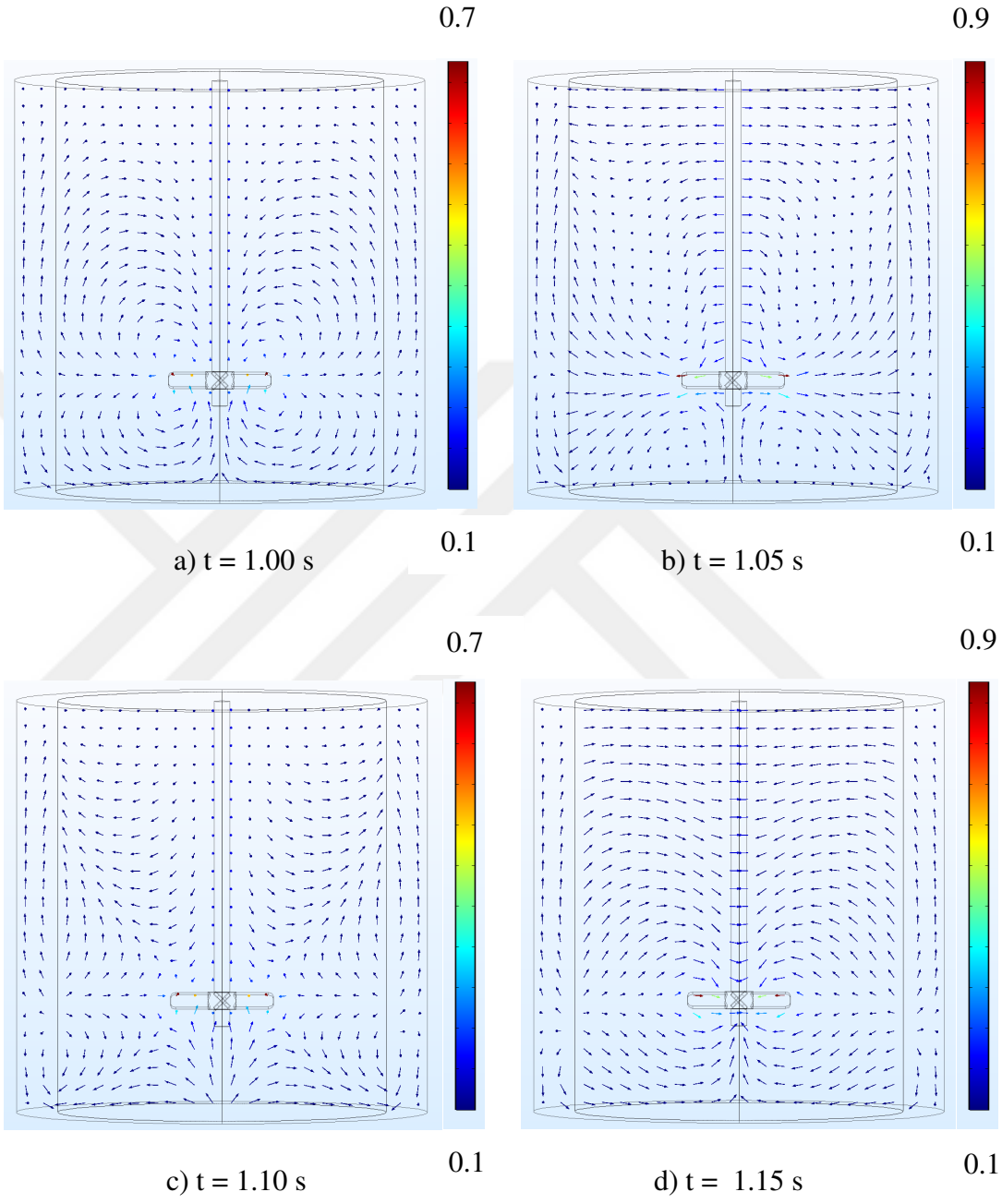

Figure 17. Velocity vectors at center of the vessel center at 300 rpm for DF-PBT

(color bars shows normalized velocity magnitudes with the tip speed)

Table 4. Specific power consumption (W/m^3) for 1.0% CMC

	E = 0		**E = 0.25**		**E = 0.50**	
rpm	**PBT**	**DF-PBT**	**PBT**	**DF-PBT**	**PBT**	**DF-PBT**
25	0.50 ± 0.04	0.53 ± 0.03	0.56 ± 0.03	0.58 ± 0.02	0.57 ± 0.006	0.52 ± 0.01
50	1.37 ± 0.03	1.41 ± 0.05	1.36 ± 0.03	1.54 ± 0.006	1.43 ± 0.05	1.36 ± 0.03
75	2.35 ± 0.06	2.45 ± 0.06	2.50 ± 0.12	2.68 ± 0.03	2.65 ± 0.18	2.48 ± 0.05
100	4.18 ± 0.11	4.04 ± 0.04	4.21 ± 0.02	4.12 ± 0.18	4.56 ± 0.27	3.94 ± 0.08
175	9.01 ± 0.09	8.96 ± 0.05	9.08 ± 0.19	8.90 ± 0.17	9.15 ± 0.03	8.97 ± 0.20
300	19.99 ± 0.53	17.33 ± 0.29	21.49 ± 0.51	18.19 ± 0.26	20.69 ± 0.24	17.45 ± 0.20
450	52.13 ± 0.19	46.06 ± 0.06	53.00 ± 0.08	48.34 ± 0.54	52.76 ± 0.23	46.53 ± 0.47

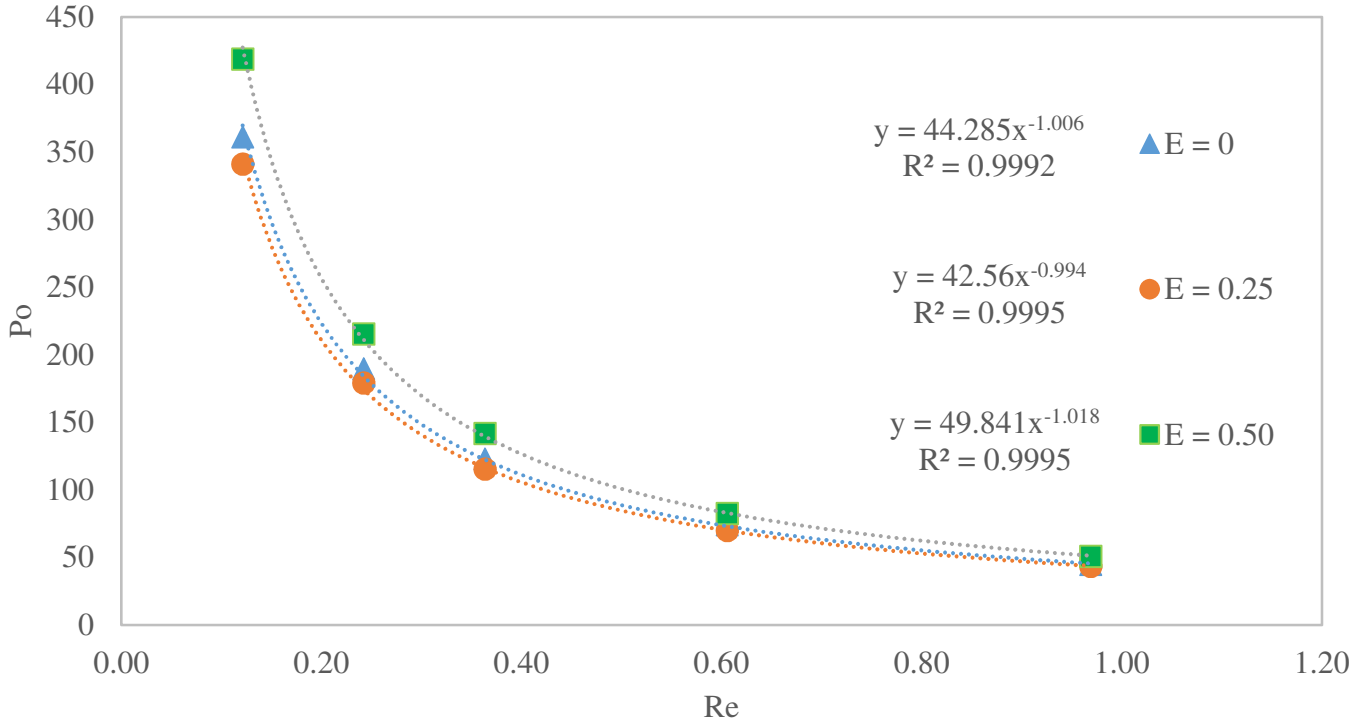

Figure 18. Power number vs Reynolds number for light corn syrup (PBT)

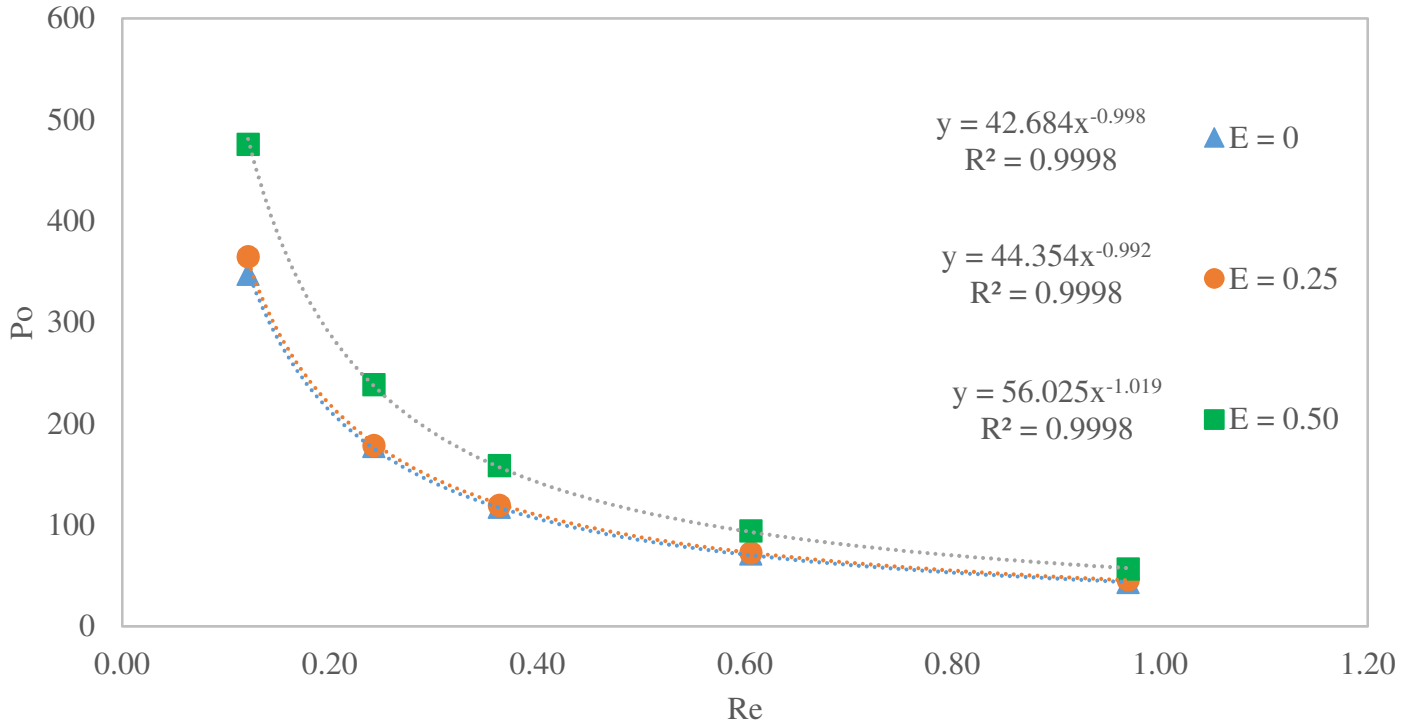

Figure 19. Power number vs Reynolds number for light corn syrup (DF-PBT)

Table 5. Experimental and numerical values of Po*Re

	PBT		DF-PBT	
E	**Experimental**	**Numerical**	**Experimental**	**Numerical**
0	44.29	48.40	42.68	48.48
0.25	42.56	48.46	44.35	48.59
0.50	49.84	49.16	56.03	49.22

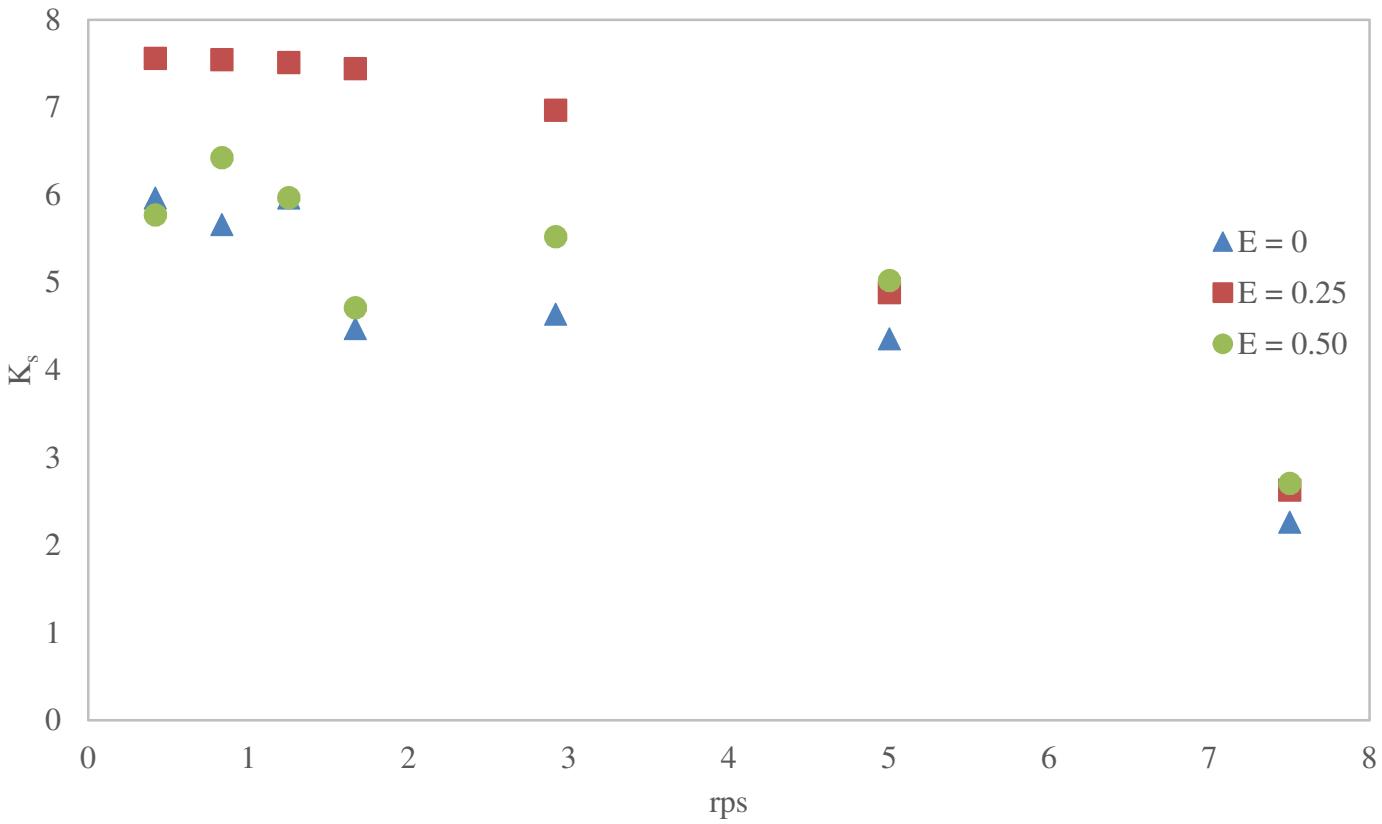

Figure 20. Effect of rps on Ks for PBT

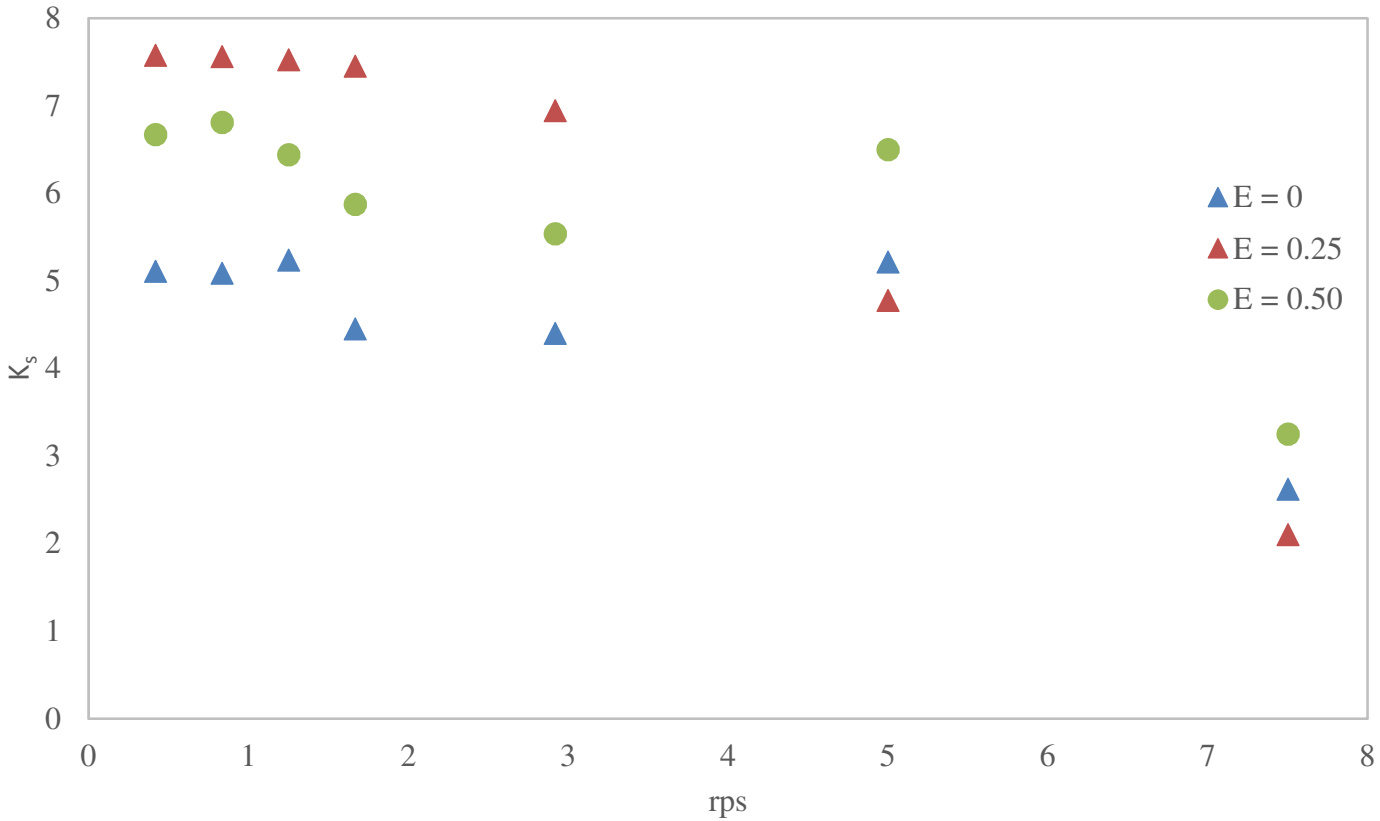

Figure 21. Effect of rps on Ks for DF-PBT

Table 6. Experimental and numerical values of K_S

	PBT		DF-PBT	
E	**Experimental**	**Numerical**	**Experimental**	**Numerical**
0	4.52	5.87	4.98	5.91
0.25	3.88	5.69	4.98	5.62
0.50	5.18	5.87	6.25	5.91

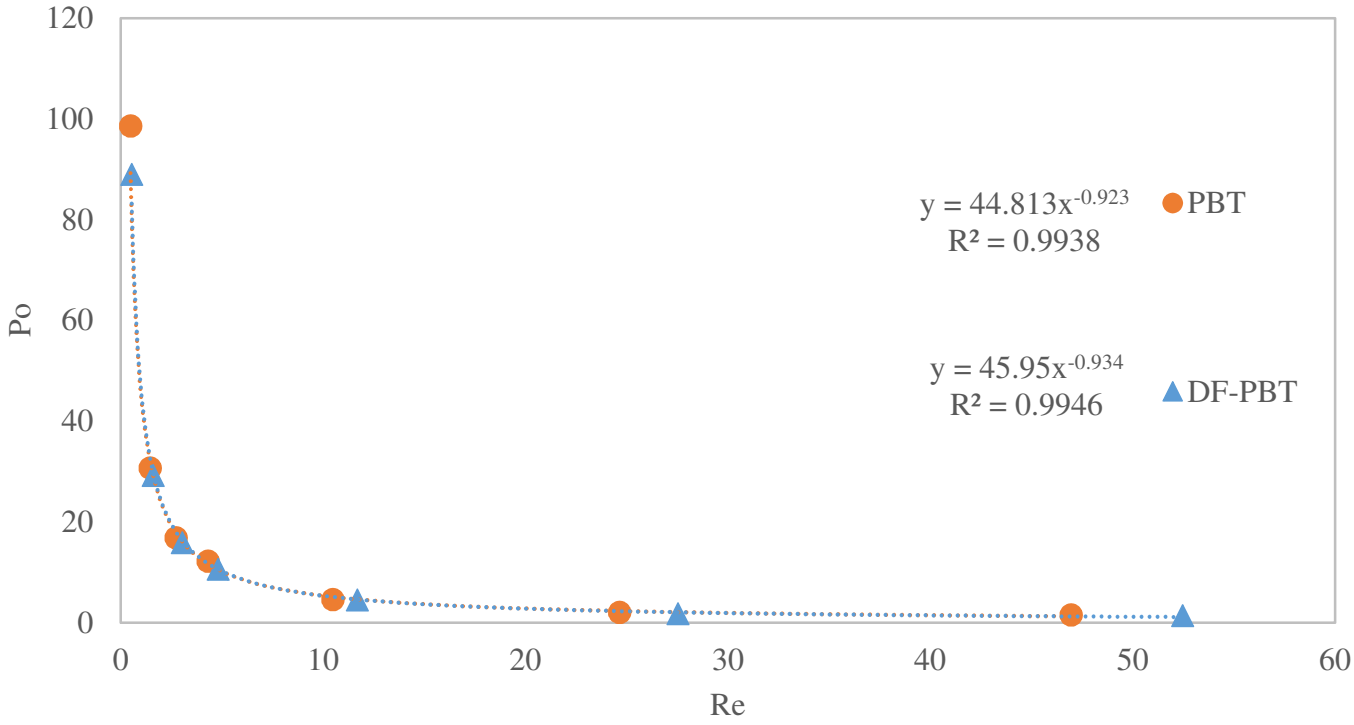

Figure 22. Non-Newtonian power curve for E = 0.50

CHAPTER 3

Shear thinning fluid mixing in unbaffled stirred vessels. Part 2: Scale-Up

Nihat Yavuz, K.P. Sandeep

Department of Food, Bioprocessing, and Nutrition Sciences, North Carolina State University, Box 7624, Raleigh, NC 27695-7624

Abstract

Mixing of a shear thinning fluid (1% carboxymethyl cellulose solution in water) was scaled-up with equal Reynolds number (Re), tip speed, and power per volume criteria. Pitched blade impeller (PBT) and dual-flow pitched blade turbine (DF-PBT) were used and located eccentrically based on the results of a previous study. The distribution of a tracer solution in terms of % uncovered area, coefficient of variation, power consumption, and flow fields were used to compare the three different scale-up criteria. Higher power consumption and less time is necessary for equal power per volume compared to that for equal Re and tip speed rules in the case of PBT. For DF-PBT, only equal Re resulted in values similar to that obtained with PBT. At a scale-up ratio of 2, the selection of scale-up rule should be based on the time and power requirements of the process.

1. Introduction

Mixing in stirred vessels is usually carried at the laboratory scale first. The important factors affecting mixing performance can be determined with reduced effort this way. On the other hand, achieving the same performance at a larger scale is still a challenging task. An ideal case of scale-up involves maintaining geometrical, kinematic, and, dynamic similarity at the same time. Geometrical similarity is achieved by keeping the ratios of different dimensions such as impeller diameter to vessel diameter same upon scale-up. Kinematic similarity is achieved by maintaining identical velocity ratios at the corresponding points of the small and large scales. Equivalent ratios between forces of viscosity, inertia, and gravity is maintained with dynamic similarity (Cullen and O'Donnell 2009). Practically, only kinematic or dynamic similarity exists with geometric similarity during scale-up. In some cases, even complete geometric similarity may not be achieved due to manufacturing limitations on the impeller geometry. The effects of such changes may affect flow profiles in stirred vessels and translated at different levels to larger scales (Wu and others 2001; Kumaresan and Joshi 2006).

Dimensional analysis is a well suited method to investigate the effects a large number of parameters on the performance of mixing in stirred vessels. A few dimensionless numbers are derived from the important parameters used to describe the entire process. The theory and details of calculations can be found in Zlokarnik (1991). Power (Po), Reynolds (Re), and Froude (Fr) numbers are only few examples of dimensionless numbers that can characterize mixing (Wilkens and others 2003; Machado and others 2012). The dimensionless number

with the most significant effect on the desired mixing performance can be kept constant for scale-up purposes and general rules of thumb have been developed over time. For example, equal Re can be used for dynamic similarity at the expense of slow production capacity. Equal tip speed should be applied for mixing of shear sensitive materials. Keeping the same mixing time as a scale-up rule is not recommended since the impeller speed must be increased to levels requiring a very large motor size and increased power consumption. Equal power per volume may be the first choice due to its moderate performance compared to other rules (Wilkens and others 2003). Additional considerations for the development of suitable viscosity and power curves at the small scale are given for scaling up power consumption with non-Newtonian fluids by Rieger and Novák (1974) and Böhme and Stenger (1988). For impellers such as planetary mixers, modifications of the dimensionless numbers may be needed to reflect the characteristic dimensions and speeds of these mixers (Delaplace and others 2005; Delaplace and others 2007; Delaplace and others 2012).

This paper is the second part of a study in which the hydrodynamics and mixing performance was studied in the first part. In this part, scale-up of an unbaffled vessel with an eccentric impeller location for mixing a shear thinning fluid is investigated. Equal Re, tip speed, and power per volume rules are applied. The effects of these rules on power consumption, evolution of a tracer solution, and, flow profiles are studied based on experimental and numerical measurements.

2. Material and Methods

2.1. Materials

Carboxymethyl cellulose (CMC) powder (Pre-Hydrated® Ticalose® CMC 2500, TIC Gums, Belcamp, MD) was used to prepare the working fluid (1% (w/v) CMC solution) which was used for the small scale experiments. The solutions were kept at ~20 ^{o}C overnight to remove air bubbles and used within 2 days before any detectable change in viscosity occurred. The flow behavior index (n) and the consistency coefficient (K) were determined as 0.41 ± 0.02 and 5.13 ± 0.57 Pa.s^{n}, respectively with a Haake VT550 viscometer (Gebruder Haake GmbH, Karlsruhe, Germany). The density (ρ) of the solution was also determined as 1001 ± 0.72 kg/m^{3}.

2.2. Mixing system

The flat-bottomed unbaffled vessel with an eccentric impeller location (E = e/r = 0.50 where 'e' is the distance between the center of the shaft and the center of the vessel, and r is the radius of the vessel) was used for the scale-up study based on geometrical similarity. The geometrical dimensions of the small and large scale vessels are given in Table 1. The scale-up ratio (R) of 2 was calculated with the following equation:

$$R = (V_2/V_1)^{1/3}$$

where V_2 and V_1 are the volumes of large and small vessels, respectively. A custom made standard 45^o four-blade pitch blade impeller (PBT) and a modified version of the same impeller (DF-PBT) were used. The impellers were attached to a Servodyne 50000-20 electrical motor operating at 3 A, 115 V (Cole-Parmer Instrument Co., Niles, IL).

2.3. Scale-up Methods

Based on a previous study, mixing at 300 rpm for an impeller position at E = 0.50 was chosen to be scaled-up. Equal Re, tip speed, and power per volume were used for scale-up. The following equations were used for determination of rpm value needed at the large scale:

$$\text{Equal Re:} \quad \frac{\rho * N_1 * D_1}{K * (K_S * N)^{n-1}} = \frac{\rho * N_2 * D_2}{K * (K_S * N)^{n-1}} \qquad (1)$$

$$\text{Equal tip speed:} \quad \pi * N_1 * D_1 = \pi * N_2 * D_2 \qquad (2)$$

$$\text{Equal Power per volume:} \quad \frac{N_1}{N_2} = \frac{(D_2)^{2/3}}{(D_1)^{2/3}} \qquad (3)$$

where N is the impeller rpm, D is the impeller diameter (m), and K_S is the Metzner-Otto constant. A subscript of 1 is used for the small scale while 2 is used for the large scale. The

average K_S values of 5.18 and 6.25 from a previous study (Yavuz and Sandeep 2016) were used for PBT and DF-PBT, respectively.

2.4. Planar Laser Induced Fluorescence Experiments

A 0.450 W diode pumped solid state laser system (RayPower 450, Dantec Dynamics Inc, Holtsville, NY) with cylindrical lenses and a digital camera (Sony Handycam HDR-CX150, Sony Corporation, Tokyo, Japan) with a narrow-band filter (9080C0541, Dantec Dynamics Inc., Holtsville, NY) was used for the large scale. To take measurements from a geometrically similar location, the laser sheet at 532 nm passed 0.1016 m away from the centerline of the vessel in the vertical plane. The procedure described by Yavuz and Sandeep (2016) was used for calibration and concentration measurements for % uncovered area and coefficient of variation (CoV).

The calibration curves (Figures 1 and 2) showed slight differences between the small and large. The uniformity of the laser sheet was tested during the calibration experiments. A higher absorption was observed at the side where the laser entered the vessel (Figure 3). The lowest CoV value when uniform distribution was maintained in the vessel was 20%. For each run, 30 mL of 68 mg/L tracer solution was injected through the surface of the CMC solution in 60 seconds to result in 20 µg/L average concentration if 100% mixing would be achieved.

2.5. Power Measurement

A torque transducer (T5-1-A1A, Interface Inc. Scottsdale, AZ) was installed between the motor and the shaft with a pillow bearing to reduce vibration. The torque values were used to determine power consumption using the following equation:

$$P = 2\pi N M_c$$

where N is impeller speed (1/s), M_c is the corrected torque (Nm) which is the difference between the measured torque with and without the working fluid. After 5 min. of warm-up time, the measurements were recorded for 3 min. at a sampling rate of 1.0 Hz.

2.5. Numerical Studies

Numerical models were developed using COMSOL 5.2 (Comsol Inc, 1 New England Executive Park, Burlington, MA) with the Rotating Machinery-Laminar Flow interface in the CFD module. Only the frozen rotor approach was used for the models due to the highly time consuming nature of time-dependent solutions for the eccentrically located impellers. The stirred vessel geometry with an outer stationary and an inner rotating domain were assembled. No slip, symmetry, and rotating wall boundary conditions were applied to the walls, fluid surface, and, impeller/shaft surfaces, respectively. A random point in the geometry was also selected for pressure constraint to define a pressure value of zero. This

way infinite number of solutions for Navier-Stokes equations were avoided. The mesh included tetrahedral, pyramid, prism, triangular, quadrilateral, edge, and, vertex elements. A built-in fine mesh setting was found to be satisfactory for convergence. Power consumption values were validated with the experimental values and velocity vectors were used to compare flow profiles at the small and large scales.

3. Results and Discussions

3.1. Determination of rpm at large scale

The rpm values used for the large scale experiments are given in Table 2. Since the impeller diameter at both scales is controlled more accurately than the fluid properties, the rpm values needed to keep constant tip speed of 1 m/s are easily adjusted. For Equal Re calculations, the Metzner-Otto constants (K_S) measured for PBT and DF-PBT at the small scale (5.18 and 6.25, respectively) are used. Böhme and Stenger (1988) pointed out that K_S is independent of the size of the mixing system. In Figures 4 and 5, the isosurfaces of the velocity magnitude at the small and large scales show that the flow is mainly taking place around the impeller and that no interaction between the impeller and vessel wall is seen. This is in agreement with the concept of K_S defining an average shear rate around only the impeller. However, numerically obtained power values are used to evaluate the dependence of K_S on scale-up. Increase in K_S from 5.87 to 6.53 for PBT and from 5.91 to 6.60 for DF-PBT show that K_S may be affected by the scale. No experimental work has been done to validate the results and hence no correction is made for the rpm values calculated. The

original rpm values calculated from Equation 3 (189 rpm) results in less power per volume than that needed for scale-up based on the preliminary experiments. On the other hand, the rpm values derived from the power curves of 1% CMC (for PBT: $Po = 44.813*Re^{-0.923}$ and for DF-PBT: $Po = 45.950*Re^{-0.934}$ from Yavuz and Sandeep 2016) return slightly higher power per volume values. Despite the same concentration of CMC being used at both scales, the change in the consistency coefficient most likely resulted in errors for the determination of rpm for equal power per volume.

3.2. Effects of scale-up on mixing performances

The changes in power consumption with scale-up are presented in Table 3. Equal Re and tip speed results in approximately quarter and half the power consumption of equal power per volume, respectively. The magnitude of this change depends on the scale up ratio (R). As R increases, a greater reduction is observed in power consumption for equal Re and tip speed scale-up rules (Wilkens and others 2005; Triveni and others 2010). Only minor differences in power consumption between the small and large scales are observed for equal power per volume. However, errors such as changes in fluid properties and fluctuations in rpm can result in bigger differences with increased R. A fairly good agreement (maximum 6% difference) is obtained between the experimental and numerical values for PBT while the differences (up to 29%) are higher for DF-PBT. With improved mechanical design to reduce vibration and increased accuracy on numerical models, power consumption upon scale-up can be better predicted so that trial and error efforts can be kept at minimum. Table 4

summarizes the effects of scale-up rules on Re and tip speed. As rpm is increased to maintain equal Re, tip speed, and power per volume, Re and tip speed also increase. The end of laminar region is associated with different Re in the literature. However, as highlighted by Lamberto and others (1999), they are generally less than 100. For each scale-up criteria, Re falls in this range. Thus, the characteristics of mixing at both scales are expected to be similar.

In Figures 6 and 7, PLIF images at the end of 3 hrs. are presented for different scale-up rules. For PBT, the tracer solution is able to cover the entire region of interest (which excludes the top and bottom of the vessel where extra reflections are seen). The bright areas at the bottom and upper right corner of the vessel indicates mixing is not complete. For DF-PBT, less area is covered with the tracer solution for equal tip speed than that for equal Re as higher rpm is required for the former. For the case of equal power per volume, the tracer solution is only able to penetrate from surface to the upper right side of the vessel. The change in % uncovered area over time is used as a quantitative measure and comparison between the small and large scales. In Figures 8 and 9, the drop in the % uncovered area happens within the first minute of mixing and reaches less than 5% in 9 and 33 min. for PBT and DF-PBT, respectively. For the large scale PBT, the drop in the % uncovered area is observed after 9, 14, and, 43 min. from the start of the experiments for equal power per volume, tip speed, and Re respectively (Figure 10). Since the distance from fluid surface to the impeller is higher at the large scale, it takes longer for the tracer solution to reach the impeller to be distributed in the vessel. As the highest rpm is used for equal power per

volume, the tracer solution reaches the impeller faster than it does for other scale-up rules. For the same reason, the shortest time to obtain less than 5% uncovered area is achieved by equal power per volume (16 min.) which is followed by equal tip speed (32 min.), and then equal Re (68 min.). In Figure 11, it is seen that only the equal Re scale-up rule works for DF-PBT. The tracer solution reaches the impeller in 28 min. and leaves less than 5% uncovered area after 105 min. While the tracer solution is able to reach the impeller during equal tip speed scale-up (75 min.), approximately 10% area is uncovered. Based on the PLIF images and the relatively flat trend seen in Figure 11, it is concluded that the tracer is unable to reach the impeller. Scale-up based on equal Re is used for dynamic similarity (Triveni and others 2010). The proposed behavior of simultaneous upward and downward flow and the possibility of these flows canceling each other may be dependent on not only the geometry of the impeller but also Re. A detailed study must be conducted to understand and improve the performance of DF-PBT. CoV values when the % uncovered area is less than 5 and at the end of 3 hrs. for each scale-up rule and impeller type are given in Table 5. For all the cases of PBT, similar CoV values are obtained. Although Kukukova and others (2009) concluded that CoV alone should not be used to define mixing, the results in Table 5 along with % uncovered area and observations from the PLIF images indicate that the same end point can be achieved with equal Re, tip speed, and power per volume with PBT.

The flow profiles determined by the numerical analysis are shown in Figures 12, 13, and 14 for the locations of the vessel center, laser measurement plane, and fluid surface, respectively. An additional circulation is more pronounced at the vessel center and a slightly

more upward flow at the laser measurement plane is observed for equal power per volume scale-up rule. The closest flow profile to the small scale is formed with equal Re which is in agreement with (Li and others 2005). The flow profile at the fluid surface shows that the separation of the flow next to the shaft is shifted towards the right side while the focus point on the opposite side of the shaft is moved to the left side as the scale-up rule is changed from equal Re to equal power per volume. The circular motion seen around the shaft at the small scale is less obvious for the large scale since the shaft diameter is kept constant due to design limitations.

4. Conclusion

The scale-up rules of equal Re, tip speed, and power per volume was applied for mixing of a shear thinning fluid (1% CMC) in an unbaffled vessel. The impellers used in the study were pitched blade turbine (PBT) and Dual-flow pitched blade turbine. Only scale-up based on equal Re was successful for DF-PBT suggesting that the flow profile of the impeller must be studied in details. The same end point of mixing (the same % uncovered area and CoV values) was achieved with different scale-up rules for PBT. The main differences between each rule were the power consumption and the time to achieve the same end point. As less time was necessary for equal power per volume, a higher power consumption was required compared to that for equal Re and tip speed rules. The numerically computed flow field was able to capture the changes due to the eccentric locations and geometrical differences. Maximum 6% difference was obtained between the numerical and experimental

power values of PBT while it was up to 29% for DF-PBT. At the scale-up ratio (R = 2) used in this study, the selection of scale-up rule should be based on the time that would be allocated for mixing and the capacity of the motor to handle the required power consumption.

References

Böhme G, Stenger M. 1988. Consistent scale-up procedure for the power consumption in agitated non-Newtonian fluids. Chemical Engineering Technology 11(1):199-205.

Cullen PJ, O'Donnell CP. 2009. Mixing in the Food Industry: Trends and Challenges. In: P.J. Cullen, editor Food Mixing. Blackwell Publishing Ltd. p 1-5.

Delaplace G, Guérin R, Leuliet JC. 2005. Dimensional analysis for planetary mixer: Modified power and Reynolds numbers. AIChE Journal. 51(12):3094-3100.

Delaplace G, Thakur RK, Bouvier L, André C, Torrez C. 2007. Dimensional analysis for planetary mixer: Mixing time and Reynolds numbers. Chemical Engineering Science 62(5):1442-1447.

Delaplace G, Coppenolle P, Cheio J, Ducept F. 2012. Influence of whip speed ratios on the inclusion of air into a bakery foam produced with a planetary mixer device. Journal of Food Engineering 108(4):532-540.

Kukukova A, Aubin J, Kresta SM. 2009. A new definition of mixing and segregation: Three dimensions of a key process variable. Chemical Engineering Research & Design 87(4):633-647.

Kumaresan T, Joshi JB. 2006. Effect of impeller design on the flow pattern and mixing in stirred tanks. Chemical Engineering Journal 115(3):173-193.

Lamberto DJ, Alvarez MM, Muzzio FJ. 1999. Experimental and computational investigation of the laminar flow structure in a stirred tank. Chemical Engineering Science 54(7):919-942.

Li M, White G, Wilkinson D, Roberts KJ. 2005. Scale up study of retreat curve impeller stirred tanks using LDA measurements and CFD simulation. Chemical Engineering Journal. 108:81-90.

Machado MB, Nunhez JR, Nobes D, Kresta SM. 2012. Impeller characterization and selection: Balancing efficient hydrodynamics with process mixing requirements. AIChE Journal. 58(8):2573-2588.

Rieger F, Novák V. 1974. Power consumption scale-up in agitating non-Newtonian fluids. Chemical Engineering Science 29(11):2229-2234.

Triveni B, Vishwanadham B, Madhavi T, Venkateshwar S. 2010. Mixing studies of non-Newtonian fluids in an anchor agitated vessel. Chemical Engineering Research & Design 88(7):809-818.

Wilkens RJ, Henry C, Gates LE. 2003. How to scale-up mixing processes in non-Newtonian fluids. Chemical Engineering Progress 9944-9952.

Wu J, Zhu Y, Pullum L. 2001. Impeller geometry effect on velocity and solids suspension. Chemical Engineering Research & Design 79(8):989-997.

Yavuz N, Sandeep, K.P. 2016. Shear thinning fluid mixing in unbaffled strirred vessels. Part 1: Hydrodynamic characterization. Unpublished.

Zlokarnik M. 1991. Dimensional analysis and scale-up in chemical engineering. Berlin: Springer-Verlag. 176 p.

Table 1. Geometrical dimensions of the small and large scale vessels

	Small Scale	**Large Scale**
Diameter (m)	0.254	0.508
Height (m)	0.254	0.508
Impeller Diameter (m)	0.0635	0.127
Impeller Clearance (m)	0.0635	0.127
Volume*10^{-3} (m^3)	12.87	102.96

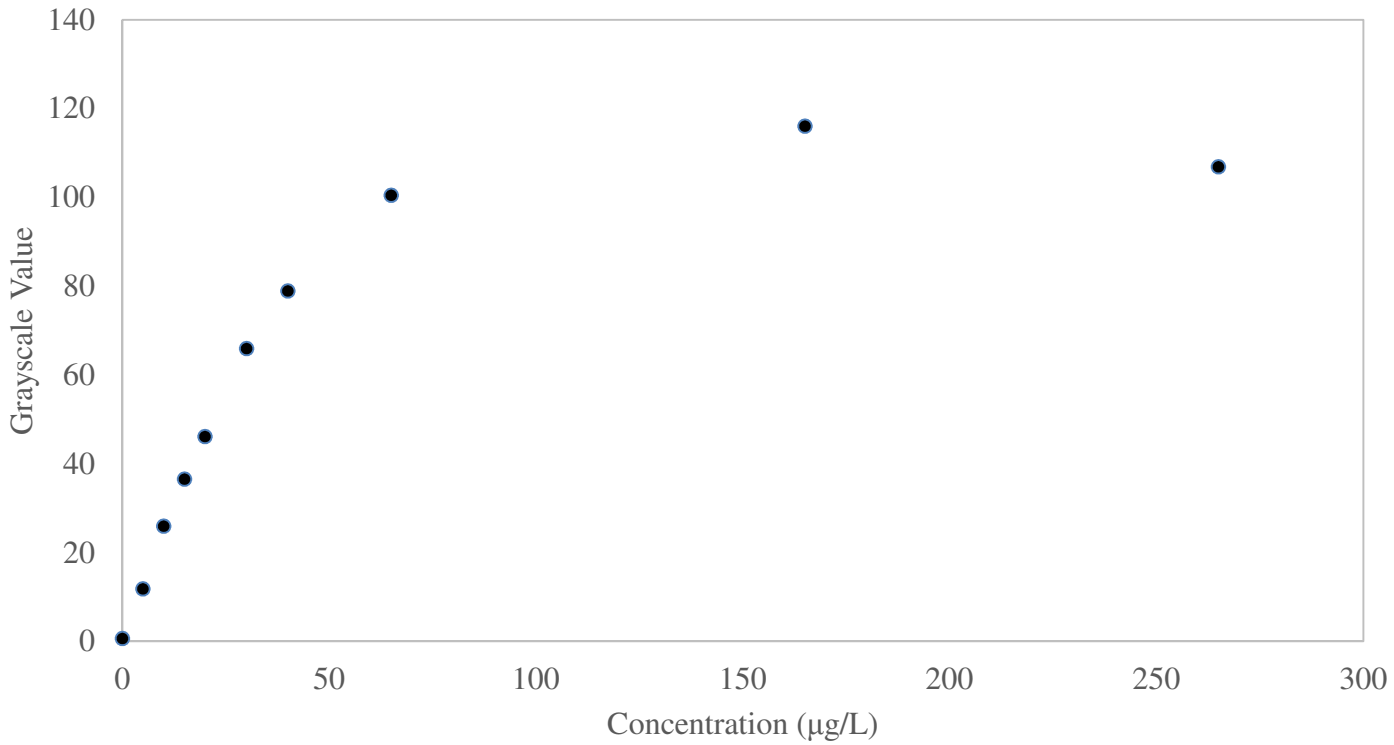

Figure 1. Grayscale vs concentration of Rhodamine 6G for large scale vessel

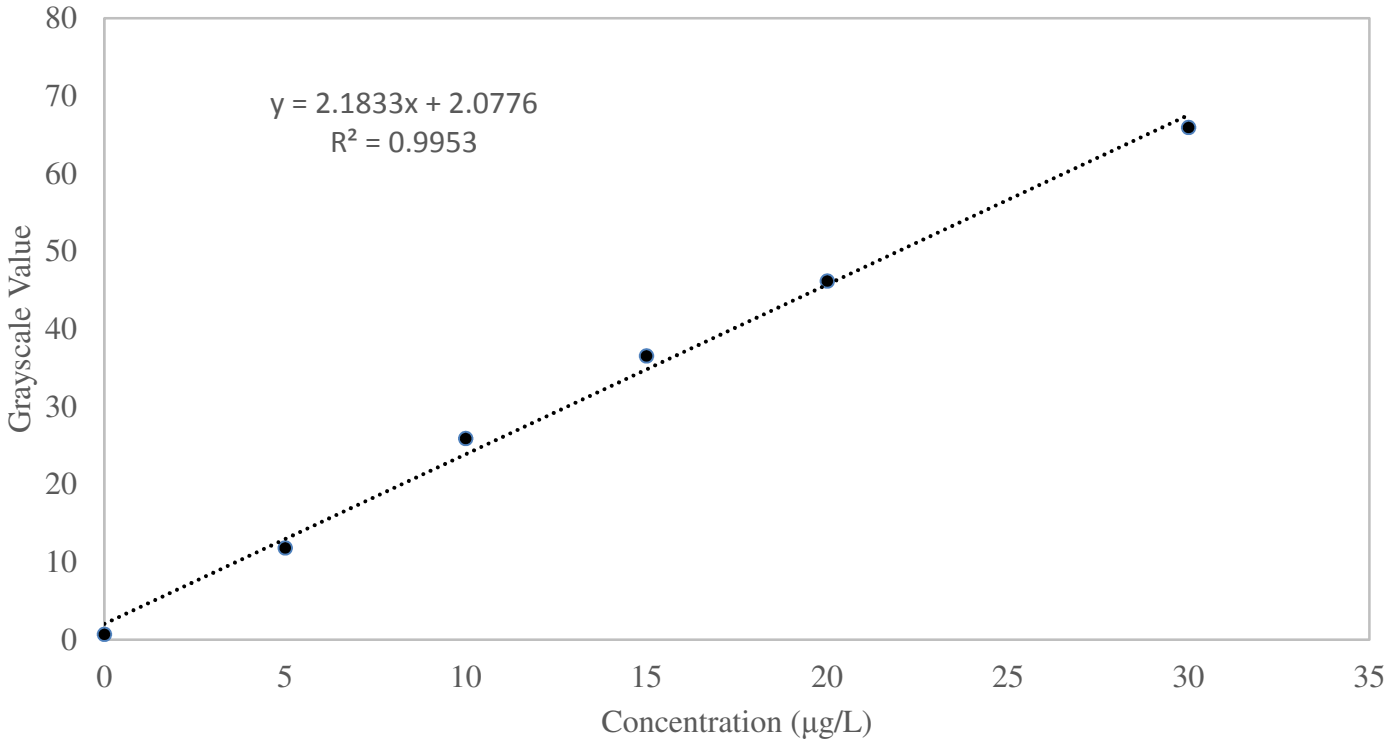

Figure 2. Linear calibration curve of Rhodamine 6G for large scale vessel

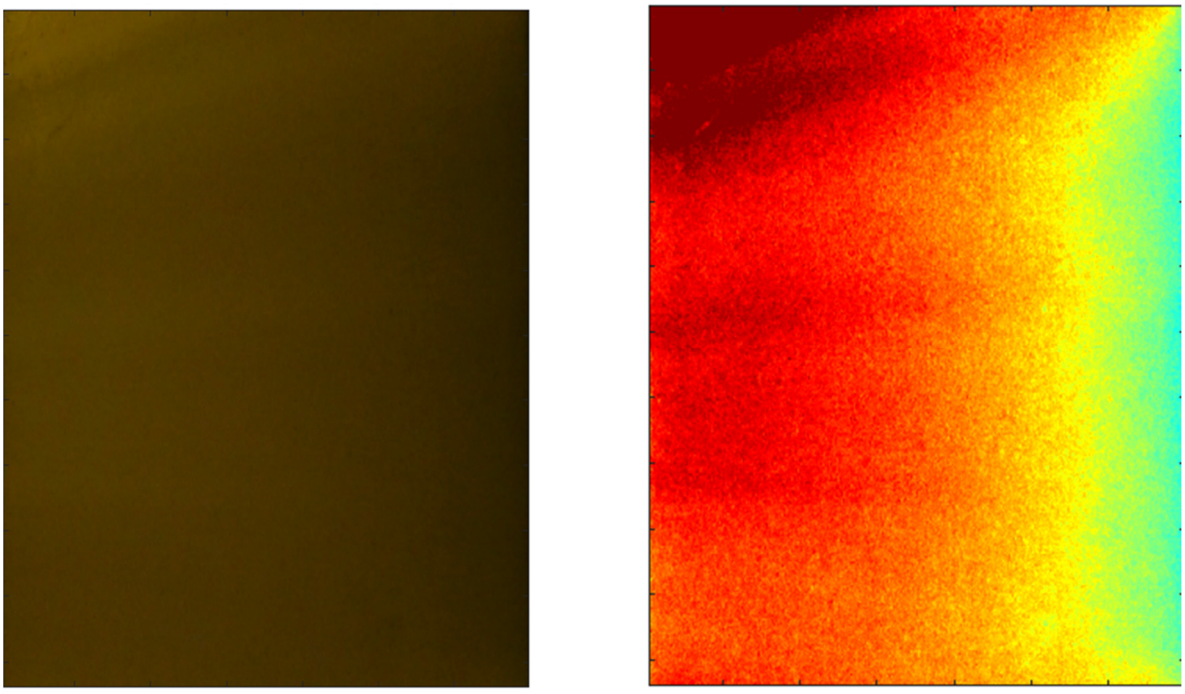

a) b)

Figure 3. Uniformity of the lase sheet for calibration image at 20 µg/L a) original image and b) colored image

Table 2. Large scale rpm values for each scale-up rule

Impeller Type	Equal Tip Speed	Equal Re	Equal Power per Volume
PBT	150	124	217
DF-PBT	150	127	210

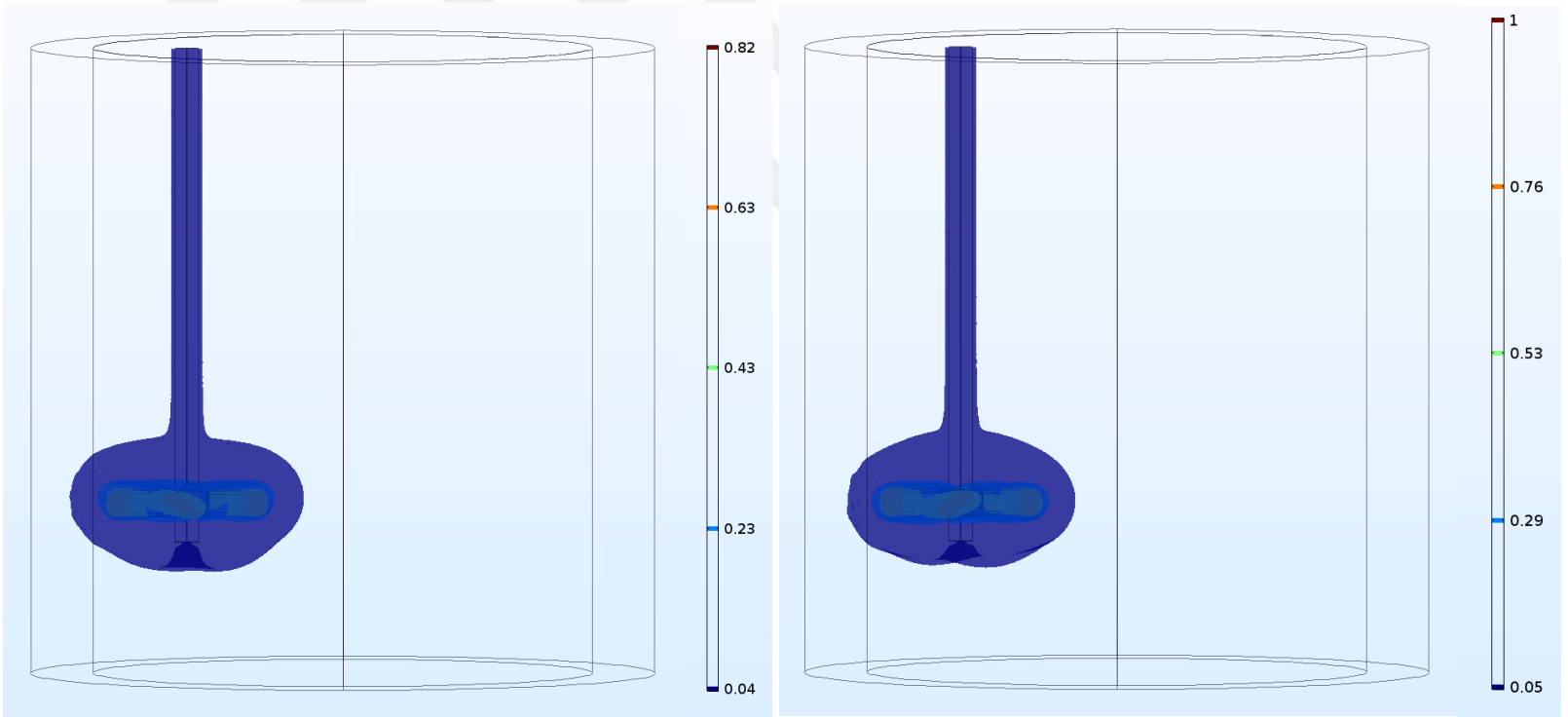

a) b)

Figure 4. Isosurface representations of velocity magnitudes at the small scale a) PBT and b) DF-PBT

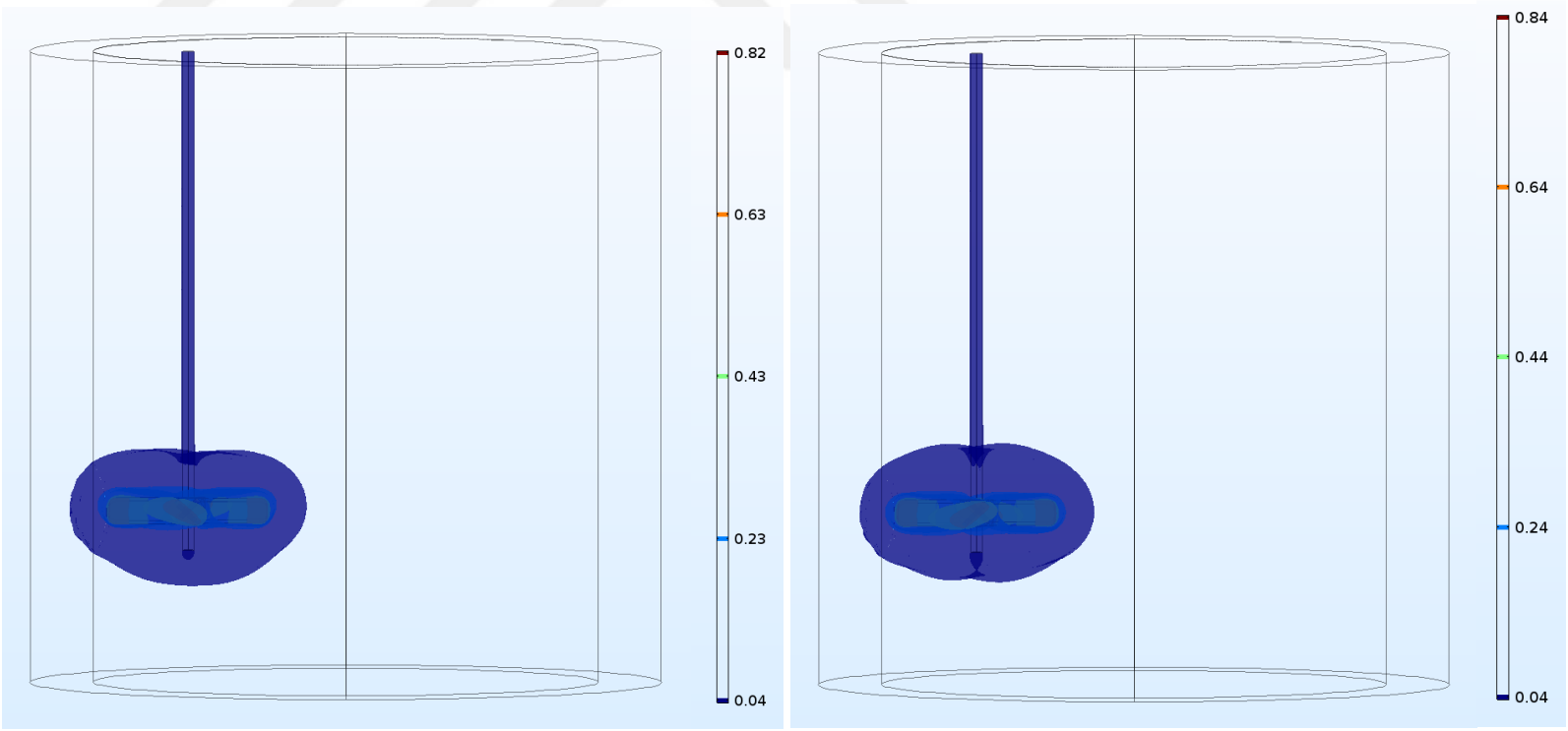

a) b)

Figure 5. Isosurface representations of velocity magnitudes on the large scale (Equal Re) for a) PBT and b) DF-PBT

Table 3. Specific power consumption (W/m^3) comparison for experimental and numerical measurements

			P (W/m^3)	
Impeller Type	**Scale-up Rule**	**rpm**	**Experimental**	**Numerical**
PBT	**Equal Re**	124	4.99 ± 0.11	5.30
	Equal Tip Speed	150	8.22 ± 0.16	8.25
	Equal Power / Volume	217	20.13 ± 0.45	20.37
DF-PBT	**Equal Re**	127	5.02 ± 0.11	5.26
	Equal Tip Speed	150	7.56 ± 0.10	8.58
	Equal Power / Volume	210	17.67 ± 0.73	22.79

Table 4. Change in Re and tip speed with scale-up

		Small Scale	**Equal Re**	**Equal Tip Speed**	**Equal Power per Volume**
PBT	**Tip Speed (m/s)**	1	0.83	1	1.44
	Re	24.2	24.2	32.7	58.9
DF-PBT	**Tip Speed (m/s)**	1	0.85	1	1.40
	Re	28.17	28.17	52.91	64.53

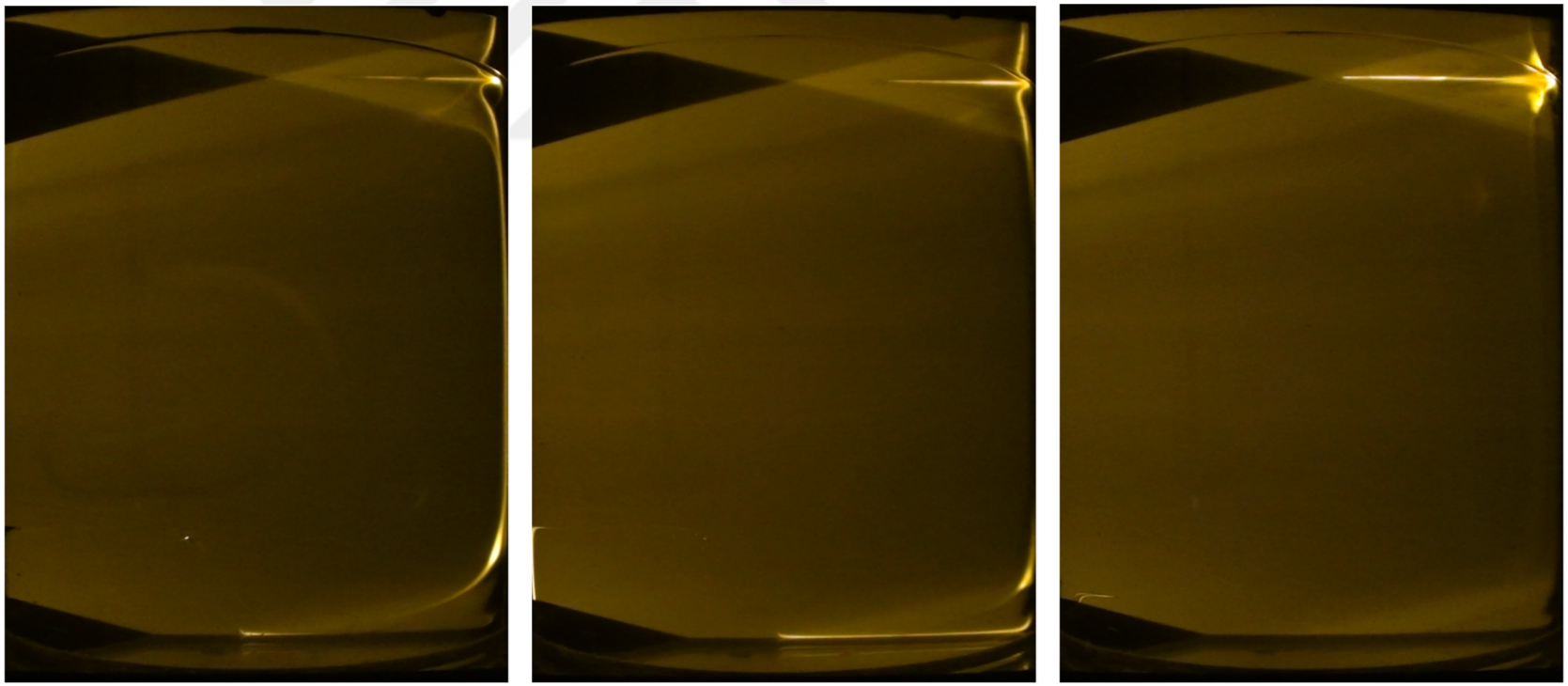

a) b) c)

Figure 6. PLIF images for PBT at the end of 3 hrs. a) Equal Re, b) Equal Tip Speed, c) Equal Power per Volume

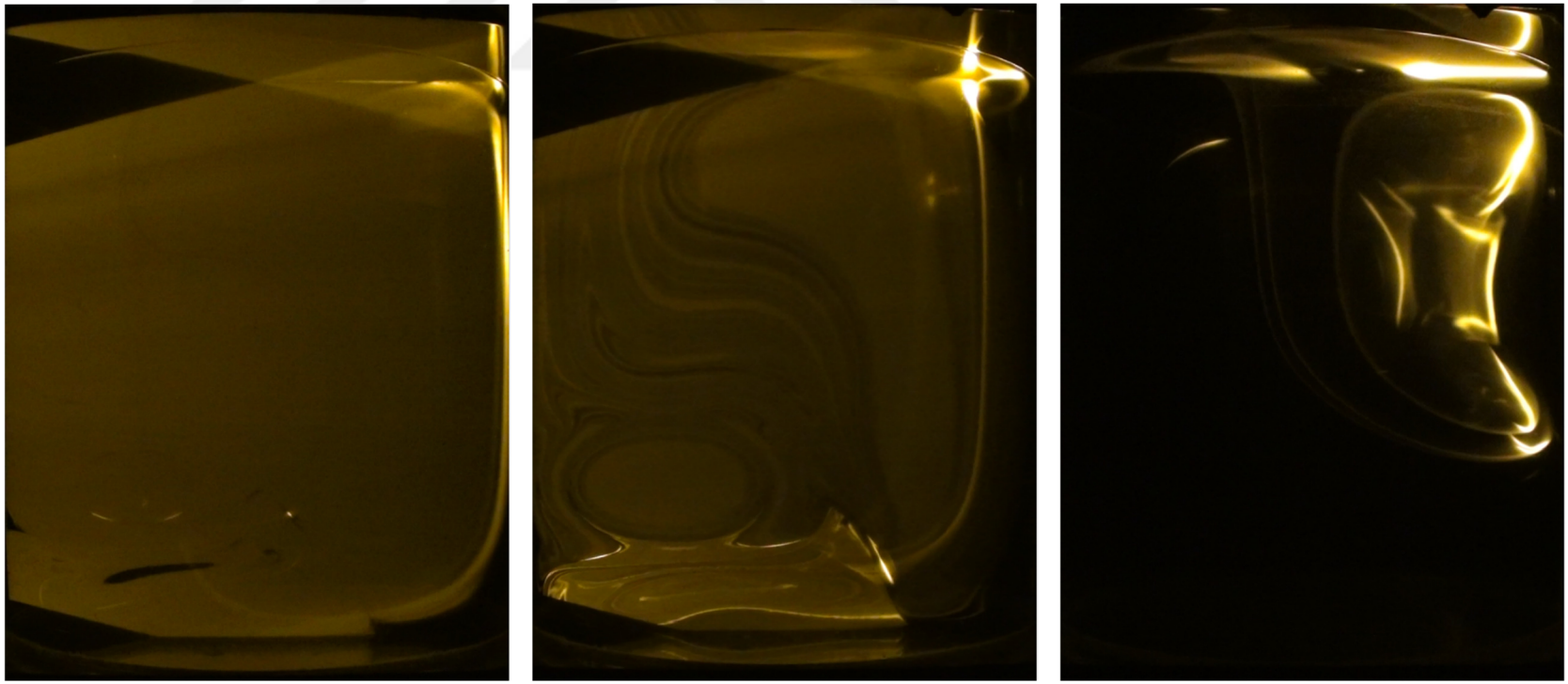

a) b) c)

Figure 7. PLIF images for DF-PBT at the end of 3 hrs. a) Equal Re, b) Equal Tip Speed, c) Equal Power per Volume

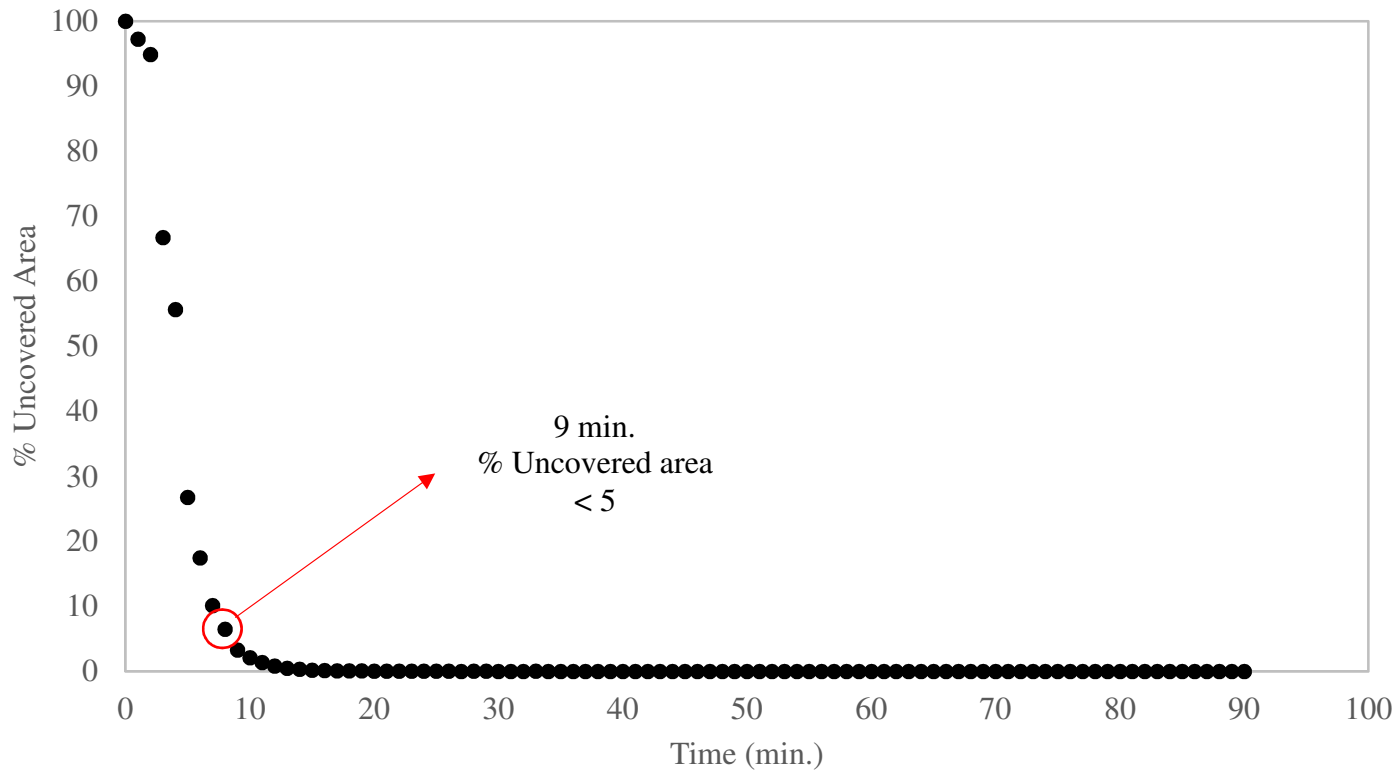

Figure 8. The change in % uncovered area% over time for PBT at small scale

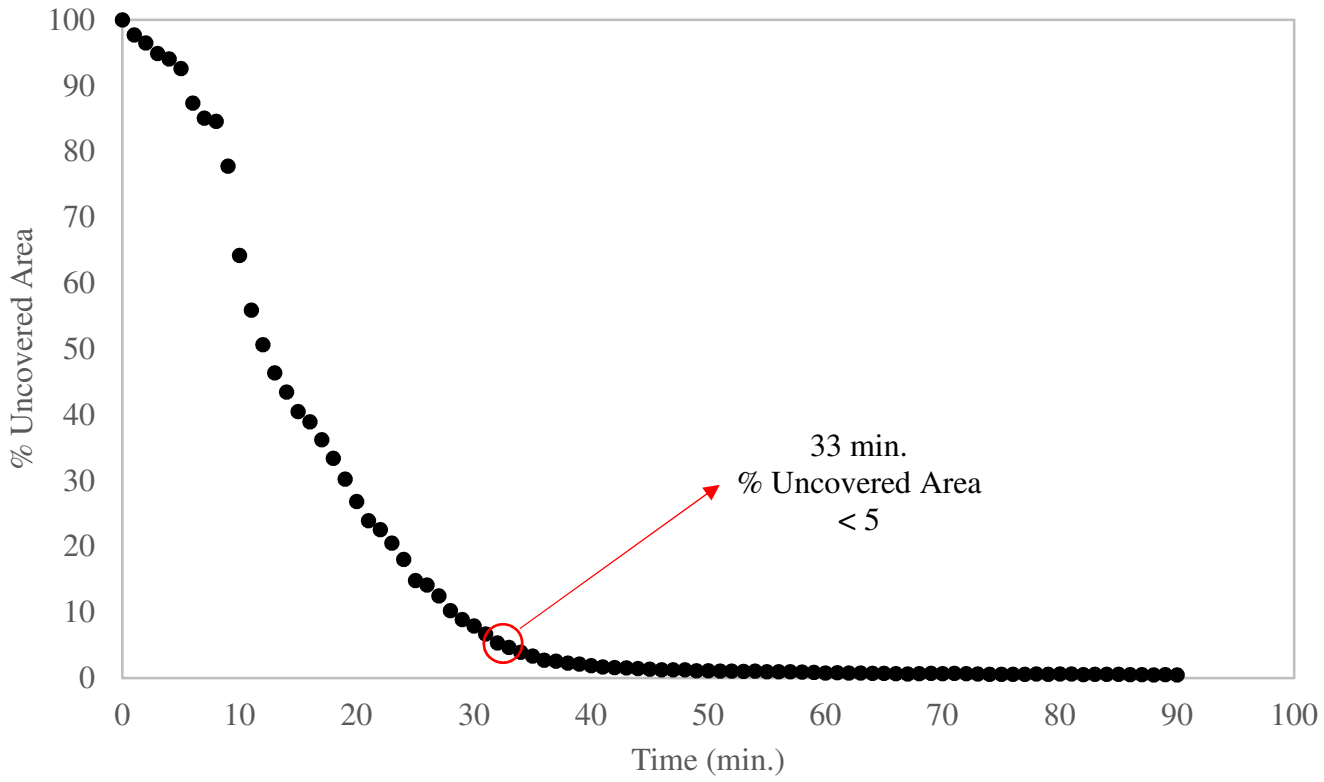

Figure 9. The change in uncovered area% over time for DF-PBT at small scale

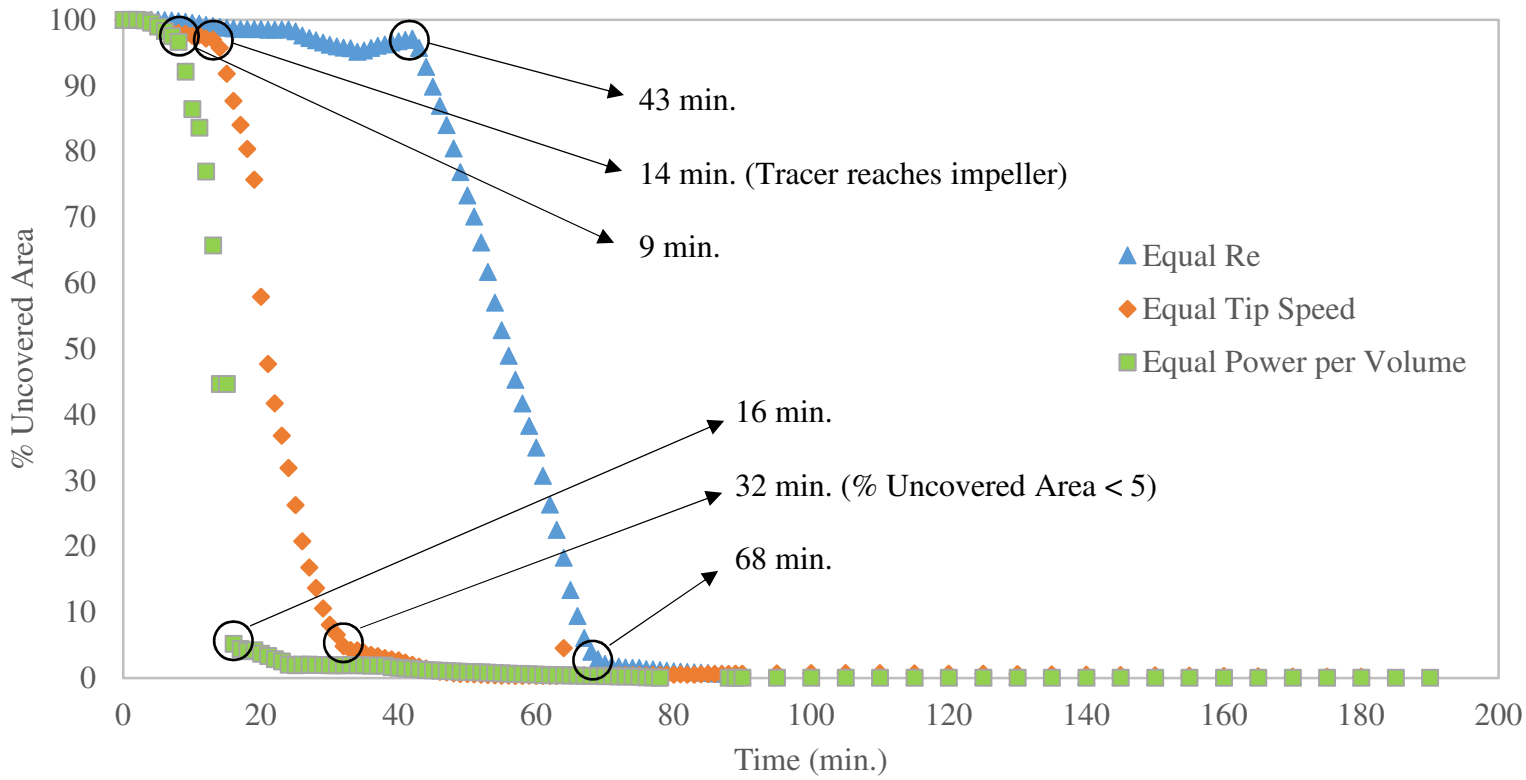

Figure 10. Change in % uncovered area over time for PBT at large scale

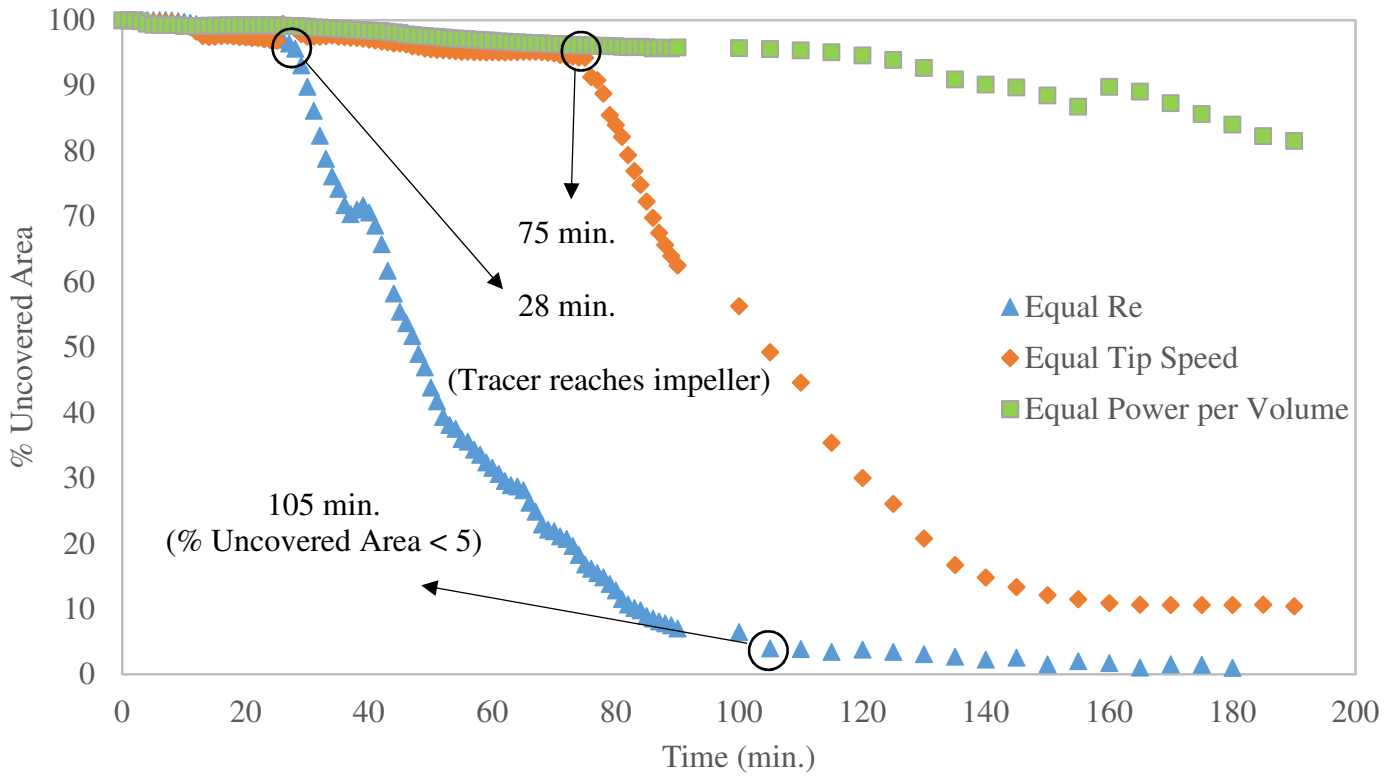

Figure 11. Change in % uncovered area over time for DF-PBT at large scale

Table 5. CoV values when uncovered area% is less than 5 and at the end of the experiments (3 hrs.)

Impeller Type	Scale-up Rule	CoV ($t_{<5\%}$)	CoV (t_{3h})
PBT	**Equal Re**	42.77 ± 2.57	26.25 ± 2.27
	Equal Tip Speed	45.01 ± 1.81	24.15 ± 0.31
	Equal Power per Volume	41.64 ± 0.39	23.18 ± 0.07
DF-PBT	**Equal Re**	34.09 ± 4.32	24.80 ± 0.93
	Equal Tip Speed	-	48.15 ± 5.84
	Equal Power per Volume	-	212.89 ± 5.36

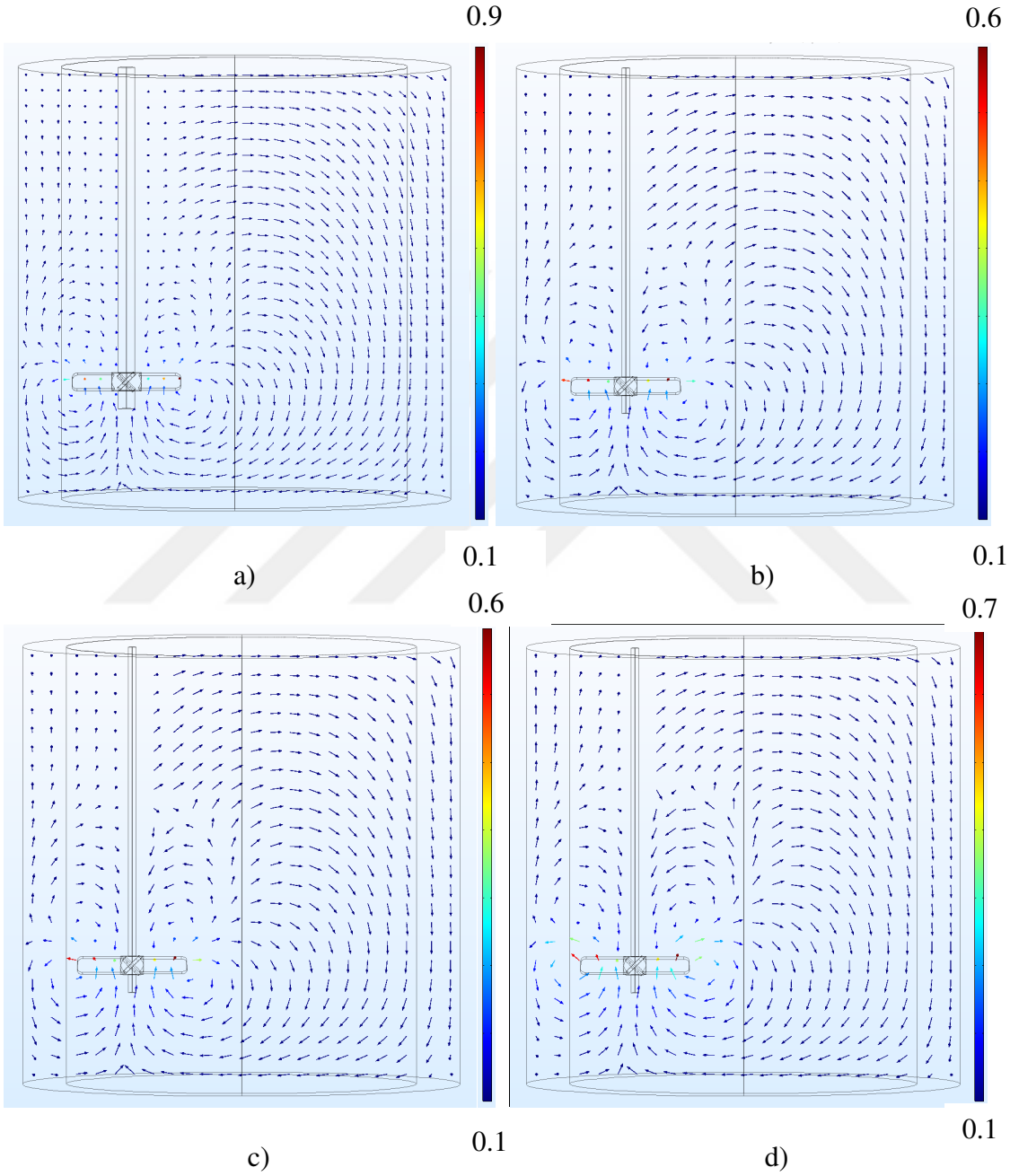

Figure 12. Velocity vectors at the vessel center for PBT a) Small scale, b) Equal Re, c) Equal Tip speed, d) Equal Power per Volume (color bars show normalized velocity magnitudes with tip speed)

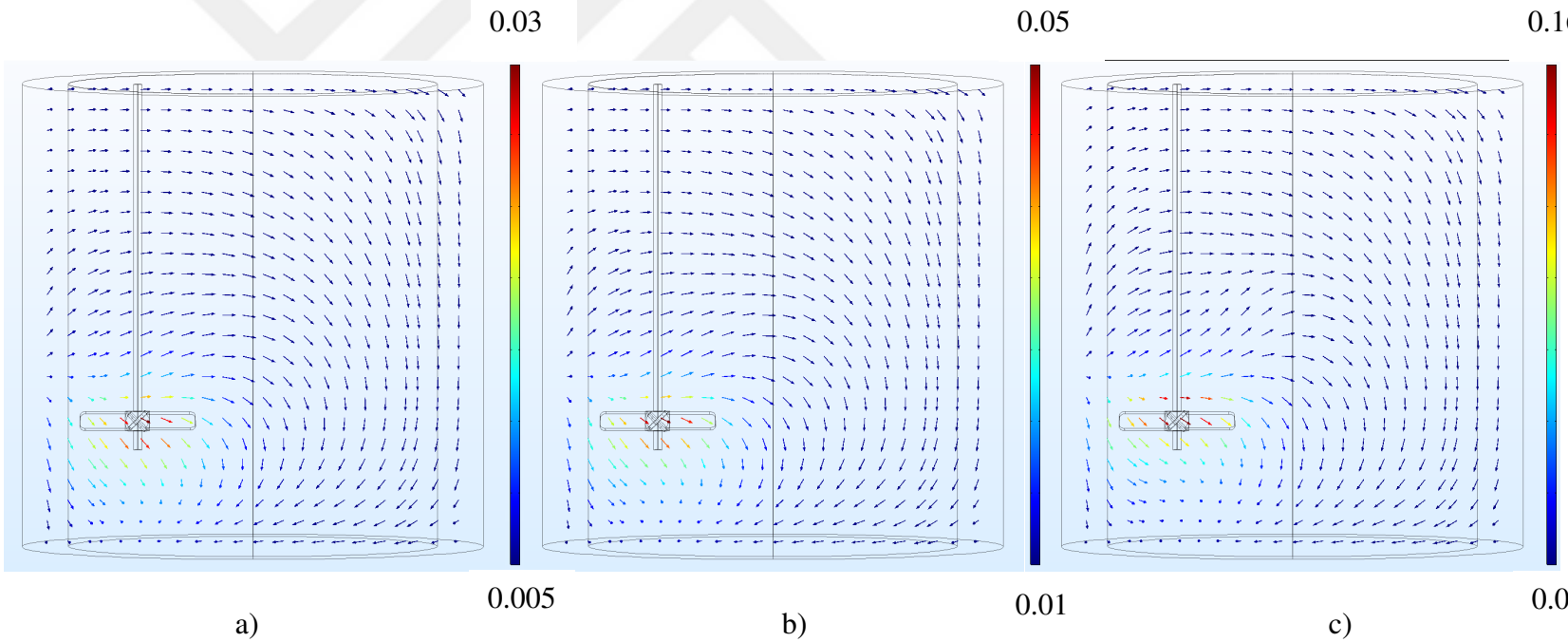

Figure 13. Velocity vectors at the laser measurement plane for PBT: a) Equal Re, b) Equal Tip speed, c) Equal P/V (color bars show normalized velocity magnitudes with tip speed)

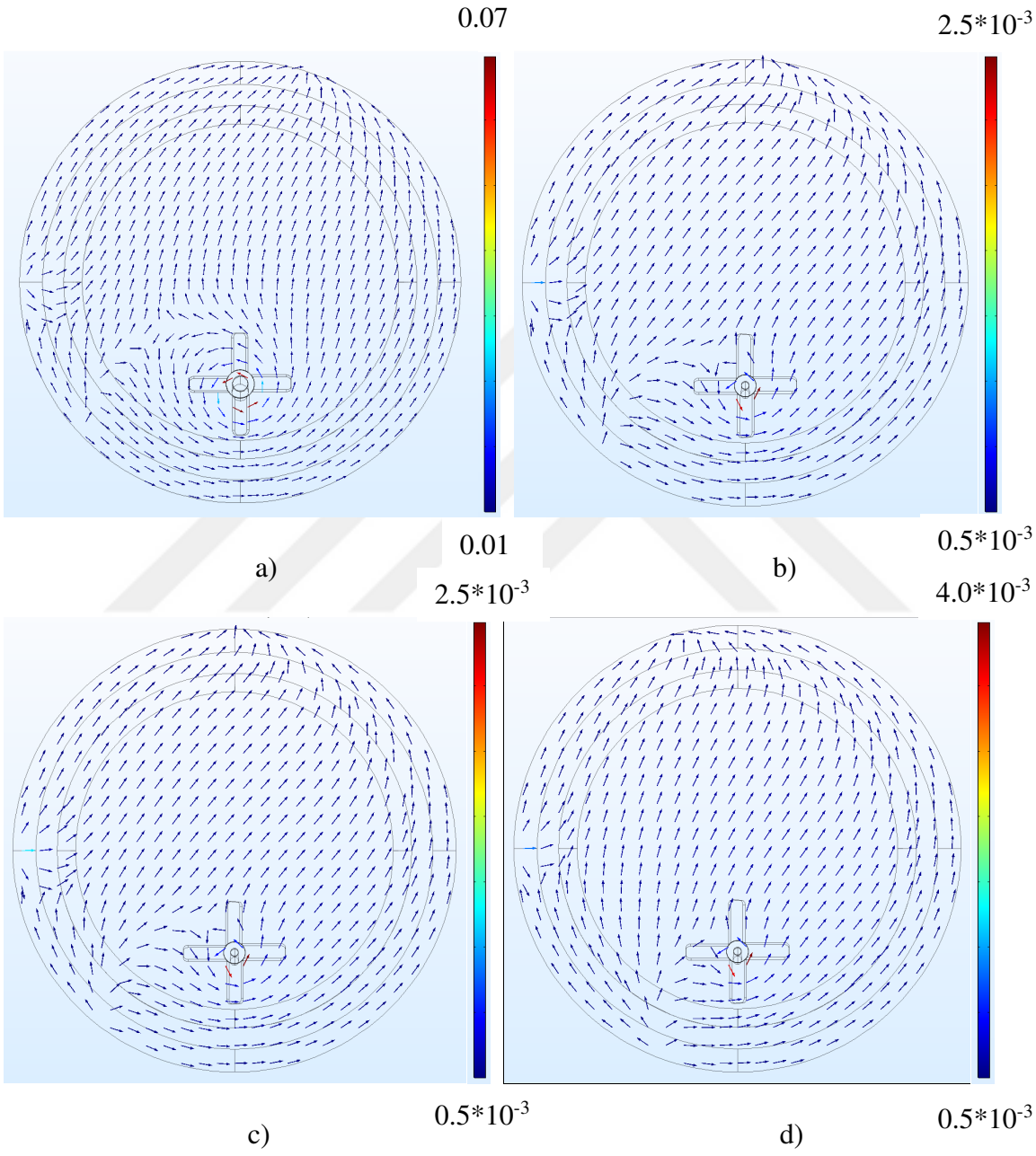

Figure 14. Velocity vectors at the fluid surface for PBT: a) Small scale, b) Equal Re, c) Equal Tip speed, d) Equal Power per Volume (color bars show normalized velocity magnitudes with tip speed)

CONCLUDING REMARKS

Mixing of highly viscous fluids in stirred vessels is usually carried out under laminar flow conditions. In this case, isolated mixing regions (IMRs), flow separation at the impeller height in radial direction, and slow mixing at the fluid surface prevent complete mixing. Methods which do not require advanced controls systems or use additional equipment to eliminate these problems may be more desirable than other complex solutions such as multiple impeller configurations or variable rotational speed/direction protocols.

Eccentrically located impellers and modification of a standard impeller were selected as two practical methods for mixing of a viscous shear thinning fluid (1.0% carboxymethyl cellulose solution). The impellers were a standard pitched blade turbine (PBT) and the modified version, Dual-Flow Pitched blade turbine (DF-PBT). The distribution of a tracer solution, power consumption, and flow profiles were used as indicators of performance. Planar laser induced fluorescence (PLIF) was used to visualize the evolution of the tracer solution (Rhodamine 6G dye) inside the vessel. The % uncovered area, which is an indicator of isolated mixing regions (IMRs), and coefficient of variation, which is a measure of concentration differences, were calculated. Power consumption in terms of W/m^3 was determined both experimentally and numerically by using a torque transducer and a commercial software. Comsol 5.2 (Comsol Inc, 1 New England Executive Park, Burlington, MA) was also used to obtain flow profiles during mixing. Average shear rate approximation based on the Metzner-Otto concept was used to plot Power number (Po) vs Reynolds number

(Re) curve to be used in the scale-up of mixing. Equal values of Re, tip speed, and power per volume criteria were used to scale-up a 12.87 L small scale system to a 102.96 L large scale system which resulted in a scale-up ratio (R) of 2.

As eccentricity increased, the size of IMRs reduced. Instead of increasing rpm to higher values without changing the location, increasing eccentricity at lower rpm resulted in wider area of coverage. This observation was important because of the fact that power consumption was not affected by eccentricity as opposed to increasing rpm. For the cases of reduced IMRs (<5% uncovered area), significant concentration variation was still present. Flow profiles showed the elimination of symmetric and slow mixing zones by eccentrically located impellers. PBT was modified to generate simultaneous upward and downward flow. However, DF-PBT did not perform better than PBT for the same rpm and eccentricity values. It was concluded that the expected chaotic flow was not developed due to the possible cancellation of flows in opposite direction. The behavior of DF-PBT was similar to that with a disc without any blade and has been shown to be an inefficient impeller in the literature. Further improvements may be done to design the appropriate geometry inducing more chaotic flow. The combined effect of eccentricity and simultaneous upward and downward flow would increase laminar mixing performance even further.

For scale-up studies at R = 2, all scale-up criteria were able to reach the same end-point in terms of % uncovered area and CoV for PBT. The main difference between each criteria was the time to reach the end-point and power consumption. The selection of scale-up criteria may be done by considering these two factors. Numerical analysis may also be

used to compute flow profiles to predict injection points on the fluid surface which will result in shorter times for the tracer to reach impeller and measurement locations which can represent the changes in mixing level better. Since only equal Re was successful for DF-PBT, a more detailed study is needed for conclusive recommendations.

RECOMMENDATIONS FOR FUTURE STUDIES

For further studies to better understand mixing and scale-up, the following points are highlighted:

- The power level of the laser source used in a planar laser induced fluorescence method should be assessed carefully by considering the size of the vessel and the concentration level of the tracer dye for measurements with minimum errors.
- The measurement location inside the vessel affects the results. Measurements at multiple locations will give a better idea of the performance of the mixing systems studied.
- Error sources such as vibration on the shaft and temperature variation during mixing of fluids with highly temperature dependent viscosities must be minimized for torque/power measurements. These errors are usually magnified for later calculations.
- Even though model development and solution in reasonable times may be hard to achieve, numerical analysis should be conducted as a prediction tool to reduce the number of actual experiments and trial and error efforts before equipment configuration is determined.

A more challenging but practically relevant scenario such as mixing of fluids with different viscosities and densities or at different temperatures may be studied with the same methods discussed in this research. Scale-up without geometric similarity

should also be considered to answer the needs where the manufacturing and processing limitations require use of different equipment at different scales.